Experimental Investigation of Energy Consumption and Performance of an Electric Vehicle Powertrain on Different Laboratory and Real-World Driving Cycles and Drive Modes

A

Thesis Submitted

in Partial Fulfilment of the Requirements

for the Degree of

DOCTOR OF PHILOSOPHY

By

Robindro Lairenlakpam

(Reg. No. 126102031)

Department of Electronics and Electrical Engineering

Indian Institute of Technology Guwahati

Guwahati - 781039, India.

2021

In the memory of

my dear Father Apabi Singh Lairenlakpam

&

To

my beloved Mother, Memton Devi Lairenlakpam,

my loving wife, Sarita and daughter, Lelinda (Babycha)

for their infinite love, trust and moral support.

Certificate

This is to certify that the thesis entitled, "**Experimental Investigation of Energy Consumption and Performance of an Electric Vehicle Powertrain on Different Laboratory and Real-World Driving Cycles and Drive Modes**," being submitted by **Robindro Lairenlakpam** (126102031), a research scholar in the *Department of Electronics & Electrical Engineering, Indian Institute of Technology Guwahati*, for the award of the degree of **Doctor of Philosophy**, has been carried out by him under our supervision and guidance. The thesis has fulfilled all requirements as per the regulations of the institute and, in our opinion, has reached the standard needed for submission. The results embodied in this thesis have not been submitted to any other University or Institute for the award of any degree or diploma.

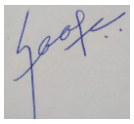

Prof. Praveen Kumar
Department of
Electronics and Electrical Engineering
Indian Institute of Technology Guwahati
Guwahati - 781039, Assam, India.
Date: 22-4-2021

Dr. Gananath D. Thakre
CSIR-Indian Institute of Petroleum
Dehradun – 248005, Uttrakhand, India.
Date: 22-4-2021

Acknowledgments

First and foremost, I would like to express my deepest appreciation to my supervisor, Prof. Praveen Kumar, for his precious support and guidance throughout my research work. His unwavering support during this work has always encouraged me. His strong knowledge in the research field, comments, and suggestions have enlightened my skills in annual progress presentations and writing this dissertation. Thank you, sir, for the time, practical inputs, and the freedom that you have given me to improve the quality of my research work, and for every moment that you added to my intellectual development. I would like to extend my deepest gratitude to my co-supervisor, Dr. Gananath D. Thakre, for his support, valuable suggestions, comments and inputs during the research work and dissertation writing. Thank you, sir.

I would also like to express my profound gratitude to my doctoral committee members, Dr. Sisir Kumar Nayak, Dr. Praveen Tripathy, Dr. Srinivasan Krishnaswamy, and Dr. Bimlesh Kumar, for their insightful assessment of my research work with wonderful suggestions and comments. My doctoral committee members are always on time and spend their precious time to evaluate my work in the annual progress seminars.

My doctoral thesis would have been impossible without the help and support of dozens of people with helping nature. My heartfelt thanks go to the former and the current Head of Department, and all faculty members of the Electronics and Electrical Engineering Department, IIT Guwahati, for their invaluable support and help during the course work. I also want to thank other faculty members and supporting staff members (especially Mr. Mukut Baruah) of the Electronics and Electrical Engineering Department, IIT Guwahati, for their kind co-operation in all academic requirements.

I would like to express my sincere gratitude to our present Director, Dr. Anjan Ray, for his relentless support and allowing me to carry out the research work at CSIR-Indian Institute of Petroleum (CSIR-IIP), Dehradun. I would like to extend my sincere thanks to our former Director, Dr.M.O. Garg, for permitting me to pursue the degree. I am also extremely grateful to my Head of Division, Mrs. Poonam Gupta of CSIR-IIP, for her pragmatic, all-time support, and untiring motivation during my bad and good times. Further, I am truly thankful to our research team, Mr. Abbal Singh Rawat, Mr. Pradeep Singh Panwar, Mr. Rajendra Badola, Mr. Yograj Singh, Mr. R.C. Semwal, Mr. R.K. Maurya, Mr. Mahesh Pal, Mr. Chander Singh, Mr.

Rajeev Sharma, Mr. Dinesh Chandra of CSIR-IIP and Mr. Iranna Gogeri (former employee of CSIR-IIP) for their immense support and help during the research works.

My special thanks go to Mr. Wittison Kamei for being a true friend of all good and bad times. He is the only witness of the whole research work and writing of this dissertation. He has been incredibly helpful during the journey of the research and completion of this dissertation. He has been my all-time company during our stay in IIT Guwahati. Thank you, Wittison. I am also indebted to my seniors, Dr.Y.K. Sharma and Mr. Amar Kumar Jain (both retired now) for their encouraging words and timely support in challenging times. I would like to acknowledge the assistance and help of Mr. Sunil K.Pathak, Mr. Ashok Kumar, Mr. Vala Vishal Magan Bhai, Mr. Om Bir Singh, Mr. Pushpraj Sharma, Mr. R.K. Joshi, Mr. Ramesh K. Kawale, Dr. Babita Bahera and the project staffs, Mr. Maibam Ardush, Mr. Vishal Maurya, Mr. Dheeraj Kanpal, during the research work. Many thanks to my researcher friends of IIT Guwahati, Dr. C. Upendra Reddy, Dr. Kashyap Kumar Prabhakar, Dr. Ankit Dalal, and Mr. Loitongbam Gyanendro Singh, for their timely help and support. I had a memorable time with Dr. Brijesh Kumar Kushwaha, Mr. Gautam Rituraj during my stay at IIT Guwahati, and thankful for their support. I must thank all those people whom I am unable to recall at this time of dissertation writing, but they helped me during my research work.

Finally, I want to thank the readers who read my thesis. I hope the readers would gain some knowledge on electric vehicle powertrain and performance evaluation in a chassis dynamometer laboratory and real-world driving conditions. I thank you one and all.
Thank you.

Date: 19-4-2021 *Robindro Lairenlakpam*

Abstract

Over the last few years, the prospect of a rapid rise in global temperature and air pollution has created concerns (about global warming, health issues) and the need to reduce the use of fossil fuels and the associated emissions. Vehicle emissions and Green-House Gases (GHGs) can have adverse impacts on health (such as cardiopulmonary diseases), environmental damage, and contribution to global warming. COP21 (also known as the Paris Agreement) has aimed to achieve a legally binding and universal agreement on climate to keep global warming below 2°C. In India, the Central Pollution Control Board (CPCB) has been operating the National Air Monitoring Program (NAMP), covering 312 cities. The NAMP is operated to improve air quality and prevent, control, or abate air pollution. Road transport is one of the major contributors to the growing air quality problems in Indian cities. There is a need for greener or alternative vehicle technologies to address the vehicle emissions issue in such situations. So, automobile companies are focused on developing alternative technologies such as hybrid electric, electric, fuel cell, and plug-in vehicles. Hence the necessity of Electric Vehicles (EVs) has been realized because of their substantial advantages over conventional Internal Combustion Engine (ICE) vehicles.

Presently, there are around 61 million in-use ICE vehicles in India, out of which passenger car contribution is 7 million. There are a few million hatchback car models of different brands of various automobile manufacturers in the country. Some of them are between 6 and 10 years old; some are between 11 and 15 years old. Many owners are still operating these old vehicles and hatchback car models. The vehicle emissions from these old ICE vehicles are a major source of air pollution in Indian cities. Therefore, the country's Supreme Court has banned BS-IV & older vehicles' sales since 1st April 2020, and operation of ICE vehicles older than 15 years old.

Meanwhile, it is essential to provide a solution for old-vehicle owners and vehicular pollution reduction. So, the Indian government has passed a legislative law, [G.S.R 167(E), 2019], which permits electric conversion of ICE vehicles into pure EVs. It paves the way for developing EV propulsion kits in the country. The Automotive Industry Standards [AIS-123 (Part-3)] lay down the procedure for Type Approval of the kits to support the legislation. The FAME (Fast Adoption and Manufacturing of EVs & HEVs) scheme also encourages the localization of the EV subsystems for import substitution. Therefore, there is a vast scope and potential for electric conversion of the old ICE vehicles (including the hatchback cars) into EVs. Electric conversion

of the ICE vehicles into EVs is a promising solution for greener transport solutions and reduces outdoor air pollution of the in-use ICE vehicles. Hatchback car models are popularly used and have a significant population in India. Presently, indigenous EV kits for passenger cars are not available in India. Therefore, it is felt to develop a prototype EV propulsion kit for the hatchback car models. In this thesis, electric conversion of two old gasoline cars into EVs is described and presented in two separate case studies. It is an experimental attempt for faster vehicle electrification and adoption of EVs. The gasoline cars are namely Maruti-800 and Maruti-Zen. Both cars belong to the entry-level hatchback segment of the M1 vehicle category.

First, the EV conversion process is described, and the conversion is carried out using local subsystems such as a local make Induction Motor (IM) and Li-ion Battery (LiB) pack. The remaining electrical subsystems are off-the-shelf components available in the market. The Computer-Aided Design (CAD) drawings for mechanical parts are prepared. The mechanical adaptors and coupling parts of the drivetrain are customized, designed, and developed in a local mechanical workshop. Secondly, evaluation tests for the converted EVs are carried out using three different driving cycles in a chassis dynamometer laboratory as per the test procedure of the prevailing Automotive Industry Standards (AIS). The laboratory study evaluates the EVs' Energy Consumption (EC) and performance using three driving cycles, and comparative analysis for the test data is performed. However, a laboratory test cannot emulate the real-world driving conditions, and it is different from a real-world test.

Finally, EV performance tests for one of the converted EVs are conducted in real-world conditions. The real-world tests are conducted on three selected traffic routes (representing low, medium, and congested traffic routes) of a Tier-II Indian city (Dehradun). The field study investigates the effect of real-world driving and drive-modes (idling, acceleration, deceleration, and cruising) on the EV's electrical parameters and performance. The distribution analysis of the drive-modes to the motor current, indirect Energy Consumption (EC_{ind}), and power consumption (PoC) are evaluated using the driving cycle analysis. The statistical, uncertainty, comparative, and sensitivity analysis are performed for the laboratory data and real-world test data. The research study is a novel attempt to convert old hatchback cars into EVs and evaluate them as per the legislation and homologation requirement. Further, the research study attempts to develop and evaluate a low-cost, prototype Electric Power-Train (EPT). Such a study can help researchers develop local EPT and conversion kits for import substitution, transport sustainability, fossil-fuel saving, and vehicular pollution reduction.

Contents

List of Figures

List of Tables

Abbreviations and Terminologies

A	Ampere
Ah	Ampere-hour
AIS	Automotive Industry Standard
Avg.	Average
BMS	Battery Management System
CAD	Computer-Aided Design
CPCB	Central Pollution Control Board
CO	Carbon Monoxide
CO_2	Carbon Dioxide
COP21	Conference of Parties (Paris Climate Agreement)
EM	Electric Motor
EV	Electric Vehicle
EPT	Electric Power Train
EC	Energy Consumption
EC_{ind}	Indirect calculated on-road Energy Consumption
EC_{tot}	Total Electrical Energy Consumption (from power meter)
FAME	Fast Adoption and Manufacturing of EVs and HEVs
FE	Fuel Economy
GPS	Global Positioning System
GVW	Gross Vehicle Weight, max.vehicle weight approved by test agencies
HC	Hydrocarbon
HEV	Hybrid Electric Vehicle
I	Current in Ampere (A)
ICE	Internal Combustion Engine
IEA	International Energy Agency
IHME	Institute for Health Metrics and Evaluation
IST	Indian Standard Time
IDC	Indian Driving Cycle
kW	kilo-Watt
kWh	kilo-Watt-hour

km/h	kilometer per hour
Kerb weight	Vehicle dry weight plus a) fuel tank filled to at least 90% of the tank capacity b) coolant and other fluids c) standard spare parts
MIDC	Modified Indian Driving Cycle
Max.	Maximum
NOx	Nitrogen Oxides
PEMS	Portable Emission Measurement System
PoC	Power Consumption from Battery
PM	Particulate Matters
R	Resistance (Ω)
SIAM	Society of Indian Automobile Manufacturers
SoC	State of Charge
THC	Total Hydrocarbon
V	Voltage
w.r.t	with respect to
WLTC	Worldwide Harmonised Light-duty Test Cycle
Wh/km	Watt-hour per kilometer

Chapter 1

Introduction

1.1 Research Background

Global warming and air pollution have brought serious impacts on production and living for the human population across the world. To address the issues of global warming and air quality, COP21 (also known as the Paris Climate Conference) has been organized, and it has targeted to achieve a legally binding and universal agreement on climate, with the aim of keeping global warming below 2°C [COP21, 2015]. Governments around the world have initiated various electric-mobility programmes [ZEV, 2016, Maya et al., 2015; NEMMP, 2012] for faster manufacturing and adoption of electric vehicles (EVs) and Hybrid Electric Vehicles (HEVs) for low-carbon footprints. In February 2020, the UK had initially planned to ban the sale of new petrol and diesel-powered cars from 2040 as part of the efforts to reduce greenhouse gas emissions. However, recently (in November 2020), the UK government has officially announced to ban new gasoline and diesel vehicles from 2030 [UK Auto, 2020]. The government expects the policy to energize the market for electric cars in the UK and help the country achieve its climate targets, including reducing greenhouse gas emissions to net-zero by 2050. India has also committed to cutting its GHG emissions intensity by 33% by 2030 [NITI Aayog, ZEVs, 2018]. On a well-to-wheel basis, GHG projected emissions from EVs would continue to be lower than for conventional Internal Combustion Engine (ICE) vehicles [IEA, 2019].

The global vehicle sales fell by 1 million units from 96.7 in 2017 to 95.7 million in 2018 (excluding two-wheeler and three-wheeler sales). The largest declines were in Asia and Europe, by 1.8% and 1.4% respectively. China, Germany, Iran, Canada, and the UK led the market down [SIAM annual report, 2018-19]. The sales figure indicates a decline in global demand for ICE vehicles. However, in 2018, the global EV share grew by 64% over 2017 to 2.1 million units, and 3 million EVs were added from 2011 to 2017. Global electric vehicle (EV) population is growing rapidly. Figure 1.1 shows the global EV demand and market projection [World Economic Forum, 2019]. In 2018, the global electric car fleet exceeded 5.1 million, up 2 million from the previous year, and almost doubled the number of new EV sales [IEA, 2019]. It is reported that China remains the world's largest EV market, followed by

Europe and the United States. Norway is the global leader in terms of EV market share. The majority of the global vehicle manufacturers have an EV model planned for launch in the Indian market. Some of them have already made their EVs commercially available [Auto-Expo, 2020].

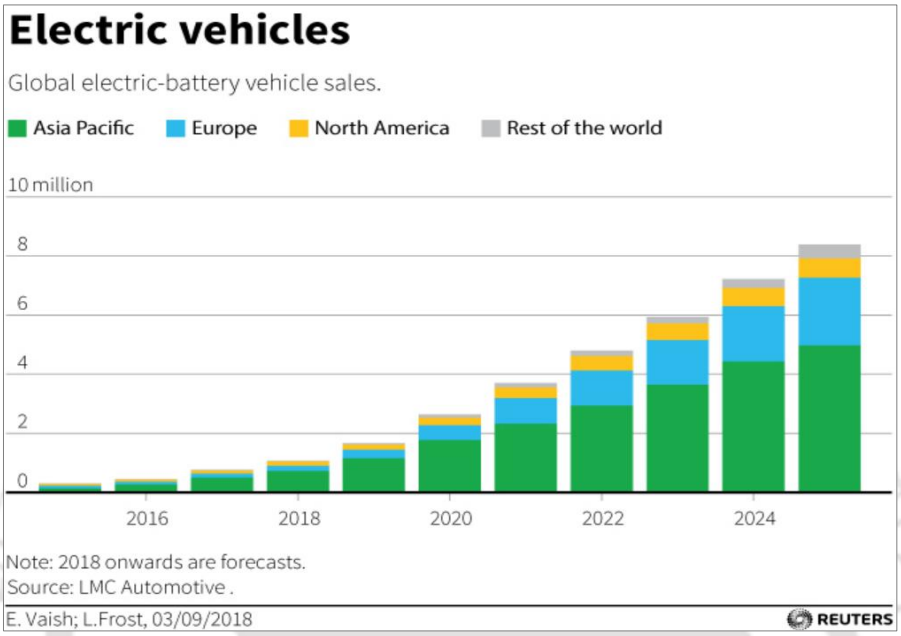

Figure 1.1: Global EV demand and market projection

Figure 1.2 shows the declining domestic sales in the car segment starting in November 2018 [Abhinav et al., 2019]. It indicates that there is a scope of domestic EVs growth and meeting the mobility demand gaps.

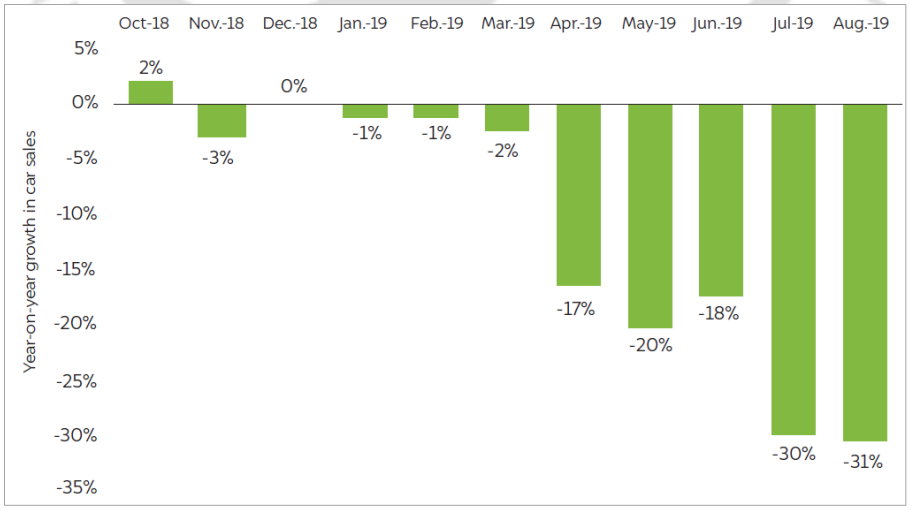

Figure 1.2: Decline in car sales since November 2018

There are also concerns about health issues and energy resource constraints due to increasing vehicle emissions and fuel consumption. Vehicle tailpipe emissions (CO, NOx, PM, HC, and others) and GHGs can have adverse impacts on health (such as premature mortality and morbidity from cardiopulmonary diseases), lower crop yields, environmental damage, and contribution to the global warming. These problems, in turn, can set back the economy. Premature mortality and morbidity can reduce productivity. Money and resources must be diverted to cleaning up the environment [Shindell et al., 2011; Nemet et al., 2010; Bollen et al., 2009]. A study has also estimated 695,000 premature deaths and a loss of 18.2 million healthy life years due to outdoor PM2.5 and ozone pollution [IHME, 2013].

In India, air pollution has also been a matter of environmental and health concerns, particularly in urban areas. Vehicle emissions are a major air pollution source in Indian cities [NITI Aayog, ZEVs, 2018]. Road transport is only one of the major contributors to the growing air quality problems in Indian cities. Among the six Indian cities (Pune, Chennai, Delhi, Mumbai, Kanpur, and Bengaluru), the share of road transport is ranged from 7% in Pune to 43% in Chennai [Guttikunda et al., 2014].

Central Pollution Control Board (CPCB) along with State Pollution Control Boards (SPCBs) has been operating National Air Monitoring Program (NAMP) covering 312 cities of the country, with an objective to improve the air quality and to prevent, control, or abate air pollution in the country [Anamika et al., 2019]. CPCB has also reported that projected Particulate Matter (PM) emission loads (tonnes/year) from vehicles have been 1624 tonnes from 1.03 million vehicles in 2018 and 1936 tonnes from 1.22 million vehicles in 2021. Similarly, Figure 1.3 shows CPCB's projection for Carbon Monoxide (CO) emission loads (tonnes/year) from vehicles [CPCB Annual Report, 2018-2019].

It is reported that estimated premature mortality due to PM pollution has increased from 438,000 in 1990 to 695,000 in 2010 in India [Guttikunda et al., 2014]. Many Indian cities are caught in a toxic web as air quality fails to meet health-based standards. Almost all cities are reeling under severe PM pollution, while newer pollutants like Nitrogen Oxides and air toxics have begun to add to the public health challenge [CSE, 2020].

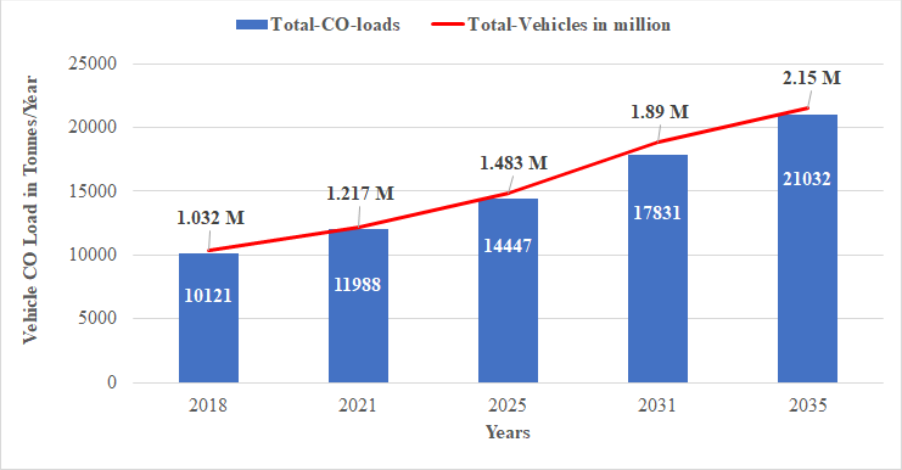

Figure 1.3: CO emission load from vehicles (tonnes per year)

Apart from vehicular pollution, fossil-fuel saving has become an important and pressing issue. Vehicle developers worldwide have been exploring and working on finding alternative technologies to address the problems of vehicular pollution and fuel savings. EVs have become a potential alternative to HEVs and ICE vehicles. In the global race of energy-saving and alternative vehicle technology, the Indian government launched the National Electric Mobility Mission Plan (NEMMP)- 2020 a few years ago with an objective to introduce 6-7 million units of EVs and HEVs, and fuel savings of 2.2-2.5 million tonnes by 2020 [NEMMP, 2012]. Under the FAME scheme, 280,000 EVs are sold, 61.10 million liters of fuel are saved, and 152.31 million kilograms of CO_2 is reduced [FAME India, 2019].

The scheme also encourages the localization of the EV subsystems for import substitution. On the other hand, in 2019, the Indian government also passed a legislative law (Gazetted notification no. G.S.R 167(E), March 1, 2019) permitting electric conversion of ICE vehicles into pure EVs. It paves the way for developing EV propulsion kits in the country. The Delhi government has recently launched Delhi Electric Vehicles Policy-2020 to establish Delhi as India's EV capital. The policy aims to increase the adoption of EVs in Delhi by incentivizing the purchase and use of EVs. [Delhi EV, 2020]. The policy seeks to drive rapid adoption of Battery Electric Vehicles (BEVs) so that they contribute to 25% of all new vehicle registrations by 2024 and bring about a material improvement in Delhi's environment by bringing down emissions from the transport sector.

These policies and legislation have significant influences on the development of electric mobility technologies. EV uptake typically starts with establishing a set of targets, followed by the adoption of vehicle and charging standards. To achieve the objectives and success of these

programmes and policies, it has become essential to develop various electric two-wheelers, three-wheelers, and passenger EVs in the next 7 to 10 years. The challenging targets of the scheme and policies have given local researchers an opportunity and 'out-of-box thinking' for developing alternative powertrain systems. A faster way to address vehicular pollution and EV deployment is developing an indigenous EV powertrain system (in the form of a kit) and converting the old ICE vehicles into EVs using the kits.

In view of the above-stated Government programmes, schemes, and policies, it is interesting and desired to conduct a research study to convert in-use ICE vehicles into EVs using local EV motors and subsystems. Therefore, the thesis's research study is carried out with an objective of electric conversion of two ICE cars into EVs and prototyping an affordable electric powertrain locally. The local motor and mechanical subsystems are selected even though imported motor subsystems are available. Further, the study investigates the energy consumption and performance of the converted EVs in a chassis dynamometer laboratory as per the guidelines and procedure of the legislation and AIS standards. It further investigates the real-world EV energy consumption and performance of the EVs in a Tier-II Indian city.

Every EV has a powertrain system consisting of subsystems like the battery pack, power converters, electric motor, motor controller, and mechanical drivetrain. An ICE vehicle also has a powertrain having an engine and mechanical drivetrain. EV's powertrain system is similar to the ICE powertrain without the engine, fuel tank, and ICE related parts. Hence, the know-how for the ICE vehicle's performance evaluation can be adopted for EV's performance evaluation with some modifications. The majority of the EVs use PM motors due to their high power and torque densities, but they are expensive. In this research study, a Three-Phase Induction Motor (3P-IM) has been used for EV applications. The detail on the Induction Motor (IM) and motor controller are described and discussed in Chapter 3.

It is learned from the literature study and above discussion that high-performance, maintenance-free, and rugged electric motors (such as IM) are preferable to reduce cost and longer life for EV applications. Therefore, the research primarily focuses on the energy consumption and performance evaluation of the EV powertrain system in a chassis dynamometer laboratory and real-world traffic conditions. The powertrain uses a local-make Three-Phase IM and LiB pack. The system integration and EV powertrain prototyping are carried out using the IM, battery pack, off-the-shelf subsystems, and mechanical subsystems.

It is essential to evaluate the powertrain performance with all subsystems working together. Therefore, the study focuses on the performance evaluation and EC analysis of the prototype electric powertrain on different driving cycles and drive-modes.

1.2 Research Motivation

At present, there are around 61 million 'on-road' (in-use) vehicles in India, out of which passenger cars contribute 7 million. Around 50.3% of the 7 million cars are less than five years old, while 29.50% are between 6-10 years old, 12.9% are between 11-15 years old. Figure 1.4 shows the domestic market share of passenger vehicles (13%) [SIAM, 2020]. It indicates the approximate passenger car population and possible candidate ICE vehicles for the electric conversion. As per the CPCB estimation, it is estimated that 60% of vehicular pollution is caused by vehicles that are older than ten years [NEMMP, 2012]. A report by the International Council of Clean Transportation (ICCT) provides an in-depth review of India's existing vehicle emissions control program—for both conventional and GHGs. The report evaluates India's vehicular emission control program through the six standards and programs, and the reductions in GHG emissions can be realized over the next 25 years [Gaurav et al., 2013].

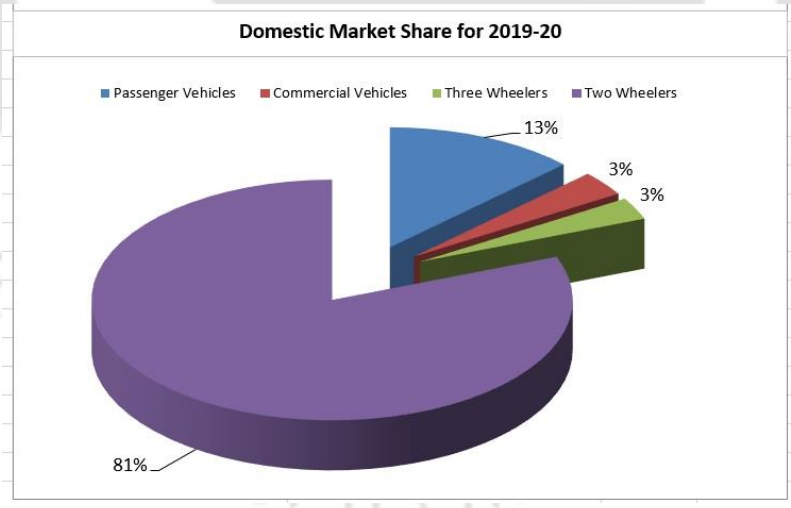

Figure 1.4: Domestic market share of vehicles in India

On the other hand, India's oil imports exceeded its domestic production for the first time in its history. In 2011, India produced about 782,000 barrels of oil per day, while it consumed nearly 3.3 million barrels per day, meaning that about 2.35 million barrels of oil used every day were imported [EIA, 2013]. A significant driver of the increase in India's oil consumption is the rapidly growing transportation sector. With rapidly growing vehicle populations and limited

oil supplies, many governments worldwide have sought to promote EVs and HEVs as suitable alternative mobility solutions. Due to low carbon footprints and zero fuel consumption, Electric Vehicles (EVs) are becoming popular and the ultimate goal for developing vehicles. At the same time, HEVs are just an interim step in the process of EVs replacing ICE vehicles [Li Z et al., 2019]. An EV generates wheel torque through an electric machine or motor that can offer more than 85% efficiency [Wu G et al., 2014], whereas an ICE can convert only 12-20% of the total fuel into useful wheel torque [Williamson et al., 2006] and have a maximum efficiency of 40% [Lukic et al., 2003].

For the passenger vehicle segment, the Global EV projection by 2020 is 5-13 million, whereas India's EV projection is 1.6-1.7 million [NEMMP, 2012]. In 2018, the EV share grew by 64% over 2017 to 2.1 million units, and 3 million EVs were added from 2011 to 2017. EVs were 69%, while PHEVs were 31%, accounting for 2.2% of total global vehicle sales [SIAM annual report, 2018-19]. Moreover, the e-mobility programme of the country's NITI Aayog also warrants minimum imports and use of indigenous technology and resources [Juyal et al., 2017].

In India, the FAME scheme and the legislation also motivate local researchers and manufacturers to carry out more EV research works and manufacture EVs with indigenous components and subsystems. The new vehicle legislation (G.S.R 167 (E)) paves many pathways for full vehicle electrification of in-use ICE vehicles into EVs using a propulsion kit. Some exemptions are also made in the import duty structure for EVs' components, such as reducing the GST rate to 5% for EVs of all categories and providing the benefit of the income tax deduction for an EV purchase. Some states have also provided the benefit of Zero Road Tax on electric vehicles [SIAM annual report, 2018-19]. All these are highly positive policy changes made in recent years to promote EVs in the country. With these favourable policies and schemes, this research study has also been motivated to carry out the electric conversion of the in-use gasoline cars into experimental EVs, using local EV motors and subsystems. The local motors and mechanical subsystems are selected even though the imported motors and subsystems are available in the market. There are around 7 million passenger cars in India, out of which a few million cars are hatchback car models of different brands of various automobile manufacturers in the country. A few thousands of them are older than ten years that can be converted into EVs for reducing vehicular pollution and fuel-saving.

There is also a wide acceptance amongst Indian consumers for LPG/CNG kits, so it is expected that the EV kits are more likely and widely to be accepted in the Indian auto market. Therefore, the thesis's research study has also focused on prototyping an EV powertrain and evaluate it as per the legislation and AIS standards. As per the Automotive Industry Standards (AIS) -123 (Part-3), the powertrain along with a programmable Vehicle Control Unit (VCU) will have to go for the Homologation requirement (Type Approval Procedure) in a later stage later. The study also focuses on creating a conversion process database, product evaluation for the EV subsystems (such as motor and battery) to align with the policies and schemes' objectives.

India has a lot to gain by converting its ICE vehicles to EVs earliest so that its oil-import bill would considerably reduce [NITI Aayog, ZEVs, 2018]. Therefore, the above-stated schemes and policies motivate researchers and manufacturers to conduct more research in developing local electric powertrains and propulsion kits for various car models in the country. The availability of several old ICE vehicles gives further incitement for the electric conversion approach.

1.3 Thesis's Objectives

In the literature study, most of the EV research studies are software simulation studies and emphasized on the techniques to develop more efficient EMs and control schemes. However, experimental studies on drivetrain topology implementation, electric powertrain's performance evaluation, and energy consumption analysis (at vehicle level) are seldom reported. There is also a lack of literature on the electric conversion of ICE vehicles into EVs. The literature review also shows a lack of research in India, especially for the detailed drive cycle analysis and performance evaluation for an EV on different laboratory and real-world driving cycles. Further, the laboratory study lacks emulation of vehicle evaluation under real-world driving conditions that are affected by traffic, weather conditions, and variations in road gradient and vehicle weights. There is also an absence of indigenous EV kits for passenger cars in India. Furthermore, the real-world implementation of a supercapacitor for EV application is seldom reported from the Indian perspective.

Based on the above-stated research gaps, the thesis's objectives are as follows:

- To conduct the electric conversion of two ICE vehicles into experimental EVs as per the AIS standards and proper selection of drivetrain topology and gear.
- Attempt to use a supercapacitor for EV application.

- To investigate the EVs' energy consumption and performance evaluation in a Chassis dynamometer laboratory using different driving cycles and drive cycle analysis.
- To investigate the real-world EV's energy consumption and performance in a Tier-II Indian city.

1.4 Contributions of the Thesis

In this thesis, actual laboratory experiments are carried out to realise the thesis objectives. The contributions are described and summarized explaining both laboratory and real-world studies. First, the electric conversion process has been described and discussed. The conversion process includes the subsystems development, selection, and system integration of the vehicle's subsystems. For a successful investigation of energy consumption and performance of the EV powertrain, the EVs are evaluated in the chassis dynamometer laboratory and real-world conditions. For the real-study, EV energy consumption and performance evaluation are carried out in a Tier-II Indian city.

1.4.1 Electric Vehicle Conversion Process

The mechanical subsystems have been designed and developed in a local mechanical fabrication shop in the conversion process. The electrical subsystems are the off-the-shelf components from the market, selected based on the specifications of the EMs and motor controller. The primary energy source is the Li-ion Battery (LiB) supplied by a local battery company. Considering the criteria of EV performance evaluation, it has also described the selection of drivetrain topology and gear selection for economic and dynamic performance. Further, the general relationship between torque and gear-ratio is discussed in the conversion process chapter. The system integration and vehicle weight distribution analysis of the EV subsystems is performed and discussed. Further, the development of a Supercapacitor (SC) bank is also described in the chapter. The study has also attempted to investigate the effect of the SC bank on the electric mileage, and same has been discussed in Chapter 4.

1.4.2 EV Energy Consumption and Performance Evaluation in Chassis Dynamometer Laboratory

For the laboratory study, three standard driving cycles are selected and used for the EV tests. The driving cycles are the Indian Driving Cycle (IDC), Modified Indian Driving Cycle (MIDC), Worldwide Harmonized Light-duty Test Cycle (WLTC). They are described in Chapter 3. The test setup for the electrified Maruti-800 (EV-I) is done on the chassis

dynamometer, as shown in Figure 1.5. The EV-I is tested using the IDC only as it has a maximum speed of 39 km/h, whereas the IDC has a maximum speed of 42 km/h. The EV-II setup is done, as illustrated in Figure 1.6. The road load simulation test for both EVs is conducted on the chassis dynamometer. The laboratory test results of EV-I and EV-II are described and discussed in Chapter 5. The statistical analysis is done for both EVs, which shows the statistical average (Avg.) and maximum (Max.) values of all the test data. The EV-II is tested using the IDC, MIDC, and WLTC. The EV's test parameters are measured and analyzed. Uncertainty analysis is done for the measured parameters of the EV-II. The detailed technical discussion on the laboratory study is described in Chapter 5.

Figure 1.5: Laboratory test set up for the EV-I (before repaint)

Figure 1.6: EV-II set up in the chassis dynamometer laboratory

1.4.3 Real-world EV Energy Consumption and Performance Evaluation in a Tier-II Indian City.

The real-world study of the EV-II is described and discussed in Chapter 6. The field study investigates the effect of real-world driving and drive-modes on the crucial EV parameters (such as total EC, battery current, input power) and vehicle performance. It also reports the real-world driving analysis to identify and understand the on-road performance and energy-

efficient routes to achieve a better driving range. Global Positioning System (GPS) mapping for the real-world EC along the vehicle GPS path is discussed in this chapter; such a GPS mapping is seldom reported in the literature from the Indian scenario standpoint. A comparative analysis for the laboratory and real-world data is discussed. Further, sensitivity analysis is performed to forecast how the target variables are affected by changes in input variables. For example, how does the kerb weight change the range of the EV-II. The performance evaluation is based on a set of crucial vehicle requirements such as vehicle speed, average speed, battery current, input power, output mechanical power, EC, and acceleration test.

Figure 1.7 shows both EVs meeting the thesis's primary objective. These two EVs have similar drivetrain and but different electric motors and controllers. The detailed technical discussion on the real-world study is described and discussed in Chapter 6.

Figure 1.7: The two converted EVs

1.5 Organization of the Thesis

The remaining thesis chapters are organized as follows:

- **Chapter 2: Literature Review.** This chapter discusses the literature study for the EV conversion process, laboratory, and real-world studies for EVs. It also discusses the research gaps found in the literature.
- **Chapter 3: Materials, Methods, and Experimental Setups.** This chapter describes the materials such as test vehicles, EV subsystems, and test instruments used for the experimental work. Then the test and analysis methods utilized for the laboratory and real-world tests have been described. Further, the experimental setups applied for the laboratory and real-world tests have been described. Furthermore, the chapter also discusses the reason for selecting the methods or subsystem and their usage for the study.

- **Chapter 4: EV conversion process.** It is the chapter that describes the EV conversion process of the two gasoline cars into EVs. The conversion is carried out using two new electric powertrains. The chapter describes the drivetrain topology and gear selection. It describes the mechanical subsystems' development process and their integration in the engine compartment of the vehicles. It also describes the electrical subsystems' selection, such as Li-ion battery and BMS, main contactors, reverse/forward contactor, pedal foot potentiometer, cable, etc. It describes and discusses the weight distribution analysis for the EV subsystems. Further, the chapter discusses an attempt to use and evaluate a supercapacitor bank for EV application.

  Chapter 5 describes and discusses the **laboratory study** conducted to investigate the EV energy consumption and performance for both EVs on different laboratory driving cycles using drive cycle analysis. The chapter is further organized into six sections; namely, i) Laboratory test description, ii) Pre-electrification vehicle performance test in the laboratory, iii) Post-electrification performance evaluation in the laboratory, iv) Experimental results and discussion for both EVs, v) Scope of further work and improvement, vi) the chapter concludes with laboratory results and the necessity for conducting a study in real-world conditions.

- **Chapter 6** describes and discusses the **real-world study** of EV-II. Some of the above-stated limitations of laboratory tests are addressed in this chapter. It describes and discusses the effect of real-world driving on vehicle parameters of the EV-II. It also describes the analysis for the test parameters with respect to the four drive-modes of the real-driving cycles. Further, it describes the sensitivity analysis done for the variables that influence the EC and driving range. The chapter is organized and discussed in five sections; namely, i) Real-world Test Description, ii) Real-world EV Performance Tests, iii) Experimental Results and Discussion, iv) Sensitivity Analysis, and v) the chapter concludes with the real-world testing perspective and potential benefits.

Chapter 2

Literature Review

The performance of an EV depends on the choice of powertrain. A modern EV powertrain system has a drivetrain (usually a 3-phase electric motor and transmission), a motor controller, dc-dc converters, and a Li-ion battery pack to provide the traction force. It is critical to select the right motor, controller, and other subsystems for an efficient powertrain for better mileage. On the other hand, the electric powertrain must meet the Automotive Industry Standards (AIS) standards for India's homologation requirement. In the country, EVs are tested for their driving performance, energy consumption, and electric range in a chassis dynamometer laboratory as per the AIS test procedure. The study has attempted to develop and evaluate a prototype powertrain (on the path of developing a kit) for the selected hatchback car models and has investigated their performance. With these broad objectives in mind, this chapter mainly emphasizes presenting the literature review in three parts. The first part of this chapter deals with the literature review on the EV conversion process, especially drivetrain topology and gear selection. The second part discusses the literature review on the laboratory study (on a chassis dynamometer) for energy consumption and performance evaluation for EVs. The third part discusses the literature review on the real-world energy consumption and performance studies for EVs.

2.1 Review on EV Conversion Process

EVs need to run at different speeds in different real-driving conditions such as city drive, highway drive, and hilly drive. EV motor is responsible for supplying a wide range of speed and torque to meet the variable-speed demand that forces the EM to run outside its efficient operating region [Ahssan et al., 2018]. The selection and design of suitable transmission GB are critical for designing an efficient drivetrain of an EV driving in Indian urban and suburban areas [Prasun et al., 2013]. Developing an efficient EV drivetrain system and integrating it with the existing ICE vehicle drivetrain can help achieve better drivetrain efficiency and vehicle performance. A motor can directly drive EV, or there might be a transmission system between motor and wheel to optimize vehicle performance [Wang et al., 2013].

An EV tends to have flexible drivetrain configurations, with or without a gears/gearbox, as the energy flows from the battery to the wheels via the flexible electrical wires and electric motor (EM). Recently, many researches have been conducted on EVs adopting different EM drivetrain configurations [Bin Wang et al., 2012; Chen et al., 2012; Yang et al., 2011]. The wheel-hub drive without a reducer (gear) is a simpler EV powertrain topology that has been widely adopted in electric bicycles and electric scooters, which have gained tremendous success in the Chinese market [Yang et al., 2011]. Although the mechanical transmission loss is eliminated in such a wheel-hub drive, the EM works mainly within the non-efficiency region of the low speed and high torque region due to the lack of reducer. A wheel-hub drive with a gear (with constant gear-ratio) is generally used to overcome this problem. The authors [Bin Wang et al., 2012] have attempted a simulation study to investigate the effect of different EV powertrain topologies on energy efficiency. Among the topologies, it has been reported that the wheel-hub drive with a gear-reducer powertrain has the highest energy efficiency. However, the control of the wheel-hub drive is more complicated due to the presence of multiple hub-motors.

Different drivetrain topologies (propulsion arrangements) can be achieved due to the flexible EV's drivetrain configurations. The choice of a drivetrain system in an EV mainly depends on the following factors: [Xue et al., 2008; Praveen Kumar, 2009-2012].

(a) propulsion mode, such as front-wheel drive, rear-wheel drive, or four-wheel drive;
(b) the number of electric motors in a vehicle;
(c) drive approach, for instance, indirect or direct drive; and
(d) the number of transmission gear levels,
(e) variations in electric propulsion and energy sources.

Therefore, there are six possible drivetrain systems reported in the literature. All six drivetrains are described in Chapter 4. Among them, the most feasible and simple topology is selected for the study, and it is also described in Chapter 4.

EV performance is generally sub-categorized into Dynamic performance and Economic performance. The study has attempted to describe and discuss both performances for the test vehicles. The criteria for EV performance are described in Chapter 4. Figure 2.1 shows a typical ICE vehicle powertrain and an EV powertrain. The figure shows the basic difference between the EV and conventional ICE vehicle powertrain.

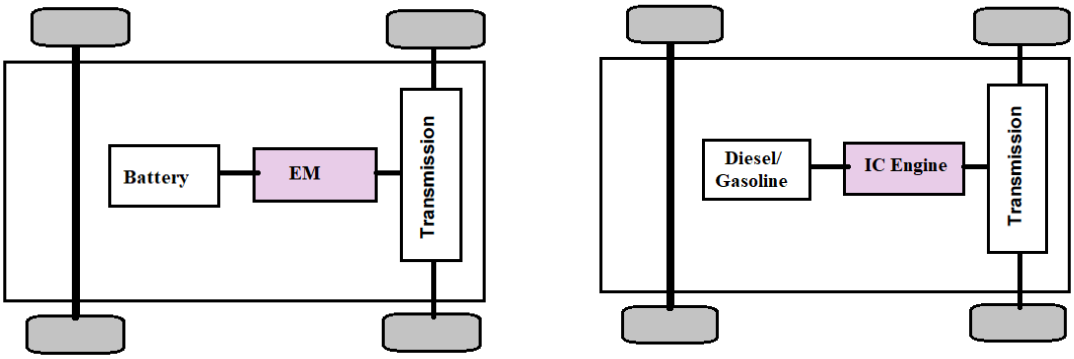

Figure 2.1: Schematic of an EV powertrain and a conventional ICE vehicle powertrain

Apart from the drivetrain selection, appropriate selection and implementation of gear and gear-ratio are also an important and challenging job for a better powertrain. The common practice to search for an optimal gear-ratio is to consider the economic performance as an objective while constraining the dynamic performance targets. For optimal gear-ratio in the transmission system, a genetic algorithm (GA) is reported in many articles [Ahssan et al., 2018; Wang H et al., 2013; Lukic et al., 2003; Yin Q et al., 2014]. In general, top gear is selected to get a maximum speed and is limited by EM or engine power, speed, and the energy economy. Lower gears are selected to get maximum speed at a maximum gradient. Lower gears are also expected to give creeping speed to avoid clutch usage and braking in city traffic [Jaideep Singh et al., 2012]. It is also reported that a suitable gear ratio is required considering the limitations of overloading and underloading operation to achieve longer mileage and safe performance of drive train [Prasun Mishra et al., 2013].

Researchers and developers are exploring the single-speed transmission system (sometimes referred to as single-gear) because it is easier to minimize the cost, volume, energy loss, or drivetrain mass. However, with a single-speed transmission system, EV powertrain performance depends on the electric motor's performance, which is not equally efficient in all speed ranges [Lukic et al., 2003]. Therefore, the right EM selection plays an essential role in this study. Researchers are also exploring various aspects of single-speed transmission in EV platforms, such as performances, gear ratio, transmission losses, cost penalties, etc. Thus, they offer potential and economical solutions for the desired EV performance. Figure 2.2 shows a typical multi-gear transmission [Multi-gear, 2020].

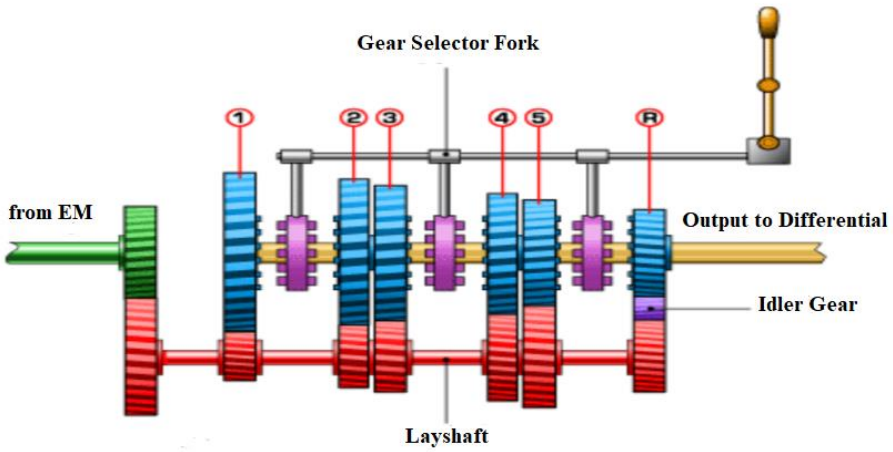

Figure 2.2 A typical multi-gear transmission

The use of a multi-gear or single-gear transmission depends mostly on the motor speed-torque characteristics. That is, at a given rated motor power, if the motor has a long constant power region, a single-gear transmission would be sufficient for a high tractive effort at low speeds. Apart from the induction motor operates very efficiently near or at the rated speed. It has low efficiency at a very high and low speed as compared to rated speed. So, a proper gearbox is designed to operate the motor in the specified efficient zone of operation. Gear shifting in a multi-gear transmission system is always associated with driving torque interruption and dynamic oscillation in output torque to the vehicle wheel [Liang Q et al., 2013].

Although many studies are based on simulation rather than an experiment, it is observed that a well-defined gear shift schedule is necessary during the gear-ratio optimization process. It increases the complexities of the drivetrain. The paper's authors [Walker et al., 2013] have reported that the gear-change causes some torque interruption in the acceleration mode in a multi-gear transmission system. They have also found that a two-speed system suffers from a lower driving range compared to that with a single-speed system. On the other hand, for large passenger vehicles, the single-speed transmission model achieves the highest driving range of 189 km, which is about 4% and 5.5% more compared to those with two-speed and three-speed transmission models, respectively [Walker et al., 2015]. When the number of gears is increased in transmission, and extra mass, transmission losses will also increase. It is reported that the multi-speed transmission system increases the losses through the clutches, gears, and driveline components [Walker et al., 2015]. Apart from the drawbacks discussed above, the additional cost is a critical issue for introducing a multi-gear system in EVs. After all, EVs do not

necessarily require many gears as they have higher torque output throughout the wider speed range of the EM [Ahssan et al., 2018]. Several authors have done many studies on electric drive systems for EVs and HEVs. Despite all these studies, the literature review shows that there is a lack of research work, especially in India, of the detailed drive-cycle analysis and performance evaluation for different power train configurations for EV applications.

Therefore, apart from the various advantages and discussions above and reported in many articles, the single-speed drivetrain (with fixed gear) is selected for this study. For the single-speed drivetrain, it is interesting to investigate whether or not it is possible to manage the efficiency of the 3P-IM so that it is operated more often in its higher efficiency region by using the gearbox (GB). It is also selected due to the simplicity discussed above. The single-speed configuration is implemented by fixing the GB at 4^{th} gear for the EV-I and 3^{rd} gear for the EV-II. Thus, the study focuses on the economical and straightforward single-speed transmission system. For a proper weight distribution of the EV subsystems in the vehicle, Indian Standard (IS) 11825: 1986 is referred to, which describes the method of weighment of automotive vehicles.

2.2 Review on Laboratory Studies for EV Energy Consumption and Performance Evaluation

The global EV market is gradually growing, with various auto-companies carrying out several EV research works and manufacturing new EV models [Global EV, 2019]. Unlike the Chinese and Indian EV market, the U.S. EV market offers many high-end and luxury brands such as Tesla, BMW, and Mercedes-Benz. The current Chinese market is dominated by small and inexpensive EVs (>80%) with the rapid growth of EVs sales in 2013–2018 [Shiqi et al., 2019]. The Indian EV market is in an initial stage, with very limited EV models commercially available. These EVs are predominantly low-speed EVs with a maximum speed of 70-80 km/h and ideal for intra-city mobility. Since the low-speed EVs are used in city traffic conditions, it is necessary to understand their performance on different city drive cycles. EVs are an alternative transport solution to the HEVs and conventional vehicles using electric motor drive systems with no fossil-fuel consumption. They are more efficient in frequent stop-go operations in city traffic [Walker et al., 2012]. The FAME scheme has aimed to support and encourage local Indian companies manufacturing EV components for import substitution. The scheme provides subsidies and incentives for those EVs that used indigenous (local) components and

parts [FAME India, 2019]. It has been strengthened by the legislation [G.S.R.167(E), 2019]. Many local researchers are motivated to conduct EV research works in view of these encouraging schemes and legislation. So, this thesis's work has been conducted to convert two pollution-causing car models, Maruti-800 and Zen, into experimental EVs by integrating local electric motors (EM). The detailed electric conversion process and performance evaluations are described in Chapters 4, 5, and 6. This study has attempted faster vehicle electrification to reduce vehicle emissions, for fuel savings, and increasing vehicle's operational life with the electric conversion.

In an EV, the Electric Motor (EM) is the only device generating traction force (torque). An electric powertrain system (EPT) of an EV is responsible for the energy conversion and transfer from the battery to the vehicle wheels. EM is a crucial part of the EPT. An EM with particular power, speed, and torque may not work properly for all the car models and segments. Therefore, the proper selection of the right EM, motor controller, and battery for the selected car model is challenging and critical for the study. The torque, power versus speed characteristics of an EM differs from that of the ICE. It is useful to discuss and understand the fundamental difference between an EV and an ICE vehicle. Study and selection of right EM and powertrain system with appropriate gear ratios are attempted by many researchers using various models, techniques, and tools like Matlab/Simulink [Prasun et al., 2013; Karen et al., 1999]. It is also observed that it is important for an EV to have the right EM and powertrain system matching with the vehicle transmission [Chang et al., 2010].

Many researchers have conducted various simulation studies to evaluate the EM performance and EC analysis of EV powertrain. One of the essential objectives of conducting drive cycle analysis is to assess the EC and performance of an EV in various drive modes and cycles. The EV performance analysis can be achieved by studying the vehicle speed profile, input power, output mechanical power, motor rpm, and torque required for the propulsion. Evaluation of the power, EC with respect to (w.r.t) the vehicle speed, can evaluate the effectiveness of energy utilization in the vehicle operation [Bor et al., 2007]. In the literature, Jorge et al. has evaluated a method for modelling the power consumption for an EV [Jorge et al., 2018]. The model is based on the identification of the parameters that relate EC from the EV with its speed, acceleration, and road slope. In another paper [Fei Lei et al., 2019], the author has studied an EV with in-wheel motors and its EC using a constrained energy approach. It is reported that

the EC is the primary concern, and vehicle ride comfort cannot be optimized simultaneously on the vehicle level.

The EV conversion process is a good alternative in terms of energy efficiency and also cost optimization [André et al., 2018]. The author has attempted to convert a vehicle into an HEV in India, and its performance study is attempted [Sudhir Gupte, 2014]. However, most of the reported works lacked information on EV performance evaluation and EC analysis using drive cycle analysis and real-world tests. In the present study, the local EM and parts are used for low-cost EPT development after considering all the selection and sizing aspects.

Therefore, the detailed discussion on the development of the new subsystems, system integration at the vehicle level, and implementing the EPT in the vehicle are described in Chapter 4. Then Chapter 5 describes the performance evaluation tests that are conducted on a chassis dynamometer laboratory. The laboratory tests use standard driving cycles. The test parameters are measured, recorded, analyzed, discussed, and presented. The test results have verified the electric powertrain (having the local EM) for EV application. The results also verify the system integration of the EPT, its implementation, and the possibility of electric conversion of similar polluting ICE vehicles into EVs. Further, the laboratory study provides useful information and data for the localization of EV subsystems.

2.3 Review on Real-world studies for EV EC and Performance Evaluation

The number of EVs is exponentially growing globally due to strong governmental incentives, which significantly lower the price of new vehicles [Efstathios, 2020]. The global EV ownership already surpassed 2 million in 2016 [IEA Global EV, 2017]. It is worth noting that nearly 900 million electric two-wheelers are in circulation in Southeast Asia Nations, China, and India [Zhenhe et al., 2019]. In September 2017, China announced that the manufacturing and selling of ICE vehicles would be stopped in the future. Similarly, some countries such as India, England, and France have also announced to ban selling conventional ICE vehicles by 2030, 2025, and 2040 [Zhenhe et al., 2019]. Under pressure from the objective environmental factors and the subjective incentives from the governments, the development of EVs will be rapid in the coming decades. It all indicates that EVs could potentially represent a significant portion of the vehicle fleet for urban mobility in the future.

In India, under the FAME scheme, 280 thousand EVs are sold, sixty million liters of fuel are saved, and more than a hundred million kilograms of CO_2 has been reduced [FAME India,

2019]. The majority of the global vehicle manufacturers have an EV model planned for launch in the Indian market. Some of them have already made their EVs commercially available [Auto-Expo, 2020]. Meanwhile, the new legislative law also allows electric conversion of ICE vehicles into EVs to support and encourage local Indian companies manufacturing EV parts for import substitution of the EV subsystems [G.S.R 167 (E), 2019].

The above information, programmes, and schemes indicate that EVs' rapid development and deployment are inevitable in India. Mass adoption of EVs seems a promising option to replace the existing ICE vehicles. However, the limited charging infrastructure and electric driving range impede the adoption of EVs. Such challenges lead to critical researches of the EV energy consumption analysis and estimation under real-world traffic conditions. Most researchers consider them fundamental to various types of EV-centered applications that aim to improve EV energy efficiency and extend the electric range [Xuewei et al., 2018].

Many researchers have carried out several simulation studies using different test methods and various simulation tools in a laboratory. In a study, the researchers use the road traffic simulator, Simulation of Urban Mobility (SUMO) to investigate a realistic, accurate, and scalable energy model to estimate the instantaneous EC for EVs. However, this SUMO model underestimates the energy consumption values in the real world [Insaf et al., 2019]. The result of a model-based study indicates that a significant accuracy improvement in the estimation of real-world EC. Specifically, the model precision increases by 25.25% in decelerating mode compared to the conventional model [Rui Zhang et al., 2015]. In another model-based study, the economical driving speeds under low, moderate, and high temperate conditions equal to 48.97 km/h, 50.89 km/h, and 51.37 km/h, respectively [Jun Bi et al., 2019]. The authors of a paper [Abousleiman et al., 2017] report a solution in the paper for energy-efficient routing problems for EVs using soft tools. The simulation results demonstrate savings in the EC of EVs when driven on the simulated routes; however, real-world test results show more than 9% EC improvements of the EV when operated on the recommended route rather than the traditional routes. The simulation presents a solution to the source-to-destination energy-efficient routing that is specific to EVs.

Further, the other paper [Rafael Basso et al., 2019] also reports the necessity of planning routes for EVs to precisely predict the energy required to drive and plan for charging whenever needed to manage their driving range limitations. The results indicate that time and energy estimations are significantly more precise than existing methods in the literature. The planned routes are

reported to be more feasible (in terms of energy demand), and that charging stops are properly included when necessary.

A model-based analysis is reported in the paper [Xinkai et al., 2015], which shows that the EV is more efficient when driving on in-city routes than driving on freeway routes. It further discusses an analytical EV power estimation model. The evaluation results show that the proposed model can successfully estimate EV's instantaneous power and trip energy consumption.

However, all these models and theoretical methods cannot accurately estimate the real-world EC_{ind}, and input power from the battery (PoC) in actual traffic roads. The models and methods also do not represent actual traffic events and generate city-specific data. In a reviewed paper, authors observe a significant gap between the laboratory and real-world data. Researchers evaluate and present a simplified EV EC model based on the Vehicle-Specific Power (VSP) on standard driving cycles [Blaž et al., 2019]. They develop the EC model based on the VSP. By coupling the model to a traffic micro simulator, the authors could determine what kind of road connection, traffic management, and traffic light control programs will yield the lowest EC. The studies discussed above also indicate that EVs require energy-efficient routes as the traditional routes are designed for fossil-fueled vehicles. Further, the studies also show the results of real-world EC study and analysis using soft tools, which predicts the possible scenarios and boundary conditions for better efficiency and driving range. However, due to the shortage of real-world data, it is challenging to build EC estimation models and get accurate verification done by the researchers doing the simulation studies.

Some researchers report actual laboratory experiments and their attempts to evaluate and establish the gap between the simulation studies and pragmatic trials. A research work says that high acceleration severely compromises the electric range and energy efficiency of the EV, regardless of vehicle speed [Zhang et al., 2018]. The research indicates that aggressive driving conditions affect EV performance in urban traffic. The trip distance, speed, temperature, and initial SoC have an impact on EC in different degrees. The change in trip distance affects EC changes. For the impact of speed, the EC will be minimized at a speed of 40km/h [Zhang et al., 2018]. Another experiment reports that the effect of speed on EC is significant in short-distance travel and concludes that the evaluation of the real-world driving EC of EVs is becoming a requirement in future vehicle regulations [Xinmei et al., 2017]. Further, another research study observes the importance of using real-world driving cycles in designing and evaluating EVs

[Hewu et al., 2015]. The simulation results and experimental measurements encourage further investigation of exploiting EVs in real-world operation.

Although several EC estimation models and experiments are reported in the literature, the investigation on the effect of the real-world driving on the EC and determination of energy-efficient routing has been limited in the Indian sub-continent. In India, the Modified Indian Driving Cycle (MIDC) is used for testing both conventional ICE vehicles and EV on a chassis dynamometer in the laboratory [Lairenlakpam, R. et al., 2019]. The driving cycle (MIDC) was developed and adopted more than 17 years ago. However, the road-use scenario, road traffic conditions in Dehradun city, and similar Tier-II Indian cities have changed significantly in the last 17 years. The chassis dynamometer tests with MIDC may not truly represent the actual on-road (real-world) driving conditions. Indian researchers need to conduct real-world studies for EV performance, total EC, and PoC for EVs in the Tier-II cities for a realistic approach and test data.

The laboratory (dynamometer) tests are standard, accurate, repetitive, and provide precise comparisons between different vehicles in a controlled test condition. However, they lack to emulate vehicle evaluation under real-world driving conditions that are affected by traffic, weather conditions, and variations in road gradient and in-vehicle weights [Ray Galvin, 2017]. The measurement of real-world speed based instantaneous EC, efficiency of EVs is also essential to determine their usability and performance in real-world conditions. The analysis of real-world EC characteristics is a necessary foundation to study the energy consumption factor for EVs. The EC factor is a correlation factor (value) to estimate and relate real-world EC to the laboratory EC data for various EV types. Researchers may find useful information and data from such a study to establish the EC factor for Dehradun and similar Tier-II cities.

Therefore, it is felt necessary to carry out this research study to evaluate the EV fitted with the prototype powertrain in real-world operation. The main objective of the real-world study is to investigate the effect of the real-world driving and drive modes on the total electrical EC, speed-based EC (indirect EC), battery current, and input power of the EV fitted with the EPT. The second objective is to use the real-world driving cycle analysis to understand and identify the usability, performance, and energy-efficient route in real-world conditions for achieving a better driving range. The knowledge of energy-efficient routes would be useful to forecast the driving range of the traffic routes and reduce the risk of running out of electricity before reaching the charging station or destination. In the study, GPS mapping is done for the real-

world EC_{ind} along the vehicle GPS path. Such GPS mapping is little found and reported in the literature from the Indian scenario standpoint. The study also investigates the test data to determine the gap between real-world and laboratory data. It could be helpful for the researchers to figure out the methods and means to overcome the driving range anxiety among drivers. The real-world studies for EVs are seldom reported in the literature from the Indian perspective.

Chapter 3

Materials, Methods and Experimental Setups

3.1 Introduction

This chapter discusses the materials such as test vehicles, EV subsystems, and test instruments used for the experimental works. Then the test and analysis methods utilized for the laboratory and real-world tests have been described. Further, the experimental setups applied for the laboratory and real-world tests have been described. Furthermore, the chapter also discusses the reason for selecting the methods, subsystems, and their usage for the study.

Test vehicles description and details of EM and controller are mentioned in Section 3.2 (Materials section). All the test instruments used for measuring test parameters of the EVs are also described in the section. Section 3.3 (Methods Section) describes the testing and measurement methods, driving cycle selection, and traffic route selection for the study. Section 3.4 (Experimental setups section) describes the experiment setup and equipment installations for the laboratory and real-world study. Each converted car is the test vehicle for the respective case-studies described and discussed in this thesis. Each powertrain of the EVs is developed by integrating a local motor, off-the-shelf motor controller, a local Li-ion battery (LiB) pack, and a mechanical drivetrain system. An electric powertrain system of an EV is responsible for the energy conversion and transfer from the battery to the vehicle wheels. Therefore, to develop an energy-efficient powertrain, the drivetrain topology and gear selection are critical for the study. Mechanical adaptors and coupling parts used for the drivetrain are customized, designed, and developed in a local workshop. The electrical and mechanical EV subsystems are essential for a complete powertrain. The selection of the EV subsystems is also described in the next Chapter. The complete conversion process is described in Chapter 4.

3.2. Materials

3.2.1 Description of the Test Vehicles

Among the passenger car models in India, both test vehicles (Maruti-800 and Zen) are two popular car models among the passenger cars in the hatchback car segment. There are a few

million hatchback car models of different brands of various automobile manufacturers in the country. Some of them are between 6 and 10 years old; some are between 11 and 15 years old. Many owners are still operating these old models and similar hatchback models such as Hyundai Santro, Suzuki Alto (first generation), Suzuki Swift, etc. During 2005-06, the total population of vehicles under the Passenger Vehicle (PV) segment is 1.14 million, out of which 882 thousand are passenger cars. In 2018-19, the total PVs sold was 3.37 million, of which 2.21 million are passenger cars [SIAM Annual Reports, 2018-19]. These vehicle numbers indicate the approximate number of 11-15 years old operational (in-use) vehicles in India. However, the exact total number of 'in-use' passenger cars is not available with the Society of Indian Automobile Manufacturers (SIAM). Meanwhile, the country's Supreme Court has banned BS-IV & older vehicles' sales since 1st April 2020, and operation of ICE vehicles older than 15 years old. Therefore, there is a vast scope and potential for electric conversion of these old ICE vehicles (of hatchback segment) into EVs.

This study's simple technical assumption is that if the EV powertrain system works for both test vehicles, the same powertrain will work for other similar hatchback cars if the powertrain is modified a little and evaluated successfully. Therefore, both test vehicles (Maruti-800 and Maruti Zen) are utilized for the research study based on availability. Maruti-800 car, popularly known as people's car, was launched in 1983 and discontinued in 2014. Maruti Zen car was launched in 1993 and discontinued from production in 2006. The powertrain specification and primary performance data of a commercial EV model (Mahindra E_2O-Plus) is considered a benchmarking reference. The EV model (E_2O-Plus) and the test EV belong to the same vehicle category (M1) and segment. Hence, E_2O-Plus's data is referred to assess how close the test EV's performance is to E_2O-Plus. The EV model's vehicle specification and data are available on the internet (on its website). The primary vehicle specifications of the test vehicles are given in Table A.1.3 in the Appendix.

3.2.2 EV Subsystems

One of the significant advantages of the electric motor (EM) is its torque characteristic, which provides maximum torque from zero up to low speeds. Then it is governed by the maximum power available as motor speed increases. EM's performance characteristic is depicted in Figure 3.1 [Ehsani et al., 2004]. The torque-speed characteristic has a significant advantage over the typical torque-speed properties of the competing ICE. It removes the need for any additional transmission – clutch or multi-gears [Ren et al., 2009]. The majority of research

studies on EV designs have exploited the torque-characteristic advantage. The motor is usually connected to the differential unit then to drive wheels via a single reduction ratio. Therefore, for EVs, high torques are always available for good acceleration, particularly from low speeds. The torque controls the vehicle's top speed on the continuous power curve, so the fixed reduction gear is typically selected to control the speed.

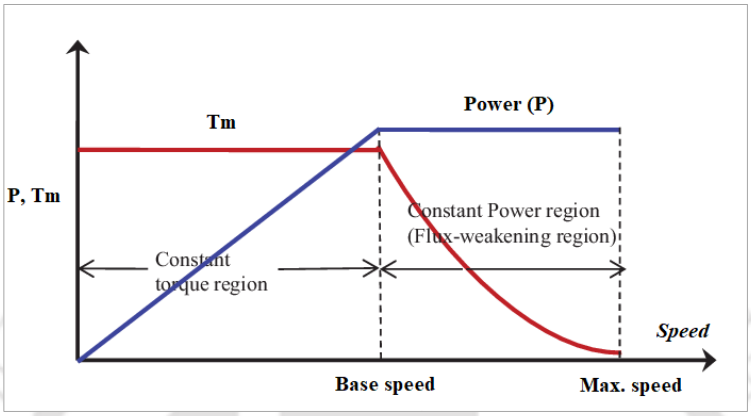

Figure 3.1: Typical performance curve of an EM drive

Researchers and system integrators are working on and exploring the use of magnet-less motors, such as Induction Motor (IM), Switched Reluctance Motor (SRM), etc., for EV applications [Boldea et al., 2014; West et al., 1994; Zeraoulia et al., 2006]. They report that Permanent Magnet (PM) motors are expensive due to the use of rare earth materials (permanent magnets). The SRM motors are attractive as they are economical but suffer from high torque ripple and electromagnetic compatibility problems due to high switching frequency and high peak currents [West et al., 1994]. A comparison for these motors is summarised in Table 3.1 [Zhi et al., 2015].

Table 3.1: Comparison of motor candidates for EV application

Parameters	**IM**	**PM**	**SRM**
Cost	Low	High	Low
Power density	Average	High	High
Reliability	High	Average	High
Torque ripple	Average	Low	High
High-speed range	High	Average	Medium
Efficiency	Average	High	Low
Control system	Moderate as it is similar to the control of a	Complex	Complex

	separately excited DC motor.		
Maintenance	Low	Low	Low
Temperature sensitivity	Low	High	---
Weight	Average	Low	High, Noisy

Therefore, one of the major candidates for EV motors is IM due to their robust construction and are less expensive than PM motors [Boldea et al., 2014; Rajashekara, 2013]. Moreover, the IMs are extensively used in industrial applications [Bose, 2002], and various speed and torque control strategies have been extensively studied [Kumar et al., 2015; Kumar et al., 2018]. The cage IMs are widely accepted and used for EVs and HEVs' electric propulsion due to their reliability, ruggedness, low maintenance, low cost, and ability to operate in harsh environments. They are particularly well suited for the rigors of industrial and traction drive environments. The thesis's research work also emphasizes the practicality and performance of the drivetrain using an IM (for the EV-II). Hence, a local-make IM is considered in this thesis.

The dynamic performance of an IM can be achieved by vector-control methods that can control the torque and flux linkage of an IM independently. Available vector-control methods are Field Oriented Control (FOC) and Direct Torque Control (DTC). Figure 3.2 shows the classification of the vector control techniques for IM control. They are better-suited control techniques for a dynamic response for EV applications [Islam et al., 1989, 1992; Kazmierkowski et al., 1995; Casadei et al., 2013]. However, the DTC suffers from high torque and flux linkage ripples [Schauder, C. et al., 1989]. Apart from information from the preceding literature, Table 3.2 describes a brief performance comparison of the IM control techniques [Mustafa et al., 2020; Vasudevan and Arumugam, 2004].

In the FOC technique, control of an IM is done by transforming the control variables from a stationary reference frame to the rotating reference frame and vice-versa [Blaschke, 1972]. The rotor-flux angle can be estimated and determined using either direct field-oriented control (DFOC) or indirect field-oriented control (IFOC).

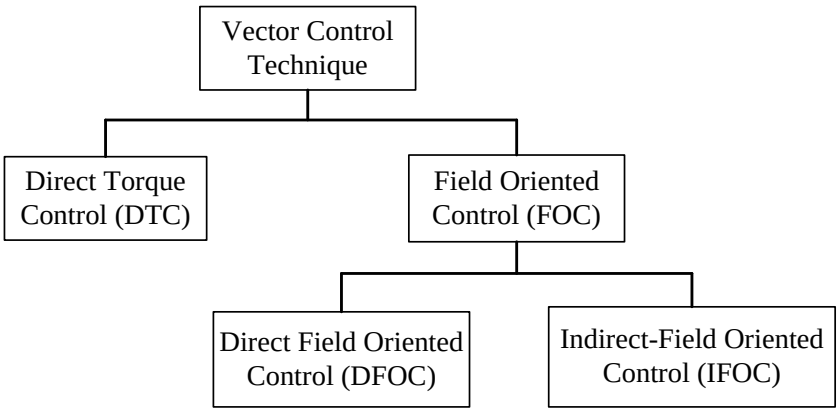

Figure 3.2: Vector Control Techniques

Table 3.2: Performance comparison between the IM control techniques

Characteristics	**DTC**	**IFOC**	**DFOC**
Dynamic torque response	Fast	Medium	Less than IFOC
Torque ripples	High	Low	Low
Current ripples	High	Low	Low
Steady-state response	Good	Very good	Very good
Low-speed operation	Poor	Very good	Very good
Cost	Low	Expensive than D-FOC due to the rotor speed sensor	Costlier than IFOC due to the presence of many sensors (such as a hall-effect sensor)
Reliability	High	High	Less reliable than IFOC due to rotor flux measurement.
Motor parameter sensitivity	Low	High	Low

Indirect Field Oriented Control (IFOC) is known to produce high performance in IM drives by decoupling rotor flux and torque, producing current-components of stator current [Kerkman et al., 1992]. In the IFOC technique, the rotor-flux angle depends on the estimation methods of rotor speed and slip speed. Therefore, IFOC generally requires accurate knowledge of the rotor-flux angle for coordinate transformation [Jacobina et al., 2000]. The 3-phase IM of the study also has an in-built encoder that provides the rotor speed and rotor position. There are also IFOC controllers available in the market. The motor controller of the IM is an off-the-shelf IFOC controller from Curtis Instruments. Therefore, the controller using the IFOC method has been selected to drive and control the IM for the study. The specifications of the electric motors

and Curtis controllers for both cases are given in the Appendix (Table A.2.3). Figure 3.3 shows the 3P-IM and controller.

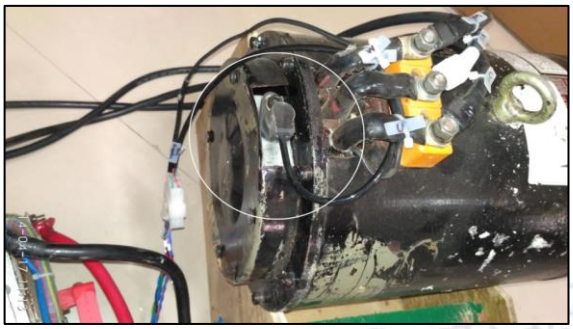

(a)

(b)

Figure 3.3: (a) Speed encoder for rotor speed & direction, (b) Curtis Controller for the IM

It is crucial to transfer the output mechanical power of the IM to the vehicle wheels efficiently. Therefore, the drivetrain subsystems like adaptor plate and axle adaptor parts must match accurately with the GB. The mechanical subsystems are customized, designed, and developed in a local workshop. The detailed development, system integration, and conversion process are described in Chapter 4.

Li-ion battery packs are used for both EVs. LiB is the primary energy source for the EVs, where chemical energy is converted to electrical energy (electrochemical energy conversion). A battery has high energy density and gets charged within a few minutes to a few hours using an appropriate charger. Researchers have used simulation models to study supercapacitors' utility (SCs) for EV applications [Shrikant Misal and Divakar, 2013]. A supercapacitor is known for its high-power density and high-current handling capability. It can get charged and discharged in a very short time. A supercapacitor bank is developed by integrating 18 cells of supercapacitors. Both energy sources can be combined to complement each other for EV applications. The practical implementation of an SC bank is attempted in this study. The SC bank is used along with the Li-ion battery for powering the EM drive system. An energy management system (EMS) can manage both battery and SC bank switching algorithm and operation-timing. However, a study on the EMS is not in this research study's scope and not reported. The specifications of the battery and Battery Management System (BMS) are given in Table A.2.5. The cell integration, development, and laboratory experiments of the SC bank are described in Chapter 4. Figures 3.4 and 3.5 show the Li-ion battery and SC bank. The

detailed design and development process, along with the complete subsystem integration, are described and discussed in Chapter 4.

Figure 3.4: Li-ion battery installation,

Figure 3.5: Integrated Supercapacitor Bank

3.2.3 Description of the Test Equipment

The sub-section describes all the test equipment used for the research study. It includes a description of the chassis dynamometer and driver's aid computer used for road load simulation tests. The subsection describes the data-logger and power-meter used for measuring battery voltage, motor current, motor rotation, and energy consumption. Further, it describes the Portable Emissions Measurement System (PEMS) used for measuring the vehicle emissions of a similar in-use car (of the same model with test vehicle). The PEMS provides the representative emissions for the test vehicle using Car chasing technique.

3.2.3.1 Chassis Dynamometer and Driver's Aid

A chassis dynamometer is a mechanical device that can simulate the road resistance forces imposed on a vehicle's wheels. The primary chassis dynamometer facility includes a roller set, power and control cabinets, a blower, a handheld remote unit (pendant), an operating PC, and safety covers and grids. They have a motor that is positioned between the pair of rollers. There are two types of chassis dynamometers, namely i) a Two-wheeled drive dynamometer having a couple of rollers, ii) a Four-wheeled drive dynamometer having two pairs of rollers. Many chassis dynamometers are two-wheel drive, thus capable of providing input to the two-wheeled drive vehicles. The problems caused by slip on rolling roads are eliminated by coupling the vehicle's drive wheels directly to the' dynamometer's hub mounts [Zhuo et al., 2018]. The test vehicle is tied and kept at a stationary state during the testing while wheels are running on load-controllable rollers. For this research work, we use an AVL chassis dynamometer of 48-inch roller diameter, 150 kW capacity with ABB drive system, and a 'Driver's Aid for the

laboratory's road simulation tests. Figure 3.6 shows the different components of the chassis dynamometer and driver's aid location.

The dynamometer testing's main advantage is that it provides a repeatable vehicle emission and EV testing condition and method. The test is relatively fast and cost-effective compared with the on-road testing. By testing the influence of changed driving behaviour on a chassis dynamometer, engineers can optimize the road design (such as crossings) and traffic management for a fluent and environmentally-friendly driving style [Van Mierlo et al., 2004]. The dynamometer testing is a standard process with a high accuracy that can benefit the comparison of performance between different vehicles. However, dynamometer testing also has some drawbacks. The most important limitation is that such testing cannot reflect real-world driving conditions. The driving situation varies each time in the real world. With the development of the cities and the improvement of living standards, it has become challenging to guarantee such a circumstance that can relieve the ever-growing traffic congestion. Another drawback is that the driving resistance exerted to vehicle wheels on the dynamometer is derived from the car coast-down test done under different conditions, which cannot precisely reflect the resistance on the real-world road [Franco et al., 2013].

Figure 3.6: Test cell description with a test vehicle mounted on the chassis dyno.

A Driver's Aid is a PC with a larger display and loaded with the software for running the driving cycles. It has data and signals acquisition hardware to configure the driving cycles and

processes (gear shifts). It receives the vehicle speed signal from the dynamometer via a speed-signal cable. The test driver sees the driving cycle on the PC display and follows the cycle's speed profile while operating the vehicle on the dynamometer. Figure 3.7 shows the driver's aid with the IDC shown on the screen.

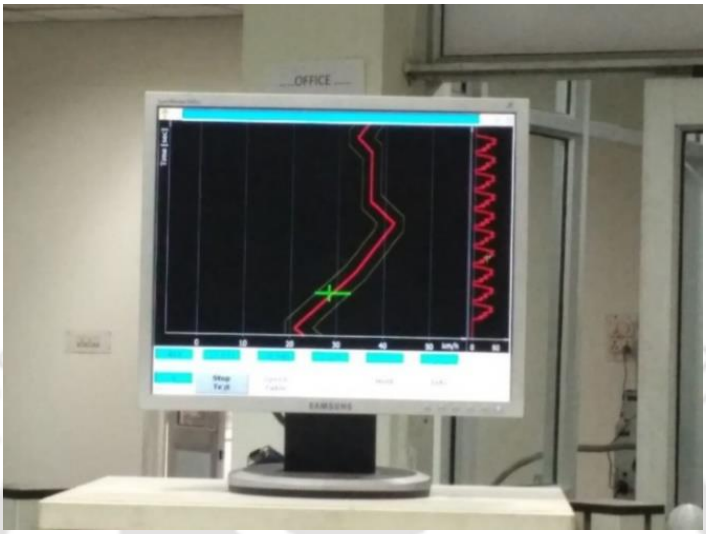

Figure 3.7: Driver's Aid with IDC

3.2.3.2 Data Logger and Power Meter

A DataTaker data logger (model DT80 from ThermoFisher Scientific) with a voltage probe and current sensor (shunt resistor) are deployed to measure the battery voltage and battery current, respectively. A photoelectric rpm sensor (of OPTEX, Japan) is used to measure motor rotation (rpm) and connected to the DT80. A power meter (Yokogawa model CW-240) is used to measure the total electrical energy consumption (kWh) required for charging the battery. Other vehicle parameters such as tractive force (F), mechanical power (kW), vehicle speed (v) are measured and recorded in the dynamometer computer. However, the mechanical torque (rotational torque) is estimated using equation (3.1). The EC (both direct and indirect measurements) is described in equation (3.4, 3.5). Figure 3.8 shows the Data-logger and power meter, and Figure 3.9 shows the schematic diagram of the wiring connection of the CW240 power meter.

Mechanical torque (Tm) = r.F (Nm) ----- (3.1)

where r = radius of the wheel in metre (m)

(a) (b)

Figure 3.8: (a) DT80 data logger setup, (b) Yokogawa CW240 Power meter

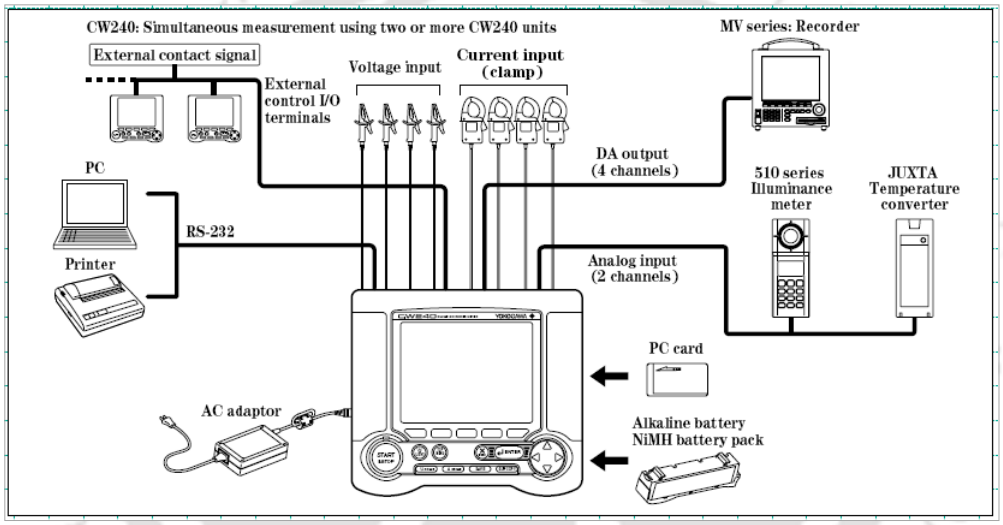

Figure 3.9: Schematic connection diagram for CW240 Power analyzer

3.2.3.3 Digital Vehicle Weighment System

Proper weight distribution plays a significant role in the design and development of motor vehicles and automotive components. It also influences vehicle dynamics, energy consumption, performance, and load capacity specifications. Indian Standard (IS)-11825 specifies the method of measuring the weight of two-wheelers, three-wheelers, cars, jeep, truck, and bus. The weight on each vehicle wheel is measured to analyze the proper weight distribution using a digital weighment system. Figure 4.30 (in Chapter 4) shows the subsystem location and distribution inside the vehicle. The subsystem's location coordinates are described in detail in Chapter 4. After removing the ICE, radiator, fuel tank, exhaust pipe, and ICE related parts, the vehicle is measured for the new G_w. The new G_w is 705 kg, along with the weight of

the EPT. Figure 3.10 shows the test vehicle mounted on the vehicle weighing system. The value of G_w is required and used to determine the coefficients obtained from the road coast-down test described in subsection 3.3.1.

Figure 3.10. Digital vehicle weighment for the test vehicle

3.2.3.4 Portable Emissions Measurement System (PEMS)

The onboard equipment used in the in-use ICE car is the PEMS (model OBS-2200 from Horiba, Japan). The PEMS is equipped with a Heated Flame Ionization Detector (HFID) for the measurement of THC, a Heated Chemiluminescence Detector (HCLD) for the measurement of NOx, and a Heated Non-dispersive Infrared Detector (HNDIR) for the measurement of CO, CO_2. It is also equipped with an inbuilt Global Positioning System (GPS) system to measure vehicle speed, distance, and location (longitude, latitude, and altitude). Figure 3.11 shows the actual PEMS setup inside the in-use car of the same vehicle model. An onboard battery supplies power to the PEMS. The PEMS uses a heated sample line along with a Pitot tube for measurement of exhaust flow. The pitot tube is connected to the vehicle tailpipe, as shown in Figure 3.12.

The equipment also provides Fuel Consumption (FC) with the help of the pitot tube. Ambient parameters such as temperature, humidity, and pressure are measured and recorded using the car roof's small weather station. The PEMS is calibrated with standard calibration gases before each test run. It provides the real-world vehicle emissions in grams per kilometer (g/km) and Fuel Economy (FE) in kilometer per liter (km/l). The PEMS is powered by an onboard battery of 24 V, 100 Ah. The basic specification of the PEMS is given in the Appendix.

Figure 3.11: PEMS inside the in-use ICE car

Figure 3.12: Pitot tube setup on the in-use ICE car

3.3 Methods

3.3.1 Coast-down Test for the vehicle

Coast-down test for a vehicle is generally conducted to determine the road-load 'F' from the vehicle deceleration by measuring the time elapsed from a speed 'v' to zero speed when the gear is in the neutral position. IS 14785: 2000 (R2016) specifies the procedure for determining the equation of road-load resistance of vehicle, including the aerodynamic and rolling resistance by the coast down technique. This data is primarily intended for the road-load simulation on the variable load curve chassis dynamometer. The road-load equation is expressed in equation (3.2).

$$F=a+bv^2, \quad \text{----------} \quad (3.2)$$

Where F is the road load in Newton (N), 'a' and 'b' are road load constants, 'v' is the vehicle speed in km/h.

However, the equation is given by the second-degree polynomial equation given in equation (2) for the road load simulation on the chassis dynamometer. The values of resistance forces are F_0, F_1, and F_2 (sometimes known as coefficients) are determined by the best curve-fitting method [IS 14785: 2000 (R2016)].

Before the conversion, a coast-down test is conducted to determine the coefficients for the test vehicle. Those values of F_0, F_1, F_2 are considered as reference coefficients for both the pre-conversion and post-conversion tests as there is a marginal difference between the vehicle kerb weights (before and after the conversion). As per the manufacturer's data, the vehicle kerb weight is 755 kg (which includes 90% of the fuel tank capacity filled with the fuel). The full

tank capacity is 35 liter (L), and fuel density is reported as 0.740 kg/L. Before the conversion, the kerb weight is taken as 735 kg because 15% of the tank capacity is filled instead of 90% during the coast-down test. Thus, the marginal weight difference is 30 kg between the vehicle kerb weights (before and after the conversion). It is assumed that the kerb weight difference of 30 kg would not make much difference in the coefficients. The ambient temperature, wind speed, and direction are considered negligible during the test. The wheel's radius and vehicle weights (before and after the retrofit) are recorded, and the equivalent moments of inertia are estimated. The vehicle's coast-down test has been carried out as per the Indian Standard, IS 14785: 2000 (R2016).

As per the polynomial equation, the resistance forces or the coefficients acting on the moving vehicle are shown in Figure 3.13.

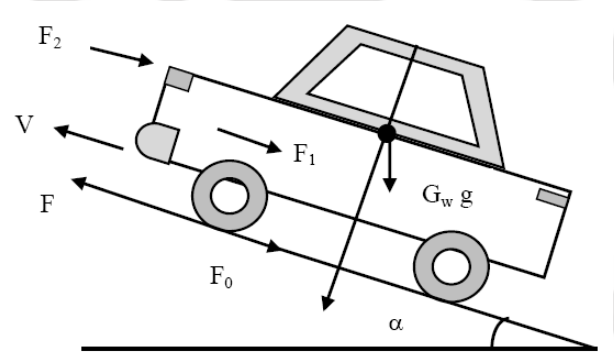

Figure 3.13. Resistance forces acting on a moving vehicle

The equation used for the road load simulation is:

$F = F_0 + F_1v + F_2v^2$ -- (3.3)

where,

F = Tractive force (N); g = gravity, 9.81 m/s^2

G_w = Vehicle reference weight (kg).

F_0 = value equivalent to rolling resistance (N);

F_1= value equivalent to losses related to chassis dynamometer

F_2= value equivalent to coefficient of aerodynamic force $(N/(km/h)^2)$

v = Vehicle speed (km/h)

α = road angle.

The term F_1v in equation (3.3) is not considered in the standard road load equation (3.2) for real-world test conditions, as the vehicle is moving and all the four wheels are rotating in the

real-world, whereas in chassis dynamometer, the vehicle is stationary and only two wheels are operated. The values of F_0, F_1, and F_2 for the EV-I and EV-II are given in Table 3.3 below.

Table 3.3: Resistance forces, F_0, F_1, and F_2 for the EV-I and EV-II

Resistance forces of EV-I	Resistance forces of EV-II
F_0= 47 N; F_1= -0.04000; F_2= 0.051900	F_0= 50.16 N F_1= - 0.7217 N/(km/h) F_2= 0.03613 N/(km/h)^2

The above coefficients are entered in the control PC of the chassis dynamometer. The road-load simulation trial test for the EV is conducted on the dynamometer to adjust the dynamometer's inertia to correspond to the vehicle weight.

3.3.2 Description and Selection of Driving Cycles

A driving cycle is representative of real-world driving conditions and patterns for a particular country or region. It may also be defined as a sequence of operating conditions (idle, acceleration, deceleration, and cruise) developed to represent a typical real-world driving condition and driving pattern of a city [Nesamani et al., 2011]. It has a series of data points representing the vehicle speed versus time. A driving cycle is formulated through statistical analysis of vehicle trip databases by carrying out extensive real-world driving experiments under varying conditions (such as different road conditions and traffic densities) to eventually represent a working day driving pattern in a region or city [Sanghpriya et al., 2009].

Driving cycles can represent the average driving pattern in a region or specific driving conditions investigated on the dynamometer. Indian auto industry follows European test methods and procedures. Hence, the Indian driving cycles are adopted from Europe. With some minor changes in the test cycle, European test procedures are followed in India for Type Approval and Certification of ICE vehicles for vehicle tailpipe emissions. Likewise, each country has its driving cycle or follows the driving cycle of a developed nation. In the research study, three different driving cycles have been selected, and they are namely, 1) Indian Driving Cycle (IDC), ii) Modified Indian Driving Cycle (MIDC), iii) Worldwide Harmonized Light-duty Test Cycle (WLTC). The IDC is the first driving cycle in India, introduced around 1985, after the extensive road tests conducted by the Automotive Research Association of India (ARAI), Pune. MIDC is a modified version of the New European Driving Cycle (NEDC) with a reduced maximum speed. The Indian auto industry adopted MIDC in 2000 [Chugh et al.,

2012]. A driving cycle's fundamental purpose is to simulate actual driving characteristics on the road for testing the vehicle tailpipe emissions and fuel consumption. However, WLTC is lately introduced in India (along with the introduction of BS-VI emission standards) with the primary objective to better match the laboratory estimation of vehicle tailpipe emissions and FC with the measurements of an on-road driving condition [Monica et al.,2015]. It aims to replace the regional NEDC and MIDC.

All three driving cycles are used for testing the experimental EV of Case-II (Electric Maruti-Zen). Two of the driving cycles are the IDC and the MIDC [TAP-115/116]. They are shown in Figure 3.14 and Figure 3.15, respectively. They are generally used for testing ICE vehicles in India. The MIDC has been adopted to test all the 4-wheeled passenger vehicles and LCVs with Gross Vehicle Weight (GVW) ≤ 3500 kg. However, the IDC has a maximum speed of 42km/h, and it is usually used for testing 2-wheeled, 3-wheeled, and smaller 4-wheeled vehicles. Therefore, due to the speed limit, the EV of Case-I (Electric Maruti-800) uses only IDC for the performance evaluation. The third driving cycle used is the WLTC, as shown in Figure 3.16. It is a new test cycle used globally to test all 4-wheeled light-duty ICE vehicles as per the latest emission test procedure [Monica et al.,2015; Norbert et al., 2015].

3.3.2.1 Indian Driving Cycle (IDC)

India first began to lower permissible vehicle emission limits following the Supreme Court's rulings in the late 1980s and 1990s [Gaurav et al., 2013]. The country started to move toward mitigating the public health impacts of vehicle exhaust emissions. The initial steps consisted of eliminating lead in gasoline fuel, switching to compressed natural gas (CNG) for autorickshaws and buses in Delhi and subsequently other cities, and establishing Euro I–equivalent emission standards known as India-1 standards for new vehicles. Thus, the Indian Driving Cycle (IDC) was first developed by the Automotive Research Association of India (ARAI) in 1985 under the Central Motor Vehicles Rules (CMVR) [Sumit et al., 2013]. The cycle is based on the actual on-road measurements conducted by ARAI, Pune. In India, IDC is still followed for emissions testing for 2, 3-wheelers. IDC is a short cycle (comprising of six sub-cycles) of 108 seconds each, as illustrated in Figure 3.14. It does not cover all the different driving conditions observed on the actual road. The average speed of IDC is 21.9 km/h and a distance of 3.94 km.

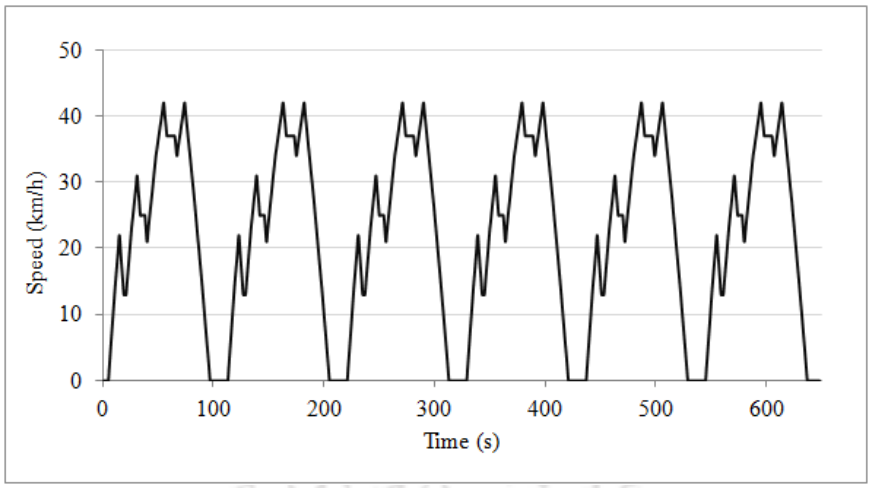

Figure 3.14. The Indian Driving Cycle (IDC).

Many researchers have raised questions on the suitability of IDC and MIDC as the standard cycles for vehicle testing in India. The IDC is reported unsuitable for evaluating fuel consumption due to its gentle acceleration, braking, and long periods spent in stationary mode [Van Mierlo et al., 2004]. Similarly, it is reported that the MIDC does not give a realistic assessment of vehicular emissions in actual on-road conditions [Franco et al., 2013]. The above researchers attribute the variations in emissions and FC data to differences in traffic density, land-use patterns, road infrastructure, and traffic management.

Based on the various studies reported in the literature, the significant limitations of the IDC can be summarized as follows [Sumit et al., 2013]:

1) the higher speeds (>42 km/h) and accelerations (>0.65 m/s^2) are not taken into account, which means the vehicles running at higher speeds or highly transient conditions can have higher tailpipe emissions. Yet, they could still pass the emission tests done using IDC.
2) It assumes all traffic to be homogenous, and it does not consider the varying conditions of the real-world traffic. In reality, traffic movement in a region or a city is highly dependent on street design, quality of roads, traffic lights, congestion levels, and driver behavior.
3) It assumes low accelerations observed in real-world driving conditions in hilly terrains and highways.

3.3.2.2 Modified Indian Driving Cycle (MIDC)

The MIDC is the same as Europe's NEDC, which comprises four Urban Driving Cycles and an Extra-Urban driving cycle (highway). However, the maximum speed of the MIDC cycle is reduced to 90 km/h considering Indian road and driving conditions. Unlike the IDC, the MIDC has two parts of the cycle, viz. the Phase-I cycle representing urban driving conditions, and the Phase-II cycle representing highway driving conditions. The Phase-II of the MIDC represents highway driving with a speed limit of 90 km/h, as shown in Figure 3.15.

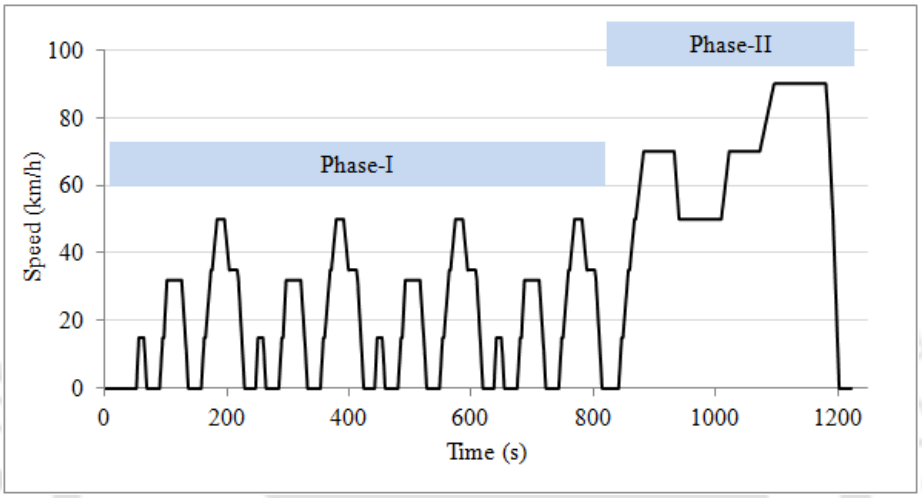

Figure 3.15. The Modified Indian Driving Cycle (MIDC).

3.3.2.3 Worldwide Harmonized Light-duty Test Cycle (WLTC)

The Worldwide Harmonized Light-duty Test Procedure (WLTP) aims to harmonize test procedures on an international level and set up an equal playing field in the global market. The WLTP is being developed by experts from the European Union, Japan, and India under the United Nations Economic Commission's guidelines for Europe (UNECE). The new WLTP procedure relies on the new driving cycles (WLTC) to measure the mean fuel consumption, CO_2 emissions as well as the emissions of pollutants by passenger cars and light commercial vehicles. There are three WLTP Test Cycles for light-duty vehicles viz. Class-1, Class-2, Class-3. For the research work, we use the WLTC (Class-2), as shown in Figure 3.16. It has three phases: Low, Medium, and High, representing driving conditions in city, highway, and expressway. The medium and high phase of the WLTC cycle has a maximum speed of 74.5 km/h and 85.2 km/h. And the test vehicle could only reach a maximum speed of 64 km/h.

Therefore, the IDC, Phase-I of the MIDC (MIDC-I), and Low-phase of the WLTC (WLTC-low) are used to test the EV-II as they represent urban driving conditions. There is no

alternative driving cycle available for EVs; moreover, the EV-II is retrofitted for utilization in the city areas.

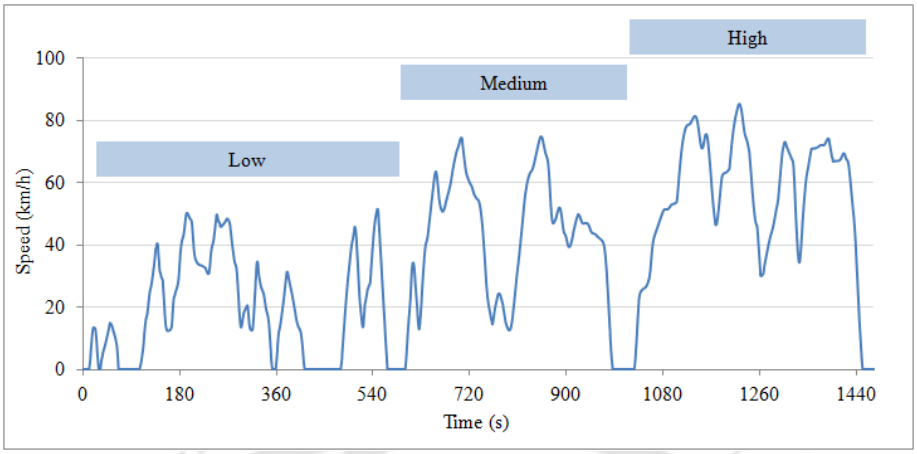

Figure 3.16. The Worldwide Harmonized Light-duty vehicles Test Cycle (WLTC, Class-2).

3.3.3 Drive Cycle Analysis

Vehicle driving is a combination of four drive modes, namely (i) deceleration, (ii) acceleration, (iii) cruising, and (iv) idling. Every driving cycle has these four modes. The test data comprising vehicle speed, battery current, input power, output mechanical power, and indirect EC are evaluated and distributed into these four modal categories. A simple computer program is developed in Microsoft Excel software, which segregates the corresponding test data to the drive modes. The simple program includes the sub-programs for each drive mode. The program flowchart is described in the Appendix (Figure A.6.1). The program checks the trend of acceleration by using the acceleration limit. The definition of idling, acceleration, deceleration, and cruising modes are given below [TAP-115/116, Issue No. 4, 2012].

The drive-mode definitions and limitations are as follows.

- Idle - speed equals zero km/h.
- Acceleration - Speed greater than 0.139 m/s^2
- Deceleration - Same as acceleration except that acceleration should be negative.
- Cruising - Speed greater than 5km/h and acceleration greater than 0.139m/s^2.

3.3.4 Energy Consumption Measurement Method

The study follows the method and procedure given in the automotive standard, AIS-039 (Rev.1), for measuring the electrical EC. The standard specifies the method for measuring electrical EC expressed in Wh/km for L, M & N categories of Electric Powertrain Vehicles as defined in Rule 2 (u) of Central Motor Vehicle Rules (CMVR). It specifies the detailed procedure for vehicle preparation, charging, discharging of the rechargeable energy storage systems, end of charge criteria, etc. It also defines the test condition specifying that all the tests are conducted at a temperature between 20 °C and 30 °C. The detail of AIS-039 (Rev.1) is given in the Appendix.

Electric energy consumption calculation is specified as follows:

$$C = \frac{E}{D} \text{ (Wh/km)} \quad \text{---} \quad (3.4)$$

Where C is the total electrical energy consumption per kilometer (EC_{tot}) expressed in Wh/km; E is the total electrical input energy in Watt-hour (Wh) reading of the power meter, and D is the distance covered (range) in kilometer (km).

$$EC_{ind} = \frac{PoC}{S} \text{ (Wh/km)} \quad \text{---} \quad (3.5)$$

Where EC_{ind} is the speed-based Indirect EC (Wh/km), sometimes mentioned as real-world EC in this report; PoC is the P_{dc} (W), and S is the vehicle speed (km/h).

3.3.5 Traffic Routes Selection

The traffic route selection in Dehradun is mainly made based on traffic density and average vehicle speed. The route selection includes different traffic roads (i.e., city driving, suburban, and highway driving) for various vehicle speeds and road gradients that can be encountered in a real-world driving situation. For Dehradun city, the maximum vehicle speed limit for cars is 70 km/h [S.O.1522 (E), 2018], whereas the actual average speed varies 40-50 km/h, depending on the city-route choice. The average and maximum speeds for the MIDC are 32 km/h, 90 km/h, respectively, whereas the on-road vehicle speeds have average speeds ranging from 12–30 km/h. A similar real-world study was conducted for an ICE vehicle that evaluated road quality and traffic management's impact on real-world vehicle emissions and Fuel Economy (FE) [Jain, A.,2011]. In another similar study, the authors utilized a GPS in a test vehicle. The vehicle was operated on various traffic routes in Dehradun for several trips for generating road

data [Pathak et al., 2016]. The road trip-data includes maximum speed, average speed, percent time spent in idling, acceleration, deceleration mode, average acceleration, average deceleration, and braking. The authors have considered these vehicle parameters for the route selection, taking reference from the laboratory cycle parameters.

Based on these studies reported in the literature [Jain et al., 2011; Pathak et al., 2016], the three traffic routes are selected, representing congested, medium, and low traffic conditions for the study. The selected routes are based on the criteria established for the on-road emissions tests for conventional ICE vehicles with the PEMS. A combination of such traffic routes truly represents the actual distribution of roads in Dehradun.

3.3.5.1 Description of the Real-world driving cycles (RDC)

The test-driver drives the test vehicle on the three traffic routes representing low, medium, and congested traffic routes. The vehicle is operated in city driving conditions fitted with the GPS to acquire the vehicle operating conditions during peak hours and off-hours (morning and evening). The portion of the National Highway (NH-72), which passes through the city's suburban area, has been considered as the low traffic route. The medium traffic passes through a place mixed with residential and commercial localities, whereas the congested route passes through the main city areas via the road to Dehradun railways station. The above-described route characteristics make the real-world driving cycles unique from the laboratory cycles. As discussed in the literature study, real-world driving cycles show a significant departure from the standard cycles in terms of the cycle parameters. The reported studies [Pathak et al., 2016; Berry et al., 2010] also bring out the significant difference between the laboratory (certification) cycle and the real-world driving cycle in key driving parameters. Real-world driving demonstrates a considerable variation from standard cycles in terms of acceleration, maximum and average speed, pointing to a large gap between real-world driving and standard cycles.

During real-world driving, one experiences frequent acceleration, deceleration, and braking. These drive modes and action keep the vehicle speed in a narrow range; such a condition makes higher power demand and more energy consumption than standard cycles. Real-world driving happens at much lower speeds because of India's traffic conditions but has much higher acceleration rates. This study is an advancement over the previous EV studies in India. It

comprehensively assesses the real-world driving pattern and EV energy consumption for the Tier-II Indian city and compares them with the standard driving cycle (MIDC).

3.3.8 Car Chasing Method

Several methods are being used to estimate travel data. The travel data may be observed in two different ways, the "stationary observer" method and the "moving observer" method [Lum et al., 1998]. The "stationary observer" method does not require a test vehicle as it uses techniques such as license plate matching, computer-based image processing, and matching techniques [Robertson et al., 1994]. The "moving observer" method needs a test vehicle as it adopts techniques such as the 'moving observer method' and 'car chasing method'. A new methodology for the car-chasing method using a Global Positioning System (GPS) and Geographic Information System (GIS) technologies has also been done [Quiroga and Bullock, 1998].

The moving observer method and car chasing method are discussed here. The moving observer method requires three persons (including the driver) in the test car. The car-chasing method only requires a test car with a driver and an observer to observe travel data for the study location. For the car chasing method, the test car is driven at another driver-desired speed. To get representative journey data, the test driver has to drive at the speed of a randomly chosen car in front. The test driver has to keep a distance from the following car within 6 seconds. The test car has to follow the other car by keeping a safe distance until it leaves the area, parks, or the 'chase' becomes unsafe and illegal maneuvers. The test driver has to drive the test car generally with respect to the present traffic condition.

As reported in the paper [Ahmad et al., 2005], it seems that the best fit (R^2) of the speed-density relationship for the Car Chasing Method is higher than the Moving Observer Method. In any statistical analysis, the best fit with higher R^2 values is always better and preferable. Due to the reason stated above and other reasons in Table 3.4, the car chasing method has been adopted for this research study.

Table 3.4: Summary of the Car Chasing methods

Car Chasing Method	Moving Observer Method
It only can obtain travel speed data.	It obtains the travel speed and traffic volume (hourly) data simultaneously.
It is applicable for either one-way or two-way routes.	It is applicable only for two-way routes where opposing traffic is visible at all times. It must be able to turn around at each end of the test sections.
It needs only two persons (including the driver).	It requires at least three persons in the test car (including the driver).
It follows the speed of the other driver (follow the speed of the chosen car).	Only the test-car driver speed (means it obeys the speed limit).
One direction is enough to get one set of data.	Travel in both directions (go & back) is required for one set of data.

3.4 Experimental Setups

3.4.1 Description of the Laboratory Experimental Setup

The chassis dynamometer laboratory consists of many hardware and software, described in the respective subsection and pre-electrification setup. The essential instruments used for EV testing are the chassis dynamometer, driver's aid, data logger, power meter. The test vehicles are set up on the dynamometer, as shown in Figure 3.17 and 3.18.

Figure 3.17. Road load simulation test of the EV-I (before repaint) on the chassis dynamometer

Figure 3.18. Setup of test vehicle EV-II on the Chassis Dynamometer

3.4.2 Description of the Real-world Test Setup

The test equipment used for testing the EV-II is the GPS data-logger (DataTaker DT80). The data-logger uses a voltage probe and current sensor (shunt resistor) to measure the battery voltage and load current motor drive system. It also uses a photoelectric rpm sensor (of OPTEX, Japan) to measures motor rotation (rpm). Figure 3.19 shows the data logger setup inside the test vehicle.

Figure 3.19. The actual setup of the GPS data logger inside the test car

The power meter (Yokogawa CW240) measures and records the total EC from the AC mains during charging. The basic description and specification of the testing equipment used for real-world testing are given in the Appendix. The PEMS (model OBS-2200 from Horiba, Japan) is the onboard equipment used in the chased in-use car. It measures real-world vehicle emissions and FE of the in-use car. It uses a Heated Flame Ionization Detector (HFID) for the measurement of Total Hydrocarbons (THC), Heated Chemiluminescence Detector (HCLD) for the measurement of Nitrogen Oxides (NOx), and Heated Non-Dispersive Infrared sensor

(HNDIR) for the measurement of Carbon Monoxide (CO), and Carbon Dioxide (CO_2). The PEMS provides the on-road vehicle emissions in grams per kilometer (g/km) and FE in kilometer per liter (km/l). It uses a pitot tube for the measurement of exhaust flow and provides FC using the carbon-balance method. It also has an in-built GPS to measure vehicle speed, distance, and location coordinates (longitude, latitude, and altitude). Figure 3.20 shows the PEMS's setup and real-world test for the in-use car and EV-II. The detail and specifications of the test equipment are mentioned in Table A.3.1 (Appendix).

(a) (b)

Figure 3.20. (a) PEMS setup inside the in-use car, (b) Real-world test for the same model's in-use car.

A preliminary real-world test has been conducted as a trial and hands-on experience using the EV-I, as illustrated in Figure 3.21. After a few real-driving trial tests, the EV-I is improved and repainted, as shown in Figure 3.22. From the trial tests, it has been attempted to understand and find out the gap between the dynamometer test and real-world test in terms of Energy Consumption (EC), power consumption, and other electrical parameters. The field trial indicates the limitations of the EV-I.

Figure 3.21: Real-driving trial for the EV-I

Figure 3.22: Improvised and repainted EV-I

Dehradun being the capital city of Uttrakhand State, represents one of the fast-developing metropolitan cities in India and is listed in the Tier-II smart cities. Therefore, it is necessary to carry out the real-world study in Dehradun (a Tier-II Indian city). Figure 3.23 illustrates the real- driving in traffic conditions.

Figure 3.23. Real-world driving and testing of the EV-II

Chapter 4

Electric Vehicle Conversion Process

4.1 Introduction

The research purpose, background, and literature review of this thesis are discussed and explained in Chapter 1 and 2. The materials and methods used for electric powertrain are described in Chapter 3. The legislation standards referred to in this study are also mentioned partly in Chapter 3.

Electric conversion of the conventional ICE vehicles into EVs is a promising solution for improving transport sustainability and reducing outdoor air pollution of current ICE vehicles running on the road. The legislative law [GSR 167 (E) March 1, 2019] allows the conversion of ICE vehicles into pure EVs. This legislation shows pathways for developing EV conversion kits in the country. The Automotive Industry Standards lay down the Type Approval procedure of the kits [AIS -123 (Part-3)]. The thesis's research study follows the guidelines and test procedure of the legislation and standard. An EV's powertrain system is responsible for energy conversion and delivering power to the vehicle wheels efficiently. The powertrain characteristics of a traction motor differ from those of an IC engine. It is required to match the traction motor with the vehicle transmission to make an EV with the same performance as that of a traditional ICE vehicle [Chang et al., 2010]. Therefore, mechanical subsystems are crucial for the vehicle transmission to couple the EM with the ICE vehicle GB.

In this chapter, the EV conversion process of the two gasoline cars into EVs is described. The conversion is carried out using two new electric powertrain systems. The chapter describes the drivetrain topology and gear selection. It describes the mechanical subsystems' development process and their integration in the engine compartment of the vehicles. It also describes the electrical subsystems' selection, such as Li-ion battery and BMS, main contactors, reverse/forward contactor, pedal foot potentiometer, cable, etc. The system integration and weight distribution analysis of the subsystems are also described and discussed in it. Further,

the chapter discusses an attempt to use and evaluate a supercapacitor bank for EV application. The specifications of the Electric Power-Train (EPT) for both EVs are given in the Appendix.

4.2 Selection of Drive Train Topology

Many researchers have started working on exploring better technologies for an electric motor, battery, and BMS. However, the transmission system (drivetrain) has soon appeared as another crucial powertrain subsystem that might enhance EVs' performances. The performance of EV depends on an energy management strategy of an EV powertrain. A modern EV powertrain system has a drivetrain (a 3-phase electric motor and transmission), a motor controller, dc-dc converters, and a Li-ion battery pack to provide the traction torque. Several authors have done many studies on electric drive systems for EVs and HEVs. Despite all these studies, the literature review shows that there is a lack of research work, especially in India, of the detailed drive-cycle analysis and performance evaluation for different power train configurations for EV applications. EV performance is generally sub-categorized into Dynamic performance and Economic performance. The battery capacity (Ah) influences economic performance, and the drivetrain influences dynamic performance. Therefore, the appropriate selection and implementation of battery-pack and drivetrain is the most critical and challenging job of the study. Figure 4.1 shows the criteria for EV performance evaluation. In this study, a simple drivetrain topology is opted and implemented for various reasons described in the next sub-section. The study has attempted to described, analyzed, and discussed both performances.

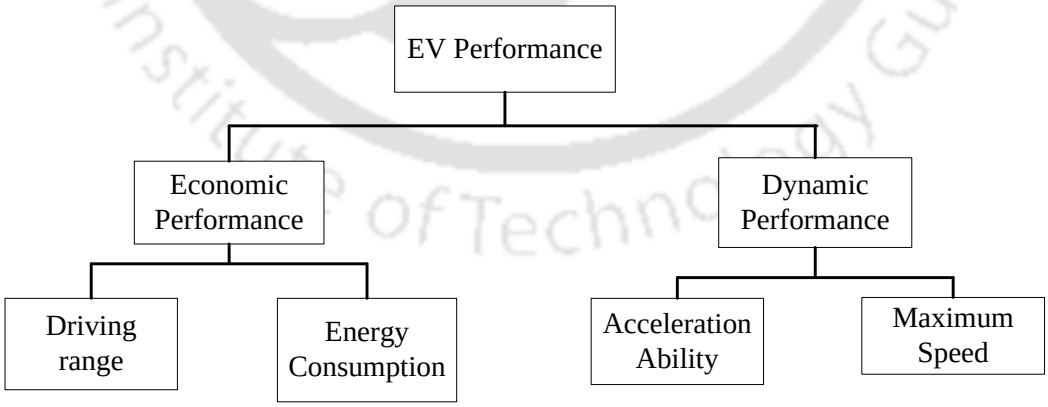

Figure 4.1: Criteria of EV Performance Evaluation

An EV tends to have flexible drivetrain configurations, with or without any gears/gearbox, as the energy flows from the battery to the wheels via the flexible electrical wires and Electric

Motor (EM). Therefore, different propulsion arrangements (drivetrain topology) can be achieved. The choice of drivetrain system in an EV mainly depends on (a) propulsion mode, such as front-wheel drive, rear-wheel drive, or four-wheel drive; (b) the number of electric motors in a vehicle; (c) drive approach, for instance, indirect or direct drive; and (d) the number of transmission gear levels, (e) variations in electric propulsion and energy sources [Xue et al., 2008; Praveen Kumar, 2009-2012]. Therefore, there are six possible drivetrain systems for EVs, and they are shown in Figure 4.2 (a-f).

i) Figure 4.2a shows a single EM configuration with a gearbox (GB) and a clutch. It is the conventional type of the drivetrain system used in an ICE vehicle, where an EM replaces the conventional ICE for a similar EV configuration. Such configuration does not change the ICE vehicle's drivetrain system; hence it can be easily implemented. The clutch enables the connection or disconnection of power flow from the EM to the wheels. The wheels have high torque, low speed in the lower gears, and high speed, low torque in the higher gears. The gear is fixed at 4^{th} gear (top gear) for the EV-I and 3^{rd} gear for the EV-II. It is reported that the amount of energy losses through clutch friction is significant [Ahssan et al., 2018]. Hence the clutch is removed and not used. Newly developed adaptors are used in place of the clutch in this research work. Due to mechanical simplicity, a single-speed drivetrain is used and implemented for this research study.

ii) Figure 4.2b shows a single EM configuration without a gearbox and clutch. The advantage of such a design is that the weight of the transmission is reduced. However, such configuration demands a more complex control of the EM to provide the wheels' necessary torque. Some existing EVs, such as Nissan Leaf and Tesla Model-S, have adopted this topology [Bin Wang et al., 2014].

iii) Figure 4.2c depicts the transmission-less type of drivetrain system. The transmission-less type of drivetrain system for EVs simplifies the conventional type, as the transmission is removed.

iv) The transmission-less type can be simplified to the differential-less type if the differential gear is removed, as illustrated in Figure 4.2d. Such topology is known as Cascaded-motors drivetrain, in which two motors are installed to give a function equal to the differential. It has a common axle for the motors to transmit power to the wheels. Such topology is also regarded as the direct-drive configuration.

v) In Figure 4.2e, another simplified version of the transmission-less type is illustrated. Two motors are used, and each fixed to the individual wheel with reduction gears to drive the

wheels. For such configuration, each motor operates independently, and there is no common axle for the motors, which makes the control system more complex.

vi) Figure 4.2f, the motors are integrated into the rear wheels themselves so that rotation can be caused directly without gear. Such motors are also known as hub-motors as the wheel-rim itself is the motor. Such direct-drive configuration is sometimes known as an in-wheel drivetrain system. A study shows that EVs using the powertrain of the wheel-hub drive with the gear reducer have lower energy consumption [Bin Wang et al., 2014].

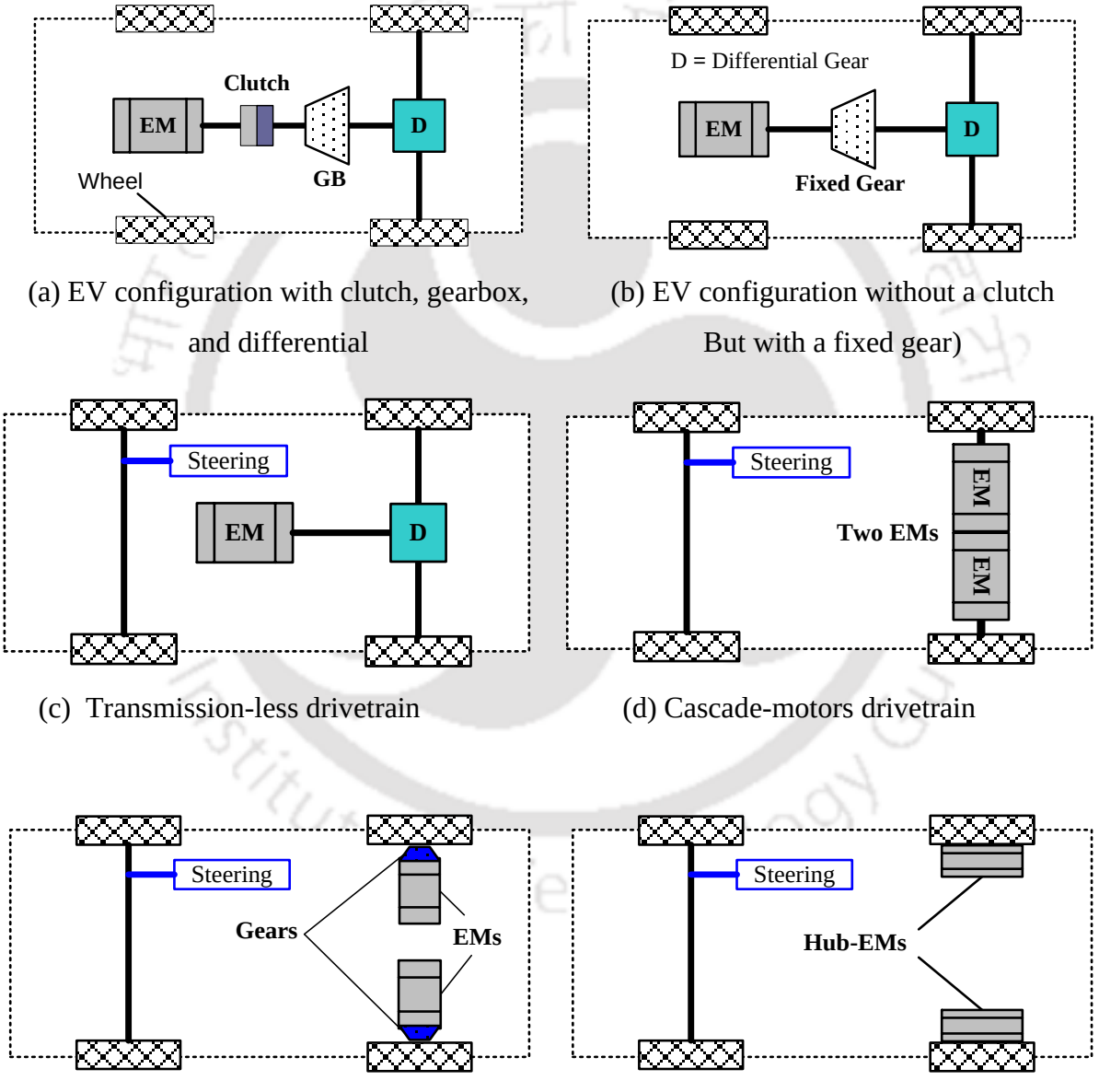

(a) EV configuration with clutch, gearbox, and differential

(b) EV configuration without a clutch But with a fixed gear)

(c) Transmission-less drivetrain

(d) Cascade-motors drivetrain

(e) In-wheel with reduction gears

(f) In-wheel direct-drive system

Figure 4.2: Different Drivetrain Topology

4.3 Gear Selection for Single-speed Transmission

In an EV powertrain, the only torque-generating subsystem is the EM, which is not equally efficient throughout a wider speed range. On the other hand, EVs need to run at different speeds in different real-driving conditions such as city drive, highway drive, and hilly drive. The electric motor is responsible for supplying a wide range of speed and torque to meet the variable-speed demand that forces the EM to run outside its efficient operating region [Ahssan et al., 2018]. So, an EM with a suitable gear system can produce and meet the torque requirement of an EV. The selection and design of suitable transmission GB are critical for designing an efficient drivetrain of an EV driving in Indian urban and suburban areas [Prasun et al., 2013]. Developing an efficient EV drivetrain system and integrating it with the existing ICE vehicle drivetrain could help achieve better drivetrain efficiency and vehicle performance. A motor can directly drive EV, or there might be a transmission system between motor and wheel to optimize vehicle performance [Wang et al., 2013].

Vehicle developers adopt the single-speed transmission system (sometimes referred to as single-gear) because it is easier to minimize the cost, volume, energy loss, or drivetrain mass. However, with a single-speed transmission system, EV powertrain performance depends on the electric motor's performance, which is not equally efficient in all speed ranges [Lukic et al., 2003]. Therefore, the right EM and gear selection play a vital role in this study. Researchers are also exploring various aspects of single-speed transmission in EV platforms, such as performances, gear ratio, transmission losses, cost penalties, etc. Thus, they offer potential and economical solutions for the desired EV performance.

The authors of the paper [Walker et al., 2013] have reported that the gear-change causes some torque interruption in the acceleration mode in a multi-gear transmission system. They have also found that a two-speed system suffers from a lower driving range compared to that with a single-speed system. On the other hand, for large passenger vehicles, the single-speed transmission model achieves the highest driving range of 189 km, which is about 4% and 5.5% more compared to those with two-speed and three-speed transmission models, respectively [Walker et al., 2015]. When the number of gears is increased in transmission, and the extra mass, the transmission losses will also increase. It is reported that the multi-speed transmission system increases the losses through the clutches, gears, and driveline components [Walker et

al., 2015]. Apart from the drawbacks discussed above, the additional cost is a critical issue for introducing a multi-gear system in EVs.

The use of a multi-gear or single-gear transmission depends mostly on the motor speed-torque characteristics. That is, at a given rated motor power, if the motor has a long constant power region, a single-gear transmission would be sufficient for a high tractive effort at low speeds. Apart from the induction motor operates very efficiently near or at the rated speed. It has low efficiency at a very high and low speed as compared to rated speed. So proper gearbox is designed to operate the motor in the specified efficient zone of operation. Gear shifting in a multi-gear transmission system is always associated with driving torque interruption and dynamic oscillation in output torque to the vehicle wheel [Liang et al., 2013]. Although many studies are based on simulation rather than an experiment, it is observed that a well-defined gear shift schedule is necessary during the gear-ratio optimization process. It increases the complexities of the drivetrain. After all, EVs do not necessarily require many gears as they have higher torque output throughout the wider speed range of the EM [Ahssan et al., 2018].

The general practice to search for an optimal gear-ratio is to consider the economic performance as the objective while constraining the dynamic performance targets. For optimal gear-ratio in the transmission system, a Genetic Algorithm (GA) is reported in many articles [Ahssan et al., 2018; Wang et al., 2013; Lukic et al., 2003; Yin et al., 2014]. In general, top gear is selected to get a maximum speed and is limited by EM or engine power, speed, and the energy economy. Lower gears are selected to get maximum speed at the maximum gradient. Lower gears are also expected to give creeping speed to avoid clutch usage and braking in city traffic [Jaideep Singh, 2012]. In other words, maximum gradeability sets the highest value of gear-ratio, and the maximum desirable speed sets the limit on the lowest gear-ratio [Sorniotti et al., 2010]. The lower value of gear-ratio also contributes to the energy economy. Gradeability is the climbing ability of a vehicle. Gradeability test is not in the scope of this research and is not covered in this report.

It is also reported that a suitable gear ratio is required considering the limitations of overloading and underloading operation to achieve longer mileage and safe performance of drive train [Prasun et al., 2013]. For the single-speed drivetrain, it is interesting to investigate whether or not it is possible to manage the efficiency of the 3P-IM so that it is operated more often in its higher efficiency region by using the Gear-Box (GB). Apart from the various advantages and

discussions reported in many articles, the single-speed drivetrain (with fixed gear) has opted for the study. It is also selected due to the simplicity discussed above. It is done by fixing the GB at 4th gear for the EV-I and 3rd gear for the EV-II. Therefore, the study focuses on the simple and economic single-speed transmission system. The relationship between gear-ratio and EM torque opted for the study is described here. Figure 4.3 illustrates the fundamental relationship between the torque and gear-ratio of a vehicle transmission system.

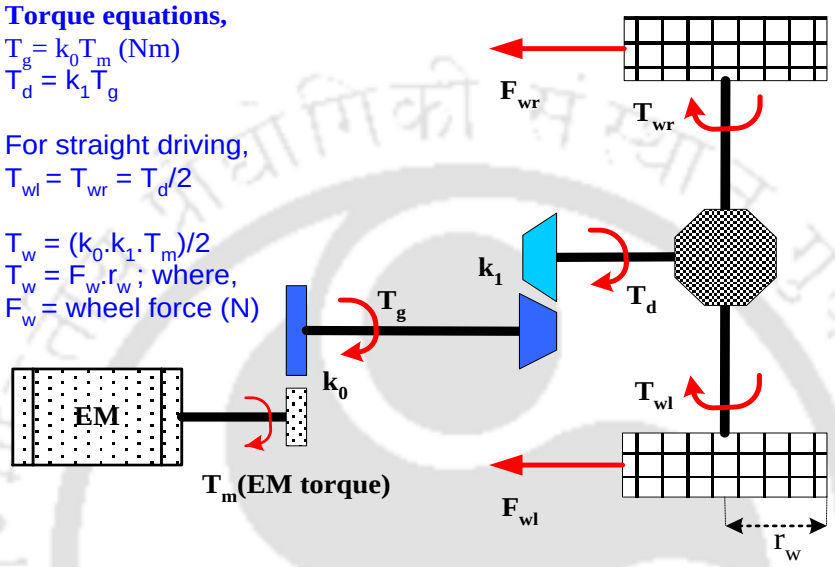

Figure 4.3: General relation of Torque and Gear ratio

Table 4.1 shows the available gear ratios of the test vehicle (EV-I; Maruti-800). However, the top gear has been selected directly for the EV-I, without analyzing the torque requirement, as a DC series motor is used, and it has high starting torque but low rpm. The detailed laboratory study for EV-I is described and discussed in Chapter 5. For the EV-II, the 3rd gear is opted, which has a gear ratio of 1.28 with the consideration of torque requirement for road gradients. Table 4.2 shows the simple calculation of the differential Torque (T_d) for the EV-II. T_d is further divided into two torques, namely T_{wr} for the right-wheel and T_{wl} for the left-wheel. The values of T_{wr} and T_{wl} depend on the angle of vehicle rotation/steering (either on the right or left). However, for straight-line driving, T_{wr} is equal to T_{wl}. Figure 4.4 depicts the torque transfer that happens from the 3P-IM to the wheels of the EV-II.

Table 4.1: Torque and Gear ratios of the EV-I

Vehicle Model		Maruti-800
Torque		58.80 Nm at 3000 rpm
Transmission System		
Transmission Gear-Ratio	1st	3.585
	2nd	2.166
	3rd	1.333
	4th (Top)	0.900
	Reverse	3.363

Table 4.2: Torque and Gear ratio of the EV-II (Maruti-Zen)

Vehicle Model	Rated torque of ICE Maruti-Zen	Rated torque of the IM (T_m)	Gear ratio (k)	Torque at differential (T_d)
Maruti-Zen	78 Nm at 4500 rpm	78 Nm	1.28	99.84 Nm

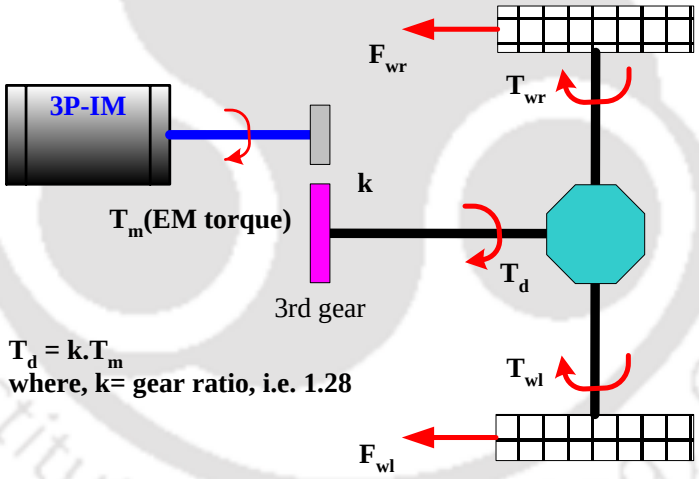

Figure 4.4: Torque and Gear ratio for the EV-II

4.4 Design and Development of Mechanical Subsystems

The drivetrain of a motor vehicle is the group of components that deliver power to the driving wheels [Bosch, 1993]. It includes the gearbox, the driveshaft, the axles, and the wheels. In the research study, the drivetrain's function is to couple the electric motor that produces the power to the driving wheels. Such a connection involves the physical linking of the two subsystems,

EM and mechanical drivetrain. The EM's motor speed and torque must be transferred to the vehicle wheels through the drivetrain having appropriate gear.

A template design of the adaptor plate between the GB and EM is first designed using a transparent acrylic sheet, as shown in Figure 4.5. It enables proper marking and pin-pointing of the GB bolt locations. Later the prototype adaptor plate (cut-out design) is developed from the template sheet, as shown in Figure 4.6. Several studies have been discussed in the previous chapter and sections. Based on the results and discussions of the studies discussed, a simple gear-ratio calculation has been done and discussed. It is also critical to transfer the output of the IM (mechanical energy) to the vehicle wheels efficiently. Therefore, the drivetrain subsystems like adaptor plate and axle coupling parts are customized, designed, and developed at a local mechanical workshop. For coupling the GB axle and EM rotor shaft, the new mechanical parts are used. Figure 4.7 shows the integration of the adaptor plate with the EM.

Figure 4.5: Template development for the adaptor plate.

Figure 4.6: Template cut-out of the adaptor plate.

Figure 4.7: Adaptor plate integration with the EM.

The IC engine and its related parts, such as exhaust pipe, fuel tank, cooling radiator, etc., are removed from the vehicle after the test vehicles' pre-conversion performance tests. The removal process for these parts is illustrated in Figure 4.8 (a-b).

(a)

(b)

Figure 4.8 (a-b): Removal process for the ICE and its parts

As shown in Figure 4.9, a level-meter is used for level-checking the EM mounting and complete drivetrain in the vehicle body. The new drivetrain (EM and GB) is carefully

integrated into the engine compartment in the vehicle. A proper alignment of the drivetrain with the vehicle differential axles is crucial and is done with extra caution and effort. Any misalignment of these parts may lead to severe vibration and damage in the drivetrain as well as in other rotating parts. It may lead to high energy consumption, a shorter life of the drivetrain.

Figure 4.9: Motor mounting and base frame for the electrical subsystems

The motor Cardan shaft adaptor, gear-shaft adaptor, adaptor plate for coupling the GB & motor, and other mounting parts for the EPT have been designed and developed in a local mechanical workshop. Simple CAD drawings of the shaft-adaptors and all other metal adaptors are designed and developed in the local workshop. The adaptor designs are shown in Figures 4.10-4.12.

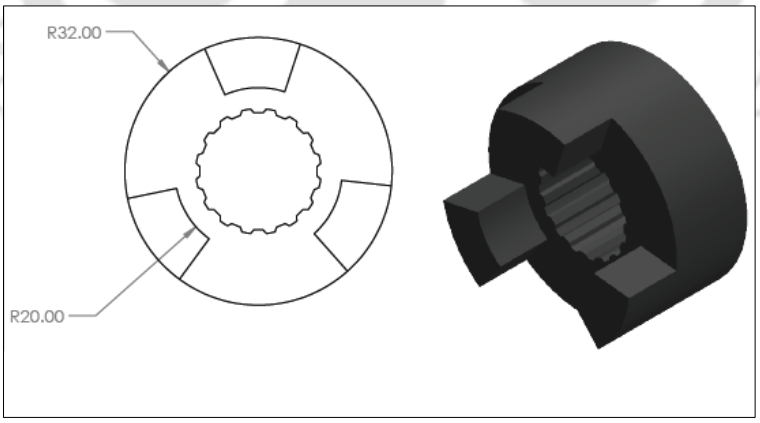

Figure 4.10. CAD diagram for the electric motor Cardan shaft (adaptor).

The GB adaptor, adaptor spider, is developed, and their integration is done with the cut-out clutch plate. The cut-out clutch plate is the re-engineered original clutch plate without the

friction plate. The metal adaptors are prepared from soft iron metal and hardened after cutting and removing the unwanted metal parts using mechanical equipment and machines in the workshop.

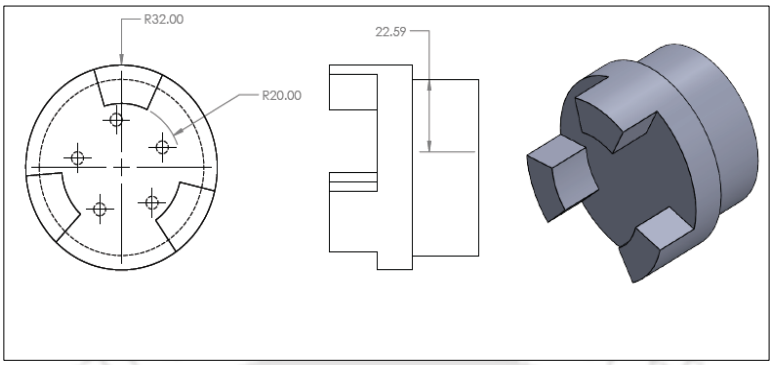

Figure 4.11. CAD diagram for the GB adaptor.

A mold of the desired spider shape is prepared using the Plaster of Paris (PoP), as per the drawing shown in Figure 4.12. With a simple molding technique, the plastic spider is developed using waste plastic materials processed and prepared in a reactor having 700 - 1000°C. However, this detailed process of using waste-plastic is not described and covered in this report. Figure 4.13 shows the hardened plastic-spider kept on the metal gear-shaft adaptor. The plastic spider is more rigid and durable than other similar rubber materials. The adaptor plate is developed using an iron metal sheet of 8mm thickness for connecting the GB and motor.

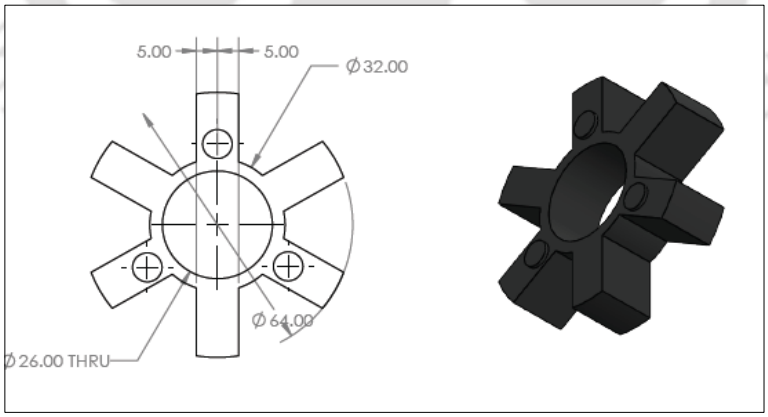

Figure 4.12. CAD diagram for the adaptor spider.

The EM rotor shaft and GB output shaft are aligned and ensured to match appropriately. The EM is correctly mounted in the ICE location using the original and new mounting parts, as

illustrated in Figure 4.9. System integration of the drivetrain, subsystems, and mounting parts are done in-house.

Figure 4.13. Plastic adaptor spider.

A short-summary algorithm for the system development and integration of the EPT components are listed below.

i. The ICE is removed and disassembled from the car GB.
ii. The GB axle center, bolt positions of the EM, and GB are measured.
iii. The CAD drawings of the new mechanical coupling and mounting parts are prepared, as shown in 10-12.
iv. The necessary hardware is developed and modified in a mechanical workshop having a lathe, machining, cutting, and grinding tools.
v. Trials for the hardware integration is done and checked for proper alignment if required, repeated the step-vi.
vi. Sub-assembled the new hardware subsystems with the EM
vii. The integration of the EM with GB is done for the new EPT.
viii. The installation of the EPT is done in the car.
ix. Installation and positioning of the battery pack, electric wiring & harness; other components are done.
x. The EPT prototyping is done using the electrical subsystems and new mechanical parts, as mentioned above.

Thus, a new EPT is prototyped for each EV. Figure 4.14 shows the block diagram of the implemented EPT. The EPT for the EV-I uses a DC series motor, Li-ion battery pack, and an

off-the-shelf Curtis controller. The EPT of the second EV is prototyped by integrating the low voltage 3P-IM, Lithium-ion Battery pack, IFOC motor controller-inverter, and a foot pedal potentiometer of 5kΩ, contactors and new mechanical parts. The EPT's basic design and prototyping detail are covered here. The EPTs for both EVs are based on a single EM integrated with the GB configured at a Fixed Gear (FG) and differential axles, but without a clutch. The configuration is similar to a modified version of an ICE vehicle's automatic drivetrain system, where the EM replaces the conventional ICE. The EV-I's EPT is configured and fixed at the top gear (4^{th} gear), having a gear ratio of 0.90:1.

Similarly, the EV-II drivetrain is configured and fixed at 3^{rd} gear having a gear ratio of 1.28:1. The gear ratio provides the right starting and operating torque for the EM. The FG can achieve the maximum possible vehicle speed and torque requirement. A pair of differential axles are used for the transmission, enabling the transfer of energy from the EM to vehicle wheels. The EPT specifications for both EVs are given in the Appendix.

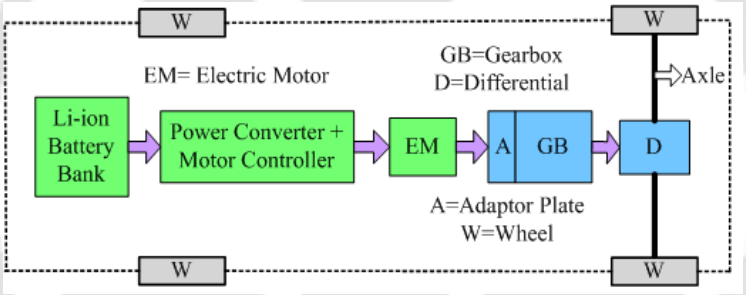

Figure 4.14. Block diagram of the EV powertrain system

The hardware required to integrate the GB and EM is designed and prototyped locally using lightweight materials. Light-weighting can reduce the EC of vehicles in many ways, and lighter vehicles mean less EC under the same condition [Shi et al., 2019]. It reduces the rolling resistance of tires and the amount of energy required to accelerate a vehicle. Light-weighting also reduces the battery energy needed for the EV to achieve the same range, resulting in the total cost reduction.

4.5 Selection of the Electrical Subsystems

The specifications of the entire power electronics, such as power converters, motor controller, and BMS, are dependent on selecting the right electric motor and its specification in terms of current & power rating [Prashun et al., 2013]. Selection of the right electric motor, converter, battery, and suitable transmission are significant issues for having an efficient powertrain of an

EV operating in Indian urban and suburban areas. The paper [Xue et al., 2008] reports the EV motor's selection technique among available electric motors and suitable electrical subsystems. While selecting authors have considered the limitations of overloading and underloading operation, to achieve longer mileage and safe performance of drivetrain. The electrical subsystems must match vehicle load characteristics and motor torque-speed characteristics within a safe, efficient operation zone for satisfactory vehicle performance.

An IM controller (model 1238E-6501) from Curtis is utilized to power and control the Three-Phase IM (3P-IM) used in the study. Figure 4.15 shows the controller and the wiring-harness. Table 4.3 gives the basic specification of the controller.

Figure 4.15: Curtis motor controller and wiring-harness

Table 4.3: 3P-IM Controller Specification:

Model	Nominal Battery Voltage (V)	2 Min RMS Current Rating (A)	60 Min RMS Current Rating (A)
Curtis 1238-6501	48-80	550	190

The test report of the 3P-IM gives the information of motor current, motor voltage, speed, and input power. The electrical subsystems such as main contactor, foot pedal, disconnect switch, forward/reverse contactor, and cable size are selected, and their ratings are decided from this information. The test report of the 3P-IM is given in the Appendix. These subsystems are off-the-shelf components available in the market. Figure 4.16 shows the electrical subsystems. A copper cable of (35 sq. mm) is used to withstand the high motor current.

Figure 4.16: Foot Pedal, Disconnect switch, BDU, F/R Contactor

4.5.1 Li-ion battery and Battery Management System (BMS)

A Lithium-ion Battery (LiB) pack is used as the primary energy source for the EV in the study. The LiB pack uses a suitable local BMS (made in India). The BMS is used to protect the Li-battery from overcharge, over-discharge, over-current, short circuit, and over-temperature operations. A LiB charger is used to charge the battery pack. The detailed specifications of the LiB pack, BMS, and charger are given in the Appendix. The Li-ion battery pack is 51.8 V, 80 Ah for the EV-I and 51.8 V, 80 Ah for the EV-II. The LiB pack cells are in the form of pouches, as shown in Figure 4.17, along with the BMS. Figure 4.18 shows both the battery and charger, along with a 1-liter water bottle (for size reference).

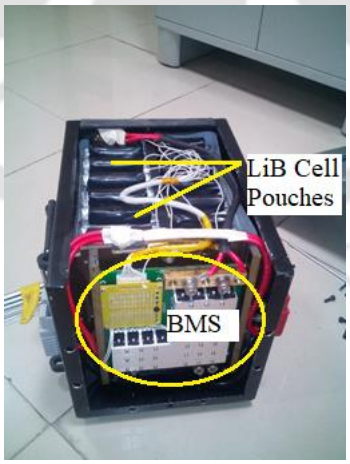

Figure 4.17: LiB cell pouches and BMS

(a)

(b)

Figure 4.18: (a) LiB pack and (b) LiB Charger

The charge has an output current of 40 A, and it takes around two hours to charge the LiB pack of 51.8 V and 80 Ah.

4.6 Supercapacitor Bank and its use for EV Application

Researchers have used simulation models to study supercapacitors' utility (SCs) for EV applications [Shrikant Misal and Divakar, 2013]. Researchers are also exploring and attempting to find a feasible method to improve an EV's performance using a supercapacitor [Jinrui et al., 2006].

The results from Jinrui's study shows that installing an SC improves the working conditions of the battery. The study further reports that a supercapacitor can provide a large current in a short time, delivering extra power to meet the power requirement as and when needed, especially during acceleration. The SC also improves the acceleration performance of the vehicle. So, a supercapacitor can be used as a secondary energy source for an EV. However, real-world implementation of supercapacitors for EV application is seldom reported from the Indian perspective. Therefore, it is essential to implement and evaluate them for their performance and suitability for EV application.

4.6.1 Charging and Discharging of a single Supercapacitor of 2.85 V, 3400 F.

A single supercapacitor (SC) cell is 2.85 V, 3400 Farad (F). A variable DC power supply unit having a capacity of 30 V, 20 A, has been utilized to charge the single SC through a wire of 1 Ω (as a single cell SC has negligible internal resistance). Figures 4.19 and 4.20 show the charging setup for a single SC, and Table 4.4 shows the charging parameters. The charged SC

has been kept in 'open' condition to check the discharge rate for a few weeks. The discharge time and parameters have been recorded, and they are tabulated in Table 4.4.

The single SC took almost 3.5 months to discharge from the initial State of Charge (SoC) of 2.53 V to 1.69 V. It shows that a single cell can hold the charge for quite a long time at 'open' condition.

Table 4.4: Charging & Discharging of a Single Supercapacitor 2.85 V, 3400 F

Experiment	**Charging Current (A)**	**Charging Time**	**Voltage (V)**
Charging	10	16 m 46 s	2.85
	20	9 m 3 s	2.85
Discharging	13th June 2018	Open Circuit	2.53
	26th September 2018	Open Circuit	1.69

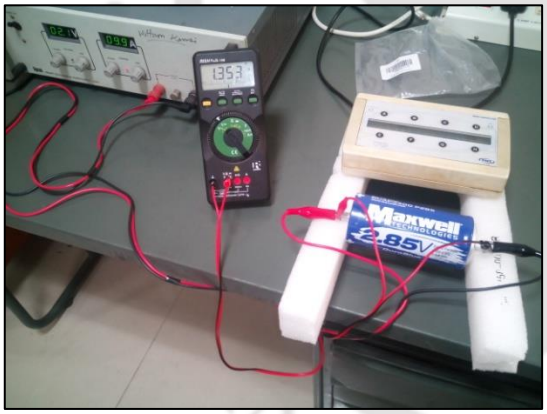

Figure 4.19: Charging setup of a single Supercapacitor of 2.85 V, 3400 F.

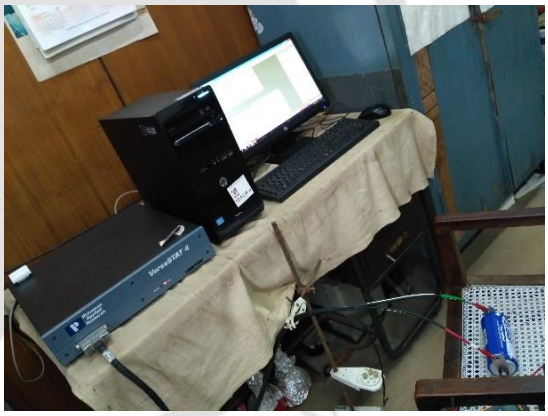

Figure 4.20: Charging/Discharging characteristics using VersaSTAT-4.

4.6.2 Charging and Discharging of an SC bank of 48 V,189 F.

A total of 18 numbers of single-cell SC are used and connected in series to make an SC bank of 48 V, 189 F. Each single cell SC is 2.85 V and 3400 Farad (F). Figure 4.21 illustrates the connection of SC cells using strap-aluminum bars. The connecting strap-aluminum bars between the SCs have been developed locally. A wooden box of appropriate size is designed and developed. The SC bank is thus assembled in the wooden box, and an Anderson connector

is installed as a charging/discharging outlet. The box is covered with a transparent plastic sheet having a 3 mm thickness for safety and protection, as shown in Figure 4.22.

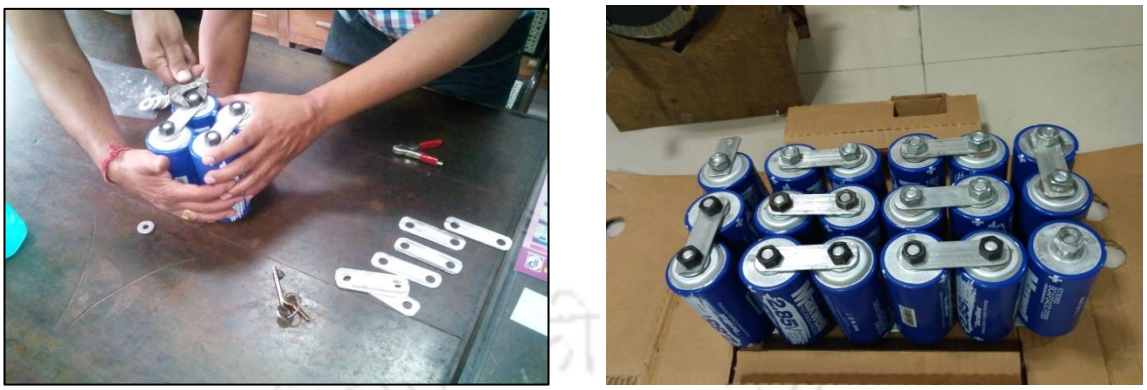

Figure 4.21: Series connection of 18 SCs for the SC bank of 48V, 189F.

Figure 4.22: An integrated SC bank of 48V, 189F.

In the literature, it is reported that SCs should not be overcharged, and they should be charged only up to 90-95% of their maximum voltage. Due to their negligible internal resistance, they may act as a short circuit if an attempt is made to charge it without any external resistor. Therefore, the SC bank (of 48 V, 189 F) is charged through a 2 mm thick Nichrome wire having a resistance of 10Ω. The charging is done using a battery charger with 34 V, 20 A at Constant Current (CC) mode. Figure 4.23 shows the charging setup for the SC bank. Table 4.5 shows the charging data. The charged SC bank is then connected to the open 3P-IM circuit for discharging. The experiments have been repeated for the charged SC bank and its usage for motor drive applications. Table 4.6 shows the discharging data.

The motor controller sets a limit of cut-off voltage (at 36 V) for the IM. It cuts the power supply from the SC bank when its voltage drops below 36V. However, unlike batteries,

supercapacitors can be discharged entirely until 0V. For storing safely, the SC bank is discharged from 36 V to 0 V through the Nichrome wire with higher heat resistivity. The Nichrome wire has experienced heating-up and became red-hot. Figure 4.24 shows the discharge of the SC using the Nichrome wire. Figure 4.25 shows the charging characteristic of the SC bank. Figure 4.26 shows the discharge characteristics of the SC bank obtained using the open IM circuit.

Figure 4.23: Charging of the SC Bank.

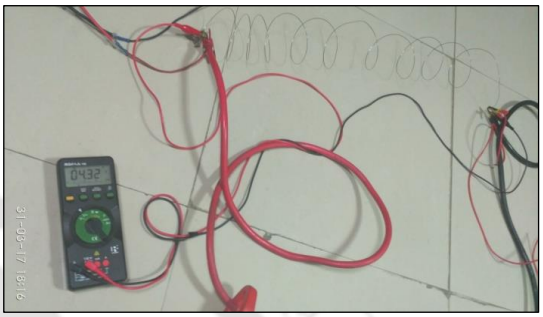

Figure 4.24: Discharging of the SC bank.

Table 4.5: Charging data of the Supercapacitor Bank of 48V, 189F

Experiment	Charging Time (s)	Initial SC Voltage (V)	Charging current (A)
Experiment-1	0	36.2	6.5
	5	37.0	6.9
	10	37.4	7.1
	405	50.2	4.3

Table 4.6: Discharging data of the Supercapacitor Bank of 48V, 189F

IM RPM	Motor Current (A)	SC Terminal Voltage (V)
200	1.80	48.80
400	2.13	48.70
600	2.53	48.50
800	2.90	48.30
1000	3.37	48.00
1200	3.60	47.70
1400	3.90	47.40
1600	5.07	46.60
1800	5.45	46.20
2000	6.00	45.60
2500	6.22	45.20

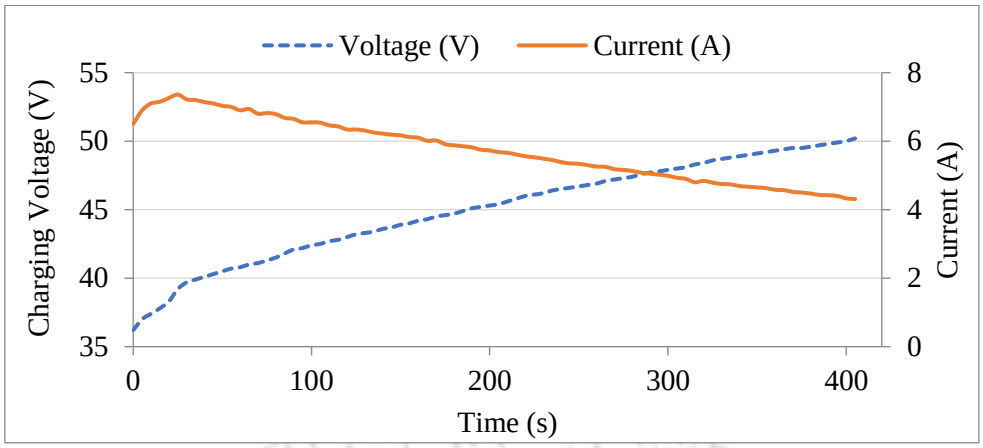

Figure 4.25: Charging characteristic graph of the SC bank

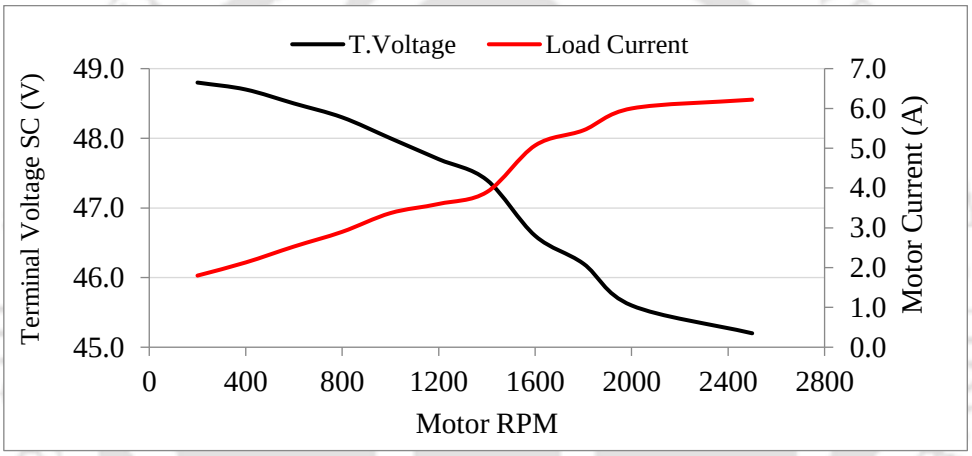

Figure 4.26: Discharging characteristic graph of the SC bank

4.6.3 Effect of a Supercapacitor Bank on Electric Range of an EV

The SC bank is installed in the engine compartment, as shown in Figure 4.27. The SC bank is charged using the LiB charger, keeping at Constant Current (CC) mode through the Nichrome wire. The SC is connected to the 3P-IM circuit of the EV-II. A test trial is conducted for the EV-II entirely powered by the SC bank alone. It is observed that EV-II is driven for around 200 meters (m) before the controller cuts the power off. It indicates that the SC bank can power the EV-II only for a short distance. Therefore, it is observed that the SC bank alone cannot be used to power the EV. It is of great interest to repeat the EV test by combining the battery and SC. Such a combination of primary energy source and the SC is known as Hybrid Energy Storage System (HESS). The utilization of a HESS for EV application would be further attempted in the future. A hybrid electronic control unit (H-ECU) can manage the switching

algorithm and operation-timing of the LiB and SC bank. The H-ECU can be a part of the HESS. The HESS and H-ECU concept and connection is depicted in Figure 4.28.

Figure 4.27: Installation of the SC bank in the EV-II

A supercapacitor can reduce the average energy consumption of the primary energy source (battery) if it works in conjunction with the battery. The average energy consumption of an EV with a supercapacitor is around 77% of that of an EV without a supercapacitor. The electric range per charge is also substantially increased [Jinrui et al., 2006]. It can be used to absorb the regenerative power during deceleration mode.

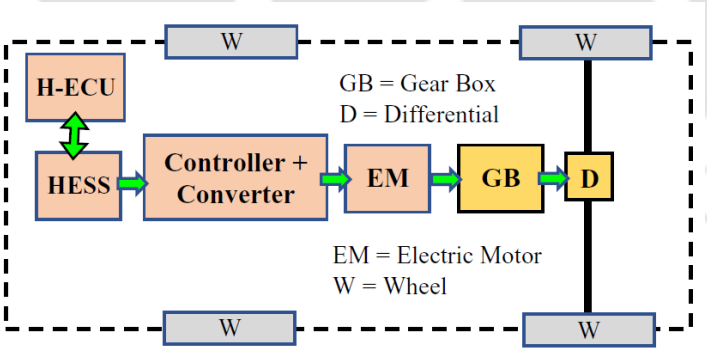

Figure 4.28: Block diagram of the EV powertrain with HESS

4.7 System Integration and Weight Distribution for the New EV Powertrain

Figure 4.29 shows the system integration of the EV subsystems inside the engine compartment. It is noticed that there is ample space available after the ICE removal. The available space can be utilized for the subsystems' optimized positioning and for keeping extra energy storage. The subsystems are positioned and fixed in a proper distributed manner so that the vehicle weight is balanced. The vehicle weight on each wheel and proper weight distribution is ensured using the digital vehicle weighment system, which is described in Chapter 3. For example, the weight on each front-wheels must be close to each other; likewise, the weight on each rear-wheels must be closer to each other. It is done to ensure the vehicle weight on each wheel is not much different from each other. A proper vehicle weight distribution is essential because uneven weight distribution may lead to undesired vehicle dynamics and dynamic performance.

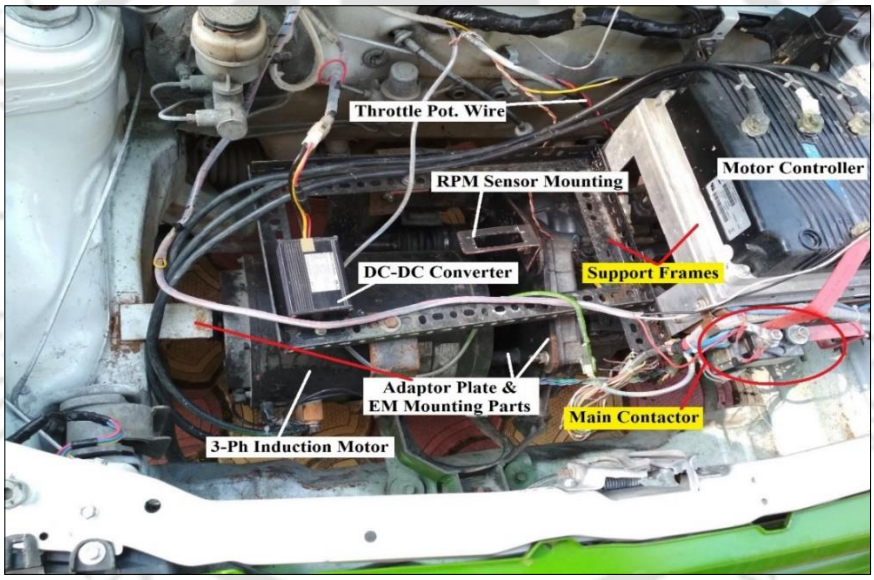

Figure 4.29. System Integration of EV subsystems inside the engine compartment

Figure 4.30 shows the weight distribution and subsystem location (XY) coordinates inside the EV. After removing the ICE, radiator, fuel tank, exhaust pipe, and ICE related parts, the vehicle is measured for the new G_w. For the EV-II, the new G_w is 705 kg, along with the weight of the EPT. The new vehicle reference weight (G_w) is determined by summing the weights on each wheel. Table 4.7 shows the weight distribution on each wheel for the EVs. It is observed that EV-I has imbalanced weight distribution having more weights on the right wheels than the left wheels. It indicates a requirement of a counter-weight to balance the distribution. However, the

weight distribution is much improved for the EV-II, having marginal weight difference between the right and left wheels.

A proper vehicle weight-distribution is desired to maintain the vehicle stability and dynamics, such as roll, pitch, and yaw parameters, within the limit. Improper weight-distribution may lead to safety compromises while braking and may have a faster wear-tear of the wheels (on the heavier side). The fundamentals of vehicle dynamics are described in the Appendix (Figure A.3.2) [Kistler vehicle dynamics, 2020; SAE Vehicle dynamics, 2020]. Table 4.8 shows the subsystems' location coordinates inside the vehicle from the global origin-coordinates (0,0). The center of each subsystem is considered the location coordinates for each subsystem. However, the detailed analysis of the vehicle dynamics is not in this thesis's scope; hence, it is not included.

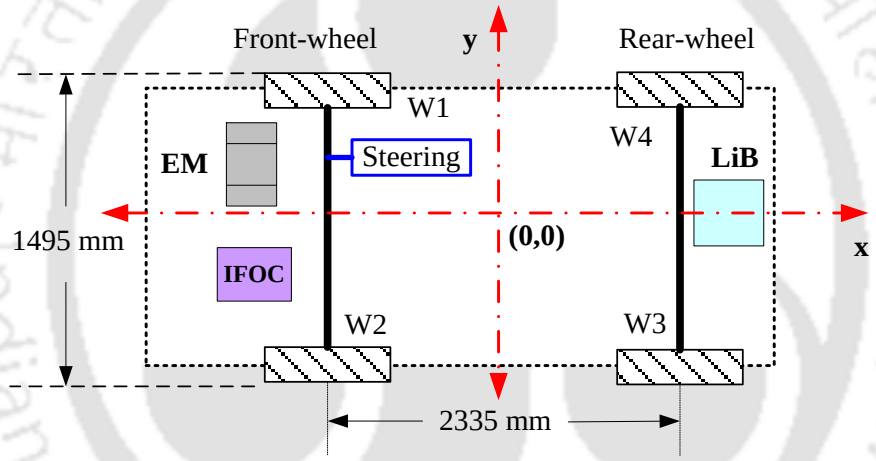

Figure 4.30: Weight distribution and x-y coordinates of the EV-II subsystems

Table 4.7: Weight distribution for the EV-I and EV-II

Weight distribution of EV-I (kg)		Weight distribution of EV-II (kg)	
Front-right wheel, W1 =	176.4	Front-right wheel, W1 =	213.2
Front-left wheel, W2 =	169.6	Front-left wheel, W2 =	211.4
Rear-left wheel, W3 =	123.8	Rear-left wheel, W3 =	139.2
Rear-right wheel, W4 =	139.2	Right-right wheel, W4 =	141.4
Total kerb weight	609.0	Total kerb weight	705.2

Table 4.8: Location (XY coordinates) of subsystems for the EV-I and EV-II

Subsystems	X-Y coordinates of subsystems for the EV-I (mm)	X-Y coordinates of subsystems for the EV-II (mm)
Electric Motor	X = 1250.00 ; Y = -150.00	X= 1390.25; Y= -170.00
Motor Controller	X = - 1015.00 ; Y = - 180.00	X= - 1370.25; Y= - 250.00
LiB	X = 1230.00 ; Y = 0.0	X= 1250.00; Y= 0.0

4.8 Conclusion

The chapter has described the complete EV conversion process, including the design, development of the mechanical subsystems, and selection of the electrical subsystems. The mechanical subsystems have been designed and developed in a local mechanical fabrication shop. The electrical subsystems are the off-the-shelf components from the market, selected based on the specifications of the 3P-IM and IFOC controller. The primary energy source is the LiB supplied by a local battery company.

- Considering the criteria of EV performance evaluation, it has also described the selection of drivetrain topology and gear selection for economic and dynamic performance.
- Further, it describes the general relationship between torque and gear-ratio. The torque and gear-ratio of the EV-II have been discussed.
- The system integration and weight distribution analysis of the subsystems are also described and performed. Proper weight distribution is critical for vehicle stability and vehicle dynamics (longitudinal, lateral, and vertical parameters).

In the chapter, the development of a SC bank is described. The SC bank is developed by integrating 18 single SCs in series connection. Further, the thesis has attempted to investigate the effect of a supercapacitor bank on the electric mileage using a SC bank of 48V, 189F.

- It has been observed that EV-II is driven a short distance of around 200 meters (m) before the controller cuts the power off to the 3P-IM. Therefore, it is concluded that the SC bank alone cannot be used to power the EV. However, the SC bank can work in conjunction with the battery so that the SC can reduce the average energy consumption of the primary energy source (battery).

After the EV conversion process, it is necessary to evaluate both EVs' performance and examine whether the subsystems are working together. Therefore, both EVs are evaluated for their performance in the chassis dynamometer laboratory described and discussed in the next Chapter 5.

Chapter 5

EV Energy Consumption and Performance Evaluation in Chassis Dynamometer Laboratory

5.1 Introduction

The detailed EV conversion process has been described in Chapter 4. The system integration of the EV subsystems into the test vehicles is done and described in the preceding chapter. After the integration, the EVs are evaluated for their performance in the chassis dynamometer laboratory. This chapter describes and discusses the laboratory study to investigate the EV energy consumption and performance evaluation for both EVs on different laboratory driving cycles using drive cycle analysis. The driving cycles used for the study are the Indian Driving Cycle (IDC), Modified Indian Driving Cycle (MIDC), and Worldwide Harmonized Light-duty Test Cycle (WLTC). The Indian EV market is presently having a few EV models commercially available in the market. Most commercial EV models (such as Tata Tigor EV, Mahindra E_2O+) are predominantly low-speed EVs with a maximum speed of 70-80 km/h and ideal for intra-city mobility. As these low-speed EVs are used for city travel in urban areas, it is necessary to understand their performance with the laboratory cycles and real-driving cycles.

Many other researchers have conducted various simulation studies to evaluate energy consumption (EC) and different EVs' performance. The authors of the paper [Jorge et al., 2018] have worked on a simulation model for power consumption analysis for an EV. The model is based on the identification of the parameters that relate EC from the EV with its speed, acceleration, and road slope. Variation of the input power, EC w.r.t the vehicle speed, is also employed to evaluate the effectiveness of energy utilization in the vehicle operation [Bor Yann et al., 2007]. However, most of the reported works lacked information on EV performance evaluation and EC analysis using drive cycle analysis and real-world testing.

In the literature, the EV conversion method is reported to be a good alternative in terms of energy efficiency and cost optimization [André et al., 2018]. In India also, researchers have attempted conversion into HEV. An Indian researcher reports that an ICE vehicle has been

retrofitted into an HEV, and its performance evaluation has been conducted [Sudhir Gupte, 2014]. However, the paper has not reported the retrofitted HEV's performance evaluation conducted in a laboratory using a driving cycle. There is also limited literature on the electric conversion of ICE vehicles into EVs.

Therefore, this chapter attempts to address the above gaps. The Maruti-800 is the first experimental EV of the study that uses a DC series motor of 4.5 kW and a suitable Curtis motor controller (off-the-shelf component). The series motor is used due to high starting torque, low-cost, hardware simplicity, and easy availability. However, the electrified Maruti-800 achieves a top speed of less than 40 km/h. Due to the low speed, the car cannot follow the IDC's speed profile or any other urban driving cycle. Apart from the speed limitation, the EV-I has technical drawbacks associated with a DC series motor, drawbacks such as lesser life and maintenance issues due to commutator and brush.

The second research work is initiated to address the above-stated limitations of EV-I by using an induction motor. The research work has converted a pollution-causing car of the same vehicle segment (Maruti Zen) into a second experimental EV by integrating a new prototype electric powertrain system (EPT). The second EV is known as EV-II in this report. The EV-II's prototype EPT has a local low-voltage 3P-IM, an IFOC vector control motor-drive system, a Li-ion Battery (LiB) pack, and new mechanical subsystems. The EV-II's subsystems are considered with all the selection and sizing aspects. The mechanical subsystems are integrated with the 3P-IM, IFOC controller, and battery to make the prototype powertrain. The prototype powertrain is then integrated into the test vehicle with the vehicle's GB configured at fixed-gear with a gear ratio of 1.28:1 (3^{rd} gear of the GB).

The laboratory study of the second EV using the 3P-IM is discussed under case study-II in this Chapter. Unlike EV-I, the EV-II uses the three laboratory driving cycles (IDC, MIDC, and WLTC). The chapter also discusses the variation of EV speed, motor rpm, battery current, torque, EC, and input and output power during the drive-modes of each driving cycle.

The present chapter is organized into five sections. The sections are i) Laboratory test description, which describes the common measurement methods and standards used for the study. It also describes the methodology and test algorithm, ii) Pre-electrification vehicle performance test in the laboratory, iii) A summary for prototype EPT and system integration, iv) Post-electrification performance evaluation in the laboratory, v) Experimental results and discussion for both the cases of EV-I and EV-II. vi) Scope of improvement and further work,

vii) the chapter concludes with critical laboratory results and the necessity for conducting a study in real-world conditions.

5.2 Laboratory Test Description

Full vehicle electrification has been carried out for the polluting gasoline cars, namely Maruti-800 and Maruti-Zen (both vehicles belong to the M1 vehicle category and small hatchback segment). The laboratory study for both EVs is described in two separate case studies in this Chapter. The electric Maruti-800 is described as EV-I in the case-study-I. The electric Maruti-Zen is described as EV-II in case study-II. Both cars were still operational and have a deteriorated IC engine with high exhaust emissions and fuel consumption until the conversion. As a standard practice, an ICE vehicle's mandatory performance evaluation is conducted in a controlled chassis dynamometer laboratory. Similarly, an EV is evaluated on a chassis dynamometer to determine its performance, energy consumption, and efficiency.

Before the vehicle electrification, the test vehicle's road resistance forces are obtained by conducting a coast-down test as per the Indian Standard [IS 14785: 2000 (Rev.), 2016]. The description of the coast-down test and second-degree polynomial equation (used for the coast-down test) is described in Chapter 3. The road resistance forces are entered into the chassis dynamometer. The regulated vehicle emissions viz. Carbon Monoxide (CO), Carbon Dioxide (CO_2), Nitrogen Oxides (NOx), and Hydrocarbons (HC) are estimated for both cars through bag analysis technique using the chassis dynamometer, emission analyzers, and Constant Volume Sampling (CVS) system. The baseline tailpipe emissions are recorded for reference and to understand the ICE condition before the electrification.

As per the Indian Automotive Industry Standards (AIS), an EV system having up to 60 Vdc is considered a low-voltage system as it has no risk of shock [AIS-138 (Part-1), 2017]. Both EV-I and EV-II are low-voltage EV systems as both use a 48 V LiB pack. After the electric conversion, both EVs' performance test is carried out using the laboratory driving cycles. EC analysis and performance evaluation are done based on the drive cycle analysis.

Two measurement methods, namely direct and indirect, are used to generate the test parameters. These measurement methods are common in both cases. The data logger uses the voltage, current, and rpm sensors for the direct measurement of the battery voltage, load current supplied to the EM, and motor rotation, respectively. A power meter measures and provides the total electrical EC (kWh) for each charging as per the Automotive Industry Standards [AIS-

039-Rev. (1)]. The [AIS-039-Rev. (1)] provides the procedure for measuring electrical EC and allows Phase-I of the MIDC for M, N category vehicles. The EV-I performance test is conducted on the dynamometer that follows the IDC's speed profile. However, EV-II uses MIDC following the AIS-039 (Rev.1) test procedure. The full MIDC is considered for research purposes for EV-II dynamometer tests, as it belongs to the M1 category (hatchback segment) vehicles.

The indirect method offers the speed-based indirect EC (EC_{ind}) values and input power of the battery (PoC) for the dynamic speed characteristic observed during the laboratory and real-world tests. The simple formula equation (5.1) estimates the total electrical EC for each test. The data logger records the battery voltage and load-current drawn by the EM drive system during the test. To understand the EC characteristics during vehicle operation, it is necessary to calculate and analyze the EC at every moment. Equation (5.2) and (5.3) calculate and offers the indirect EC and PoC for every data point, in terms of Watt-hour per kilometer (Wh/km) and kilo-Watt (kW), respectively. The dynamometer gives the vehicle tractive force (F), mechanical power (kW), vehicle speed (v).

$$C = \frac{E}{D} \text{ (Wh/km)} \quad \text{---} \quad (5.1)$$

Where C is the total electrical energy consumption per kilometer, EC_{tot} (Wh/km), E is the total electrical input energy in Watt-hour (Wh) reading of the power meter, and D is the distance covered (range) in kilometer (km).

$$P_{dc} = VI \text{ (W)} \quad \text{---} \quad (5.2)$$

Where P_{dc} is the power input (PoC) from the battery, V is the battery voltage in Volts (V), and I is the battery current in Amps (A).

$$EC_{ind} = \frac{PoC}{S} \text{ (Wh/km)} \quad \text{---} \quad (5.3)$$

Where EC_{ind} is the speed-based Indirect EC (Wh/km), sometimes mentioned as real-world EC in this report; PoC is the P_{dc} (W), and S is the vehicle speed (km/h). The above equations (5.1, 5.2, 5.3) are commonly used standard formulas for both EVs in this study.

The standard methodology and test algorithm used for both cases are explained in Figure 5.1. The performance evaluation tests are described in the respective sub-sections.

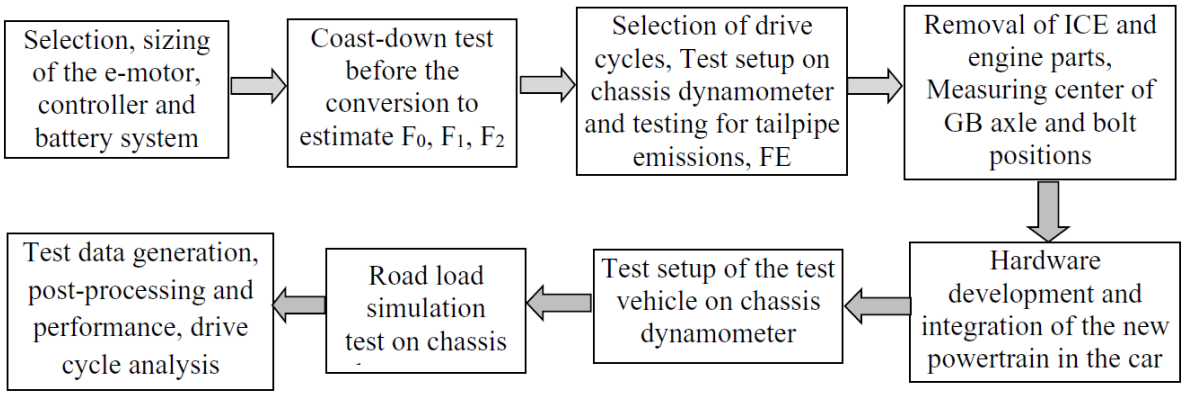

Figure 5.1. Methodology and Test algorithm

5.3 Pre-electrification Performance Test in Laboratory

Generally, a standard vehicle emission test is conducted in a controlled mass emission laboratory where the real-world driving conditions are simulated using a chassis dynamometer, which follows a driving cycle. Figure 5.2 illustrates an ICE vehicle's setup in the dynamometer laboratory to evaluate the vehicle tailpipe emissions. The vehicle tailpipe emissions are measured through bag analysis technique using the emission test systems. The tailpipe emissions and FE are obtained in gram per kilometer (g/km) and kilometers per liter (km/l), respectively. The emission analyzer bench is equipped with a Non-Dispersive Infrared Detector (NDIR) for the measurement of CO and CO_2, Chemiluminescence Detector (CLD) for the measurement of NOx, Flame Ionization Detector (FID) for the measurement of HC.

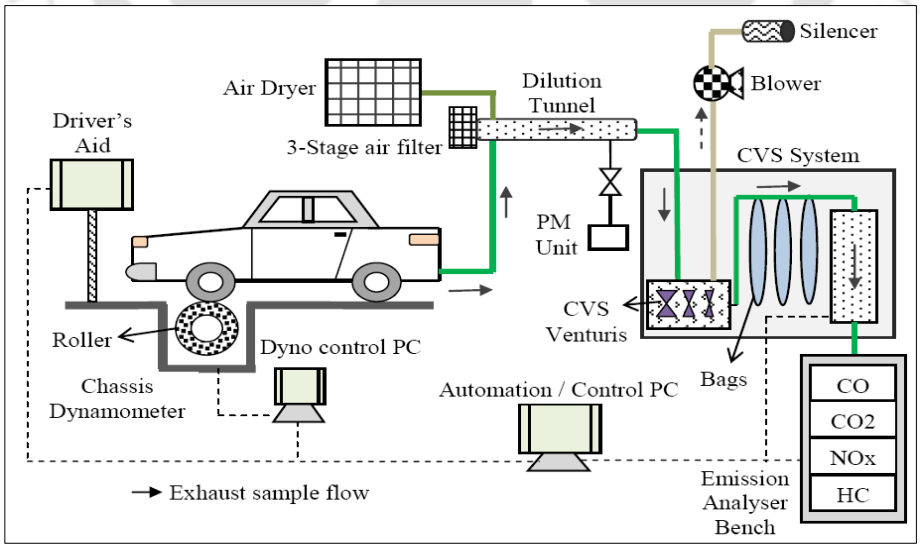

Figure 5.2. Pre-electrification vehicle set up in the chassis dynamometer laboratory.

Before the vehicle electrification, like the ICE vehicle testing, both test cars are set up on the dynamometer, as illustrated in Figure 5.2. The IDC cycle is loaded in the Driver's Aid computer and used for both cars' vehicle emissions tests. As per the Type Approval test procedure, an emissions test is conducted for each car to determine the regulated tailpipe emissions, i.e., CO, CO_2, NOx, HC, and FE. A test driver operates the vehicle on the dynamometer and follows the IDC's speed profile for both cars. Such an emissions test is done for reference and to understand the ICE condition before the electrification.

5.3.1 Case-I: Electric Maruti-800 (EV-I)

Before the electrification, the test vehicle (EV-I) is tested for the regulated tailpipe emissions. After the electric conversion, the test equipment is deployed, and the performance test is again conducted for the test vehicle with the same driver and the same cycle. Test data acquired from the 'before and after' the vehicle's electrification is given in Table 5.1.

Table 5.1: Test Results (Before and After conversion) for EV-I

Before electric conversion	**After electric conversion**
Vehicle Emissions HC – 1.12 g/km NOx – 3.17 g/km CO – 6.73 g/km CO_2 – 140.16 g/km	Zero Emissions ▪ Environmental friendly
Max. Speed: 100 km/hr	38.9 km/hr
Fuel Economy: 15.45 km/l	Zero fuel; Electric range: 30 km/full charge; Battery SoC: 25-95%
Kerb weight: 620 kg	586 kg
Acceleration test: 0-20 km/hr in 5.1 s	0-20 km/hr in 6.0 s

5.3.2 Case-II: Electric Maruti-Zen (EV-II)

Similarly, the pre-electrification vehicle emissions test for the vehicle (EV-II) is conducted using the same IDC for reference data. The performance test result acquired before and after

the electrification is given in Table 5.2. The efficiency of an ICE is assumed as 40% [Lee et al., 2017].

Table 5.2: Test Results (Before and After conversion) for EV-II

Before electric conversion	After electric conversion
Average vehicle Emissions and FE (using the IDC) HC – 1.76 g/km NOx – 2.01 g/km CO – 5.92 g/km CO_2 – 151.21 g/km	Zero vehicle emissions
Max. Speed: 120 km/h	64.0 km/h
FE (IDC): 16.1 km/l	Zero fuel; Avg. electric range: 25 km/full charge; @Battery SoC: 20-100%
1 liter of gasoline = 9.10 kWh Assuming an efficiency of ICE=40% EC: 3.64 kWh for a liter of gasoline 226.10 Wh/km	106.23 Wh/km
Maximum Torque: 79 Nm @ 4500 rpm	78 Nm @ 1112 rpm
Kerb weight: 735 kg	705 kg

5.4 Prototype of EPT and System Integration

The prototyping process of the electric powertrain (EPT) is described in Chapter 4. The EV subsystem integration is also described and discussed in Chapter 4. The specifications of the prototype EPTs are described in Table A.2.1 and A.2.2 in the Appendix. It is desirable to design the hardware required to integrate the GB and EM using lightweight materials. Using lightweight material in EVs is beneficial for better energy efficiency. In the literature study, it is reported that light-weighting can reduce the EC of vehicles in many ways, and lighter vehicles mean less EC under the same condition [Shi et al., 2019]. It reduces the rolling resistance of tires and the amount of energy required to accelerate a vehicle. Light-weighting also reduces the battery energy needed for the EV to achieve the same range, resulting in the

total cost reduction. Mechanical designs, along with the design drawings for the motor Cardan shaft, gear-shaft adaptor, and adaptor plate, have been described in Chapter 4.

5.5 Post-electrification Performance Evaluation in Laboratory

The road load simulation test (sometimes referred to as 'electrical simulation of inertia') for the EVs is conducted on the dynamometer. The electrical inertia simulation is performed to adjust the dynamometer's inertia to correspond to the real vehicle weight.

The coefficients F_0, F_1, and F_2 are manually entered into the dynamometer computer. Tractive force (F) is estimated according to the standard equation mentioned in Chapter 3, which is executed in the dynamometer computer. The three driving cycles (IDC, MIDC, and WLTC) are configured in the Driver's Aid computer. Figure 5.3 shows the two EVs having similar drivetrain and but different electric motors and controllers.

Figure 5.3. The test vehicles EV-I and EV-II

5.5.1 Case-I: EV-I Setup

The vehicle setup is done as per the standard procedure and service manual of the dynamometer. The IDC is loaded into the driver's aid computer. The IDC is the only cycle used for EV-I testing. The electrical inertia simulation is conducted with the dynamometer for the EV-I. The test setup and representative testing for the electrified Maruti-800 (before repaint) are shown in Figure 5.4.

Figure 5.4. Road load simulation test of the EV-I on the chassis dynamometer

5.5.2 Case-II: EV-II Setup

The EV-II setup is done, as illustrated in Figure 5.5. The road load simulation test for the EV-II is conducted on the dynamometer. The three driving cycles are used for EV-II testing. The electrical inertia simulation is again performed with the dynamometer for the test vehicle.

Figure 5.5. Test setup and road load simulation test of the EV-II on the chassis dynamometer.

5.6 Experimental Results and Discussion

The laboratory test results are discussed in this section. The section describes the analysis techniques used for both EVs. The section is divided into two sub-sections. The first sub-section describes and discusses the performance and drive cycle analysis for the EV-I. The

second sub-section describes and discusses the performance evaluation, drive cycle analysis, and comparative analysis of energy consumption for the EV-II.

5.6.1 Case study-I: Electric Maruti-800 (EV-I)

The sub-section describes the first feasibility study carried out for vehicle electrification of the pollution-causing old Maruti-800 car into an EV. The performance evaluation and drive cycle analysis of the EV are studied and presented here. As described earlier, the new EPT is prototyped for the electric conversion by integrating the DC series EM, battery, and controller with the vehicle's gearbox system. The new mechanical subsystems are developed and used in the EV. The post-conversion performance tests are carried out on the dynamometer. The distribution of drive modes (idling, deceleration, acceleration, cruising) to the torque, input, and output power is calculated using a computer program, and results are analyzed and presented. The simple computer program is developed (using Microsoft Excel software) and used for the data segregation, especially for the acceleration data. The program flowchart is described in the Appendix (Figure A.6.1). The program checks the acceleration trend using the acceleration limit (instead of performing the time-consuming manual checks). In totality, the study and test results verify the new powertrain parts and feasibility of the electric conversion approach for faster adoption of EVs. The post-electrification performance tests are conducted using the Indian Driving Cycle (IDC) only.

5.6.1.1 Performance Evaluation of the EV-I

Test data are measured and recorded for the entire period of the test cycle (648 seconds). The statistical average (Avg.) and maximum (Max.) values of all the test data are given in Table 5.3. The maximum power efficiency observed for the EV is 54.15% (electrical input power to mechanical output power at the wheel). The average electric range is observed to be 30 km/full charge.

Table 5.3: EV-I Performance test results

Statistical values	Speed (km/hr)	Motor Current (A)	Torque (Nm)	Output Power (kW)	Input Power (kW)	EC (Wh/ km)
Avg.	21.84	51.81	18.01	0.58	2.61	94.71
Max.	38.91	182.90	211.20	4.83	8.92	458.6

A few free acceleration tests are carried out on the dynamometer to measure the time and the maximum motor-current drawn during the sudden acceleration. The test data are given in Table 5.4. The motor current is observed to reach a load current of 250-260 A momentarily.

Table 5.4: Acceleration test result for the EV-I

No. of Accel. Test	Vehicle Speed (km/hr)	Test Duration (s)	Accel. (m/s^2)	Motor Current (A)
1.	0-10	3.50 s	0.79	250A
2.	0-20	6.02 s	0.92	255A
3.	0-30	14.30 s	0.54	260A

5.6.1.2 Drive Cycle Analysis for EV-I

The EV's characteristic graphs are plotted and analyzed for the test-data for the entire test cycle. The variation of EV speed (km/hr), motor current (A), torque (Nm), input electrical power (kW), output mechanical power (kW), and indirect EC (Wh/km) with reference to the cycle is shown in Figures 5.6-5.10. It is observed that the load current follows the vehicle speed closely, and it drops to zero-current as soon as the driver releases the accelerator-pedal while braking and during the deceleration-mode. Such a situation is illustrated in Figure 5.6. During the deceleration-mode, the vehicle is still moving due to the inertia. The EV-I is not powered by the electric machine, and no load-current is drawn from the battery. Such a condition is also depicted with negative torque in Figure 5.7.

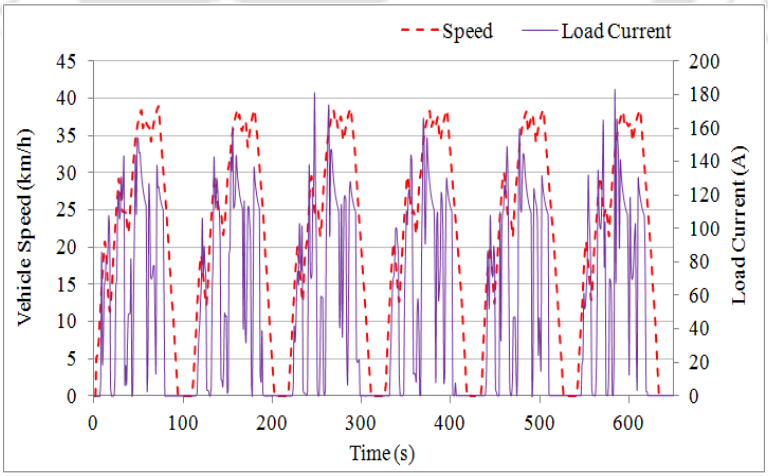

Figure 5.6. Variation of load current and EV speed with the IDC

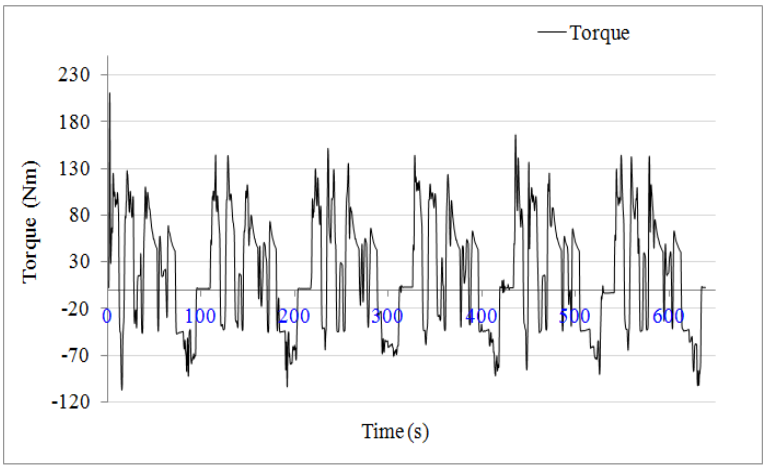

Figure 5.7. Variation of torque with the IDC

The input power is proportional to the motor current. Therefore, the input power graph is similar to the load-current graph, and it also varies with the vehicle speed, as illustrated in Figure 5.8. The output (mechanical) power is proportional to the torque. Therefore, the output mechanical power graph is similar to the torque graph, as shown in Figure 5.9. Energy (Wh) is the function of power and time. Indirect energy consumption, EC_{ind} (Wh/km) is calculated from the power and speed, and the EC_{ind} graph with respect to the EV speed is shown in Figure 5.10.

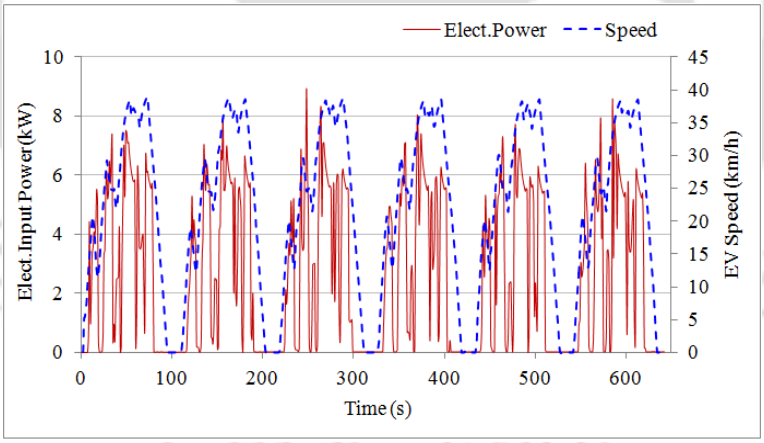

Figure 5.8. Variation of input power and EV speed with the IDC

The analysis of load current and vehicle speed indicates that the EV powertrain system needs to be improved for better vehicle performance, especially vehicle speed. The vehicle speed can be increased by using a higher-speed motor. At the same time, the load current needs to get reduced. The I^2R (Ohmic) losses and cable conductor size can be minimized by reducing the load current, which would impact the overall cost reduction. The case-I study provides a pathway for further EV research for improving vehicle performance. It also shows the

importance of the selection of the right EM and drive system. It leads to the second phase of the EV research, which uses an induction motor with higher power and motor speed.

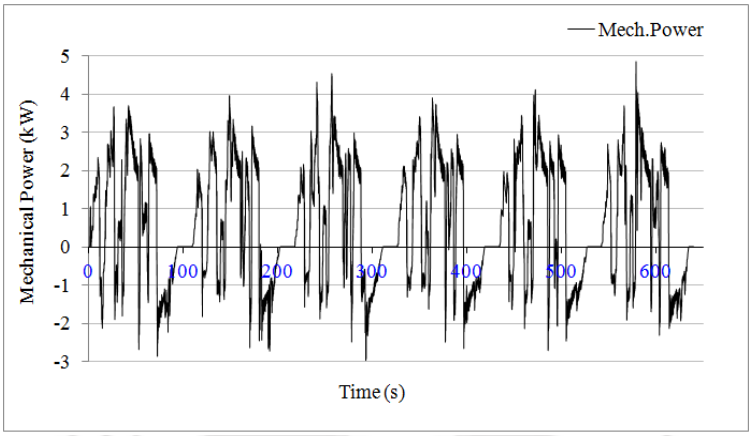

Figure 5.9. Variation of output power with the EV speed w.r.t the IDC

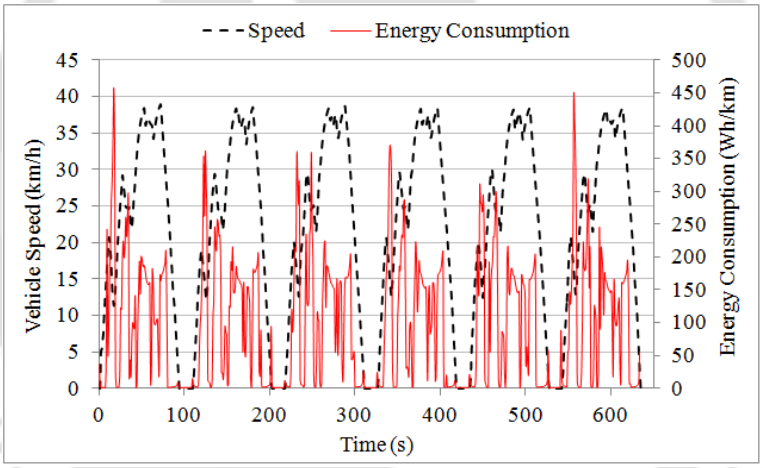

Figure 5.10. Variation of EV speed and EC_{ind} with the IDC

5.6.1.3 Distribution of Input Power, EC for the Different Drive Modes for the EV-I

The percentage distribution of each drive mode and corresponding test data are studied and analyzed for the IDC using the computer program and statistical analysis. The test results are given in Table 5.5. It is noticed that most of the power is consumed during the acceleration-mode, which can be further investigated for improvement.

Table 5.5: Percentage Distribution of Drive Modes to Powers, Torque

Drive modes/ Parameters	Time	Input Power	Torque	Output Power
Percentage	%	%	%	%
Idling	15.74	0.00	0.00	0.00
Acceleration	38.89	97.12	96.58	96.10
Deceleration	30.56	1.30	0.32	0.20
Cruising	14.81	1.58	3.10	3.70

5.6.2 Case study-II: Electric Maruti-Zen (EV-II)

The EV-II is set up on the dynamometer using the vehicle mounting, clamps, and fastening parts, as illustrated in earlier Figure 5.5. The vehicle setup is done like the one described for the EV-I. The road load simulation test for the EV-II is again conducted on the dynamometer. The driving cycles (IDC, MIDC, and WLTC) are loaded, one after another, in the Driver's Aid computer. The road load simulation test is performed again in the same manner described in the previous section. It is done to adjust the dynamometer's inertia that corresponds to the real vehicle weight.

The coefficients F_0, F_1, F_2, and tractive force (F) of the EV-II are determined with the same procedure as per the (IS 14785: 2000). They are manually fed into the dynamometer computer. In this case, the EV-II is tested on the dynamometer using all the three driving cycles, the IDC, MIDC-I, and WLTC-low. The test equipment measures the electrical input power, EC, vehicle speed, tractive force, and vehicle's output mechanical power. The test cycle duration and distance are 648 seconds and 3.94km for the IDC, 780 seconds, and 4.03km for the MIDC-I, 589 seconds, and 3.09km for the WLTC-low, respectively. Test data are measured and recorded for the entire period of the cycles.

5.6.2.1 Performance Evaluation of the EV-II

The performance evaluation is based on a set of crucial vehicle requirements (such as vehicle speed, average speed, battery current, input power, output mechanical power, EC, and acceleration test. The maximum speed test shows a top speed of 64 km/h for the EV. The

average electric range observed is 25 km/full charge (at Battery SoC: 20-100%) due to the smaller battery pack. The total EC_{tot} is evaluated using the standard formula given in equation (5.1), and it is proportional to the input electrical power (kW). Fundamental statistical analysis is done for the test data. The average (avg.) and maximum (max.) values of the test data for the EV are given in Table 5.6.

Table 5.6: EV-II performance test result

Driving Cycle/ Distance	Statistical value	EV speed (km/h)	Battery current (A)	Input power (kW)	Mech. power (kW)	EC_{tot} Wh/km
IDC 3.94 km	Avg.	21.82	45.47	2.11	1.053	106.23
	Max.	42.14	260.59	11.15	7.462	1974.64
MIDC-I 4.03 km	Avg.	17.75	37.98	1.71	0.842	110.91
	Max.	51.50	255.01	10.72	7.163	2604.13
WLTC-low 3.09 km	Avg.	19.57	41.18	1.83	0.915	87.35
	Max.	51.86	249.70	10.23	6.798	1182.36

The acceleration ability is measured by the time required to reach 60 km/h or 100 km/h from the stop position. Passing acceleration ability is the overtaking ability and is usually measured by the time required to reach 80 km/h from 60 km/h [Ahssan, M., 2018].

A few free acceleration tests are carried out to measure the time (in seconds) to reach from 0 to 20,40,60 km/h speed and the corresponding maximum battery currents. Three readings are taken for each experiment (e.g., three readings for 0-20 km/h test). The average values of the readings are tabulated in Table 5.7. The battery current is noticed to reach a load current of 245 to 301 A momentarily.

Table 5.7: Acceleration test result for EV-II

Acceleration test	Speed (km/h)	Average time (s)	Average battery current (A)
1.	0-20	4.76	245.25
2.	0-40	9.07	296.40
3.	0-60	25.95	301.80

Steady speed tests at 20, 40, 60 km/h are also conducted on the dynamometer for the EV-II, and the steady speed characteristic (vehicle speed, motor speed, and battery current) is shown in Figure 5.11. It shows the range of load current required to move the vehicle from a standstill condition as well as the current range required to accelerate the vehicle from a steady-speed to a higher speed.

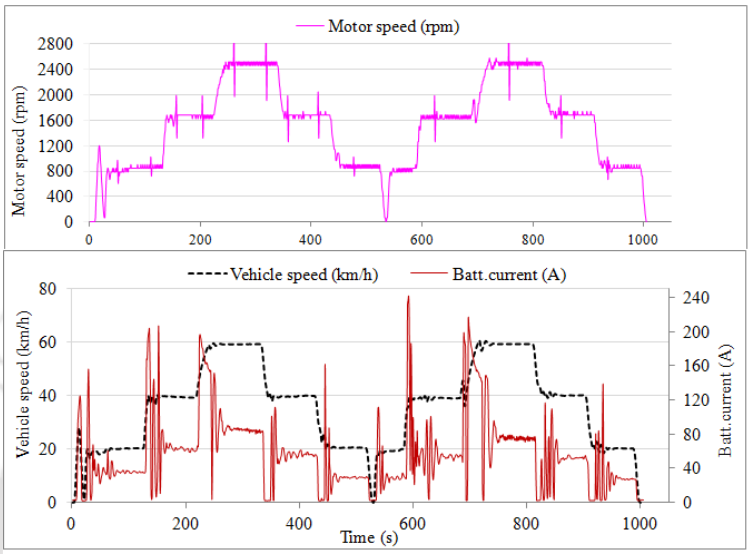

Figure 5.11. Steady speed characteristics for the EV-II.

5.6.2.2 Drive Cycle Analysis for the EV-II

Vehicle driving is a combination of four drive modes, namely (i) deceleration, (ii) acceleration, (iii) cruising, and (iv) idling. The test data comprising vehicle speed, battery current, input power, output mechanical power, and EC are evaluated and distributed into these four modal categories. The simple program developed in Microsoft Excel software segregates the corresponding test data to the drive modes [Lairenlakpam et al., 2018]. The program includes the sub-programs for each drive mode. The definition and calculation of idling, acceleration, deceleration, and cruising modes are described earlier and followed as per the method described in the paper [Nesamani et al., 2005]. The deceleration and acceleration limits are defined and followed as per the 'TAP' documents [TAP-115/116, Issue No.4, 2012]. The percentage (%) distribution of time spent on each drive-mode is estimated for the entire IDC, MIDC, and WLTC cycles for reference, and they are shown in Figure 5.12.

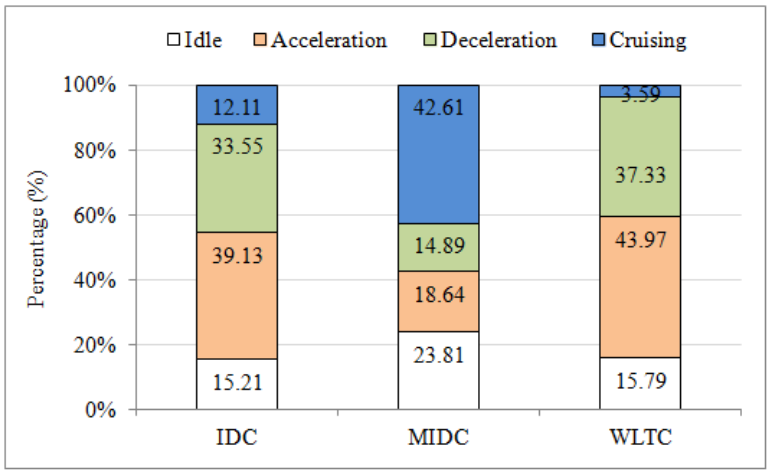

Figure 5.12. Distribution of drive modes for the IDC, MIDC, and WLTC.

The EV's test parameters are measured and analyzed. Analysis graphs are drawn for the test data along with the selected drive cycles. Figures 5.13-5.15 show the battery current variation with the actual vehicle speed w.r.t the driving cycles. It is observed that the battery current follows the vehicle speed closely during the acceleration and cruising modes, and they drop to zero as soon as the driver releases the accelerator while applying brake during deceleration mode. The test results indicate that the battery current is proportional to the dynamical vehicle speed. The electric drivetrain has drawn an average battery current of 45.47A for the IDC, 37.98A for the MIDC-I, and 41.18A for the WLTC-low cycle. The maximum battery current is observed in the range of 249 to 260A during the EV's acceleration mode. The operation of the LiB with such a high current is highly undesirable and must be minimized. The dynamic test data would be useful for studying and improving the dynamic characteristic of the LiB and the high-current part of the operation. Battery chemistry under high-current stress would require further investigation, and its improvement with additional hardware may be studied.

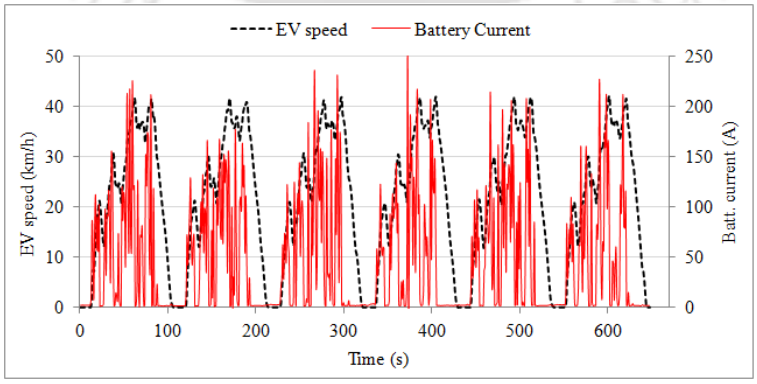

Figure 5.13. Variation of Battery current and EV speed w.r.t the IDC.

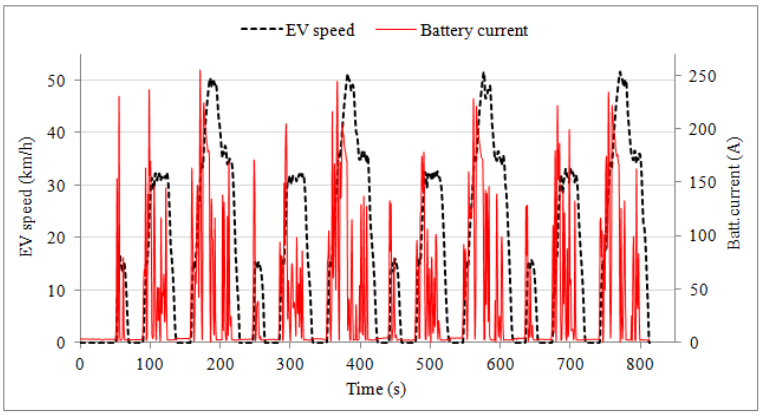

Figure 5.14. Variation of Battery current and EV speed w.r.t the MIDC-I.

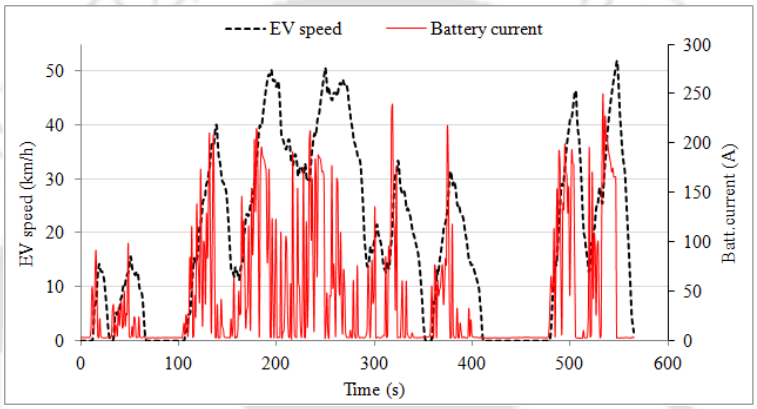

Figure 5.15. Variation of Battery current and EV speed w.r.t the WLTC-low.

Figures 5.16-5.18 show the variation of input power with the actual vehicle speed w.r.t the cycles. The input electrical power is the product of battery voltage and current; hence, it also closely follows the vehicle speed whenever the battery current and vehicle speed are greater than zero.

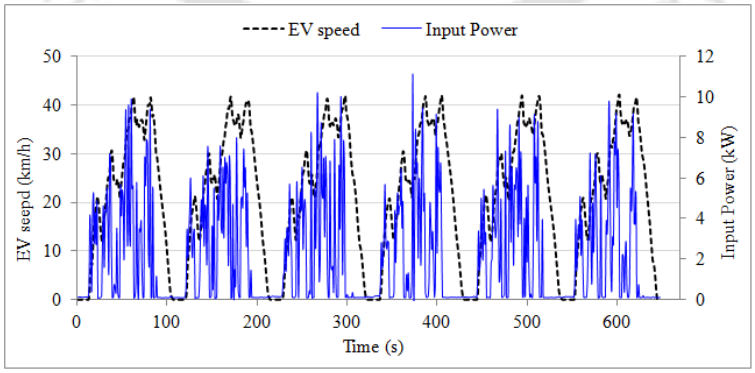

Figure 5.16. Variation of Input power and EV speed w.r.t the IDC.

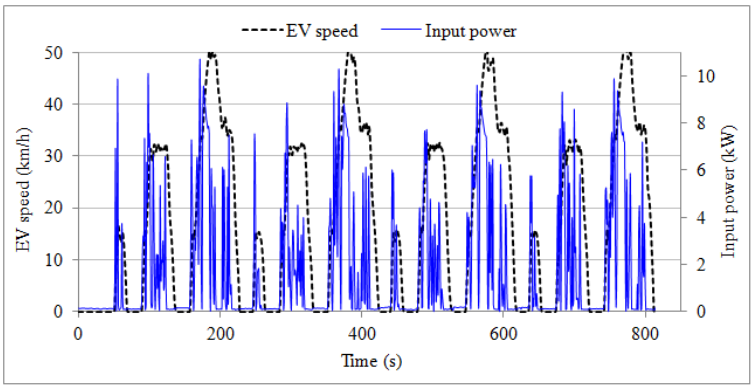

Figure 5.17. Variation of Input power and EV speed w.r.t the MIDC-I.

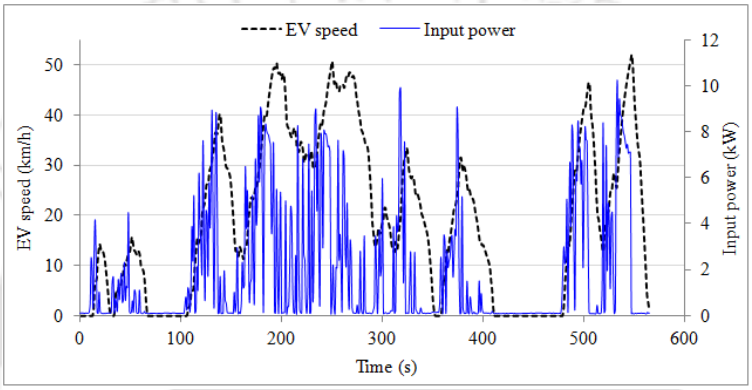

Figure 5.18. Variation of Input power and EV speed w.r.t the WLTC-low.

The 3P-IM does not propel the wheels during the deceleration mode, but the vehicle wheels are still rotating due to the inertia. During the deceleration, negative mechanical power is observed in each cycle, which is the regenerative power for the EV, and the same is illustrated in Figure 5.19, 5.21, 5.23. The regenerative power is recoverable and can be stored back in a power storage device (such as a supercapacitor); however, the said power is not recovered in the study due to hardware and equipment limitations.

Figure 5.20, 5.22,5.24 shows the variation of motor rpm and torque w.r.t to the cycles. They are kept next to the corresponding graph of speed and mechanical power for better analysis and understanding. It is observed that most of the positive torque varies from 0 to 200 Nm for the IDC, 0 to 400 Nm for the MIDC, and 0 to 200 Nm for the WLTC-low, respectively. It indicates that the 3-ph EM can deliver more torque than the required torque. The average and maximum torques are 38.14 Nm and 329.81 Nm for the IDC, 38.10 Nm, and 446.80 Nm for the MIDC-I. The average and maximum torques are 35.28 Nm and 334.73 Nm for the WLTC-low. More electric power (with a high battery current) is required due to the high torque requirement

during the acceleration mode. Therefore, it can be considered to redesign and redevelop the motor with reduced maximum torque and operating torque, which needs to be further studied and optimized.

It is also observed that there is unexpectedly high torque (more than the required torque) observed at the beginning of every sub-cycle, especially for the MIDC-I cycle. Such high torque at the starting of every sub-cycle exceeds the minimum torque required for the acceleration. It shows that the motor's maximum torque needs to be reduced and limited to an optimum value for regular operation, which can reduce battery current significantly.

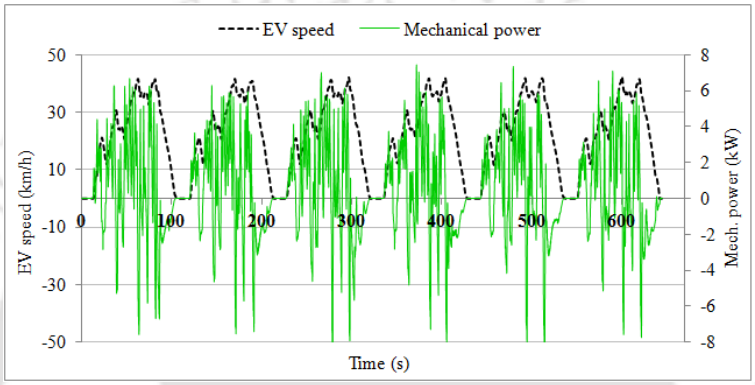

Figure 5.19. Variation of Mechanical power and EV speed w.r.t the IDC.

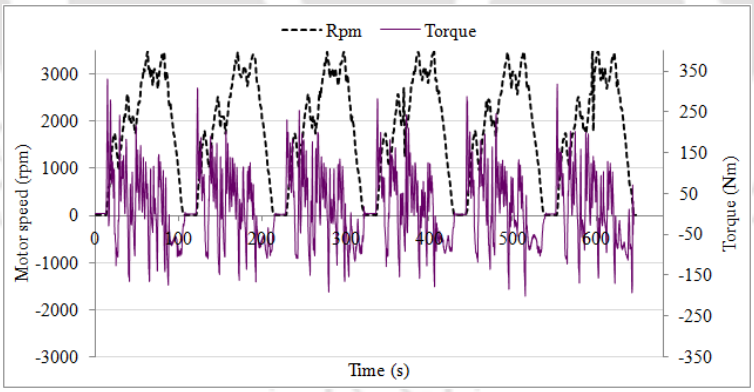

Figure 5.20. Variation of Torque and Motor speed w.r.t the IDC

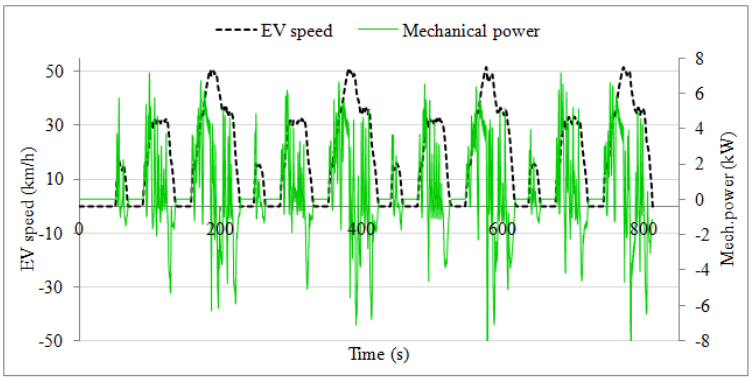

Figure 5.21. Variation of Mechanical power and EV speed w.r.t the MIDC-I.

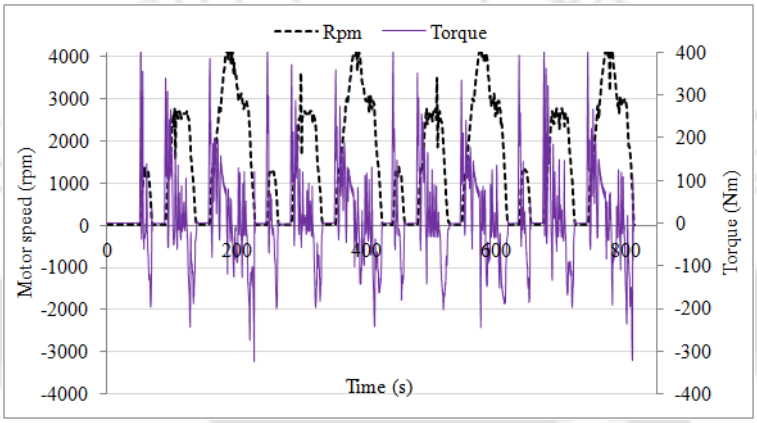

Figure 5.22. Variation of Torque and Motor speed w.r.t the MIDC-I.

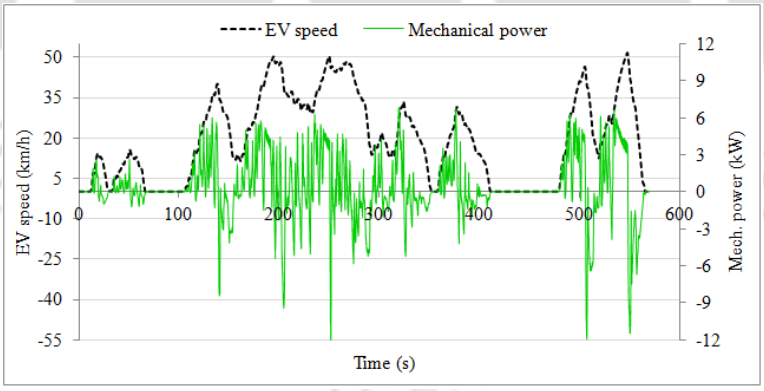

Figure 5.23. Variation of Mechanical power and EV speed w.r.t the WLTC-low.

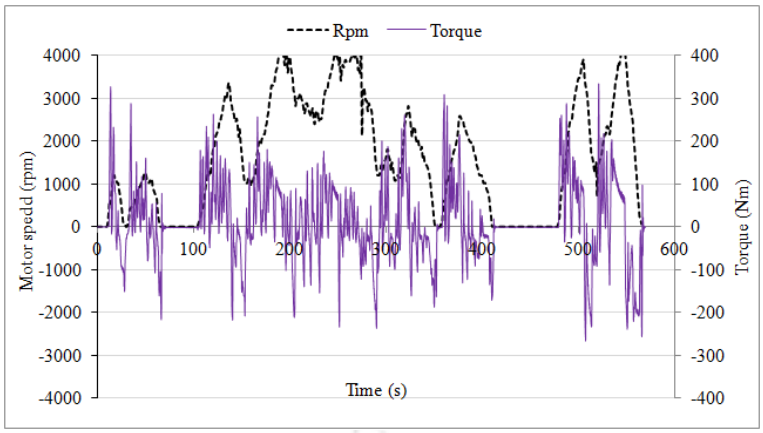

Figure 5.24. Variation of Torque and Motor speed w.r.t the WLTC-low

5.6.2.3 Distribution of Input Power, EC for the Different Drive Modes for EV-II

The percentage (%) contribution of each drive mode and corresponding test parameter, i.e., time spent, input power, and EC_{ind} data, are evaluated and analyzed for the IDC, MIDC-I, and WLTC-low cycles using the computer program. The distribution of data is provided in Table 5.8. It is observed that most of the input power and EC_{ind} are consumed during the acceleration mode, which can be further investigated and improved for less power consumption from the battery.

Table 5.8: Distribution of test data for the drive modes (EV-II)

Driving cycles	Drive modes	Time (s) (%)	Input power (kW) (%)	EC_{ind} (Wh/km) (%)
IDC	Idling	15.21	0.78	0.00
	Acceleration	39.13	66.54	64.47
	Deceleration	33.56	5.79	6.09
	Cruising	12.11	26.86	24.86
MIDC-I	Idling	35.29	3.55	0.00
	Acceleration	17.65	64.15	60.24
	Deceleration	16.65	1.90	3.20
	Cruising	30.40	30.37	18.40
WLTC-low	Idling	21.53	2.99	0.00
	Acceleration	38.82	77.98	73.22
	Deceleration	37.72	16.77	16.45
	Cruising	1.95	1.86	0.70

Figures 5.25-5.27 indicate the percentage distribution of time spent, input power, and EC_{ind} to the four drive modes. It is observed from the statistical analysis that 64 to 77% of the total input power is consumed during the acceleration mode. The percent EC_{ind} is more in the cruising than the deceleration for the IDC and MIDC-I; however, for the WLTC-low, the percent EC_{ind} is less in cruising than the deceleration mode. It is also observed that the acceleration and cruising modes are significant contributors to the total EC. For example, for the test conducted using the MIDC-I cycle, the acceleration and cruising mode accounts for more than 60% and 18% of the total EC, respectively. The overall observation indicates that the focus area of improvement for the EV is during the acceleration and cruising mode for better performance, efficiency, and less energy consumption.

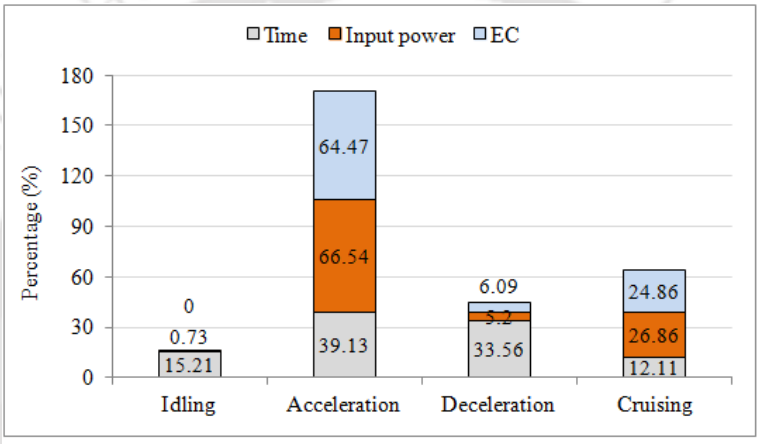

Figure 5.25. Percentage distribution of time spent, electrical input power, and EC w.r.t the IDC's drive modes.

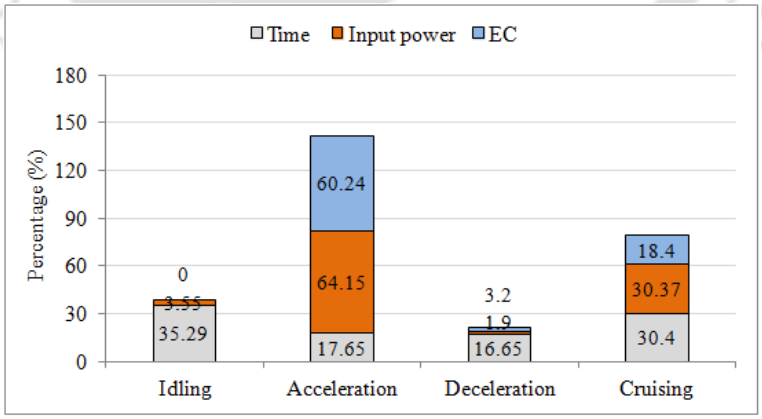

Figure 5.26. Percentage distribution of time spent, electrical input power, and EC_{ind} w.r.t the drive modes of the MIDC-I.

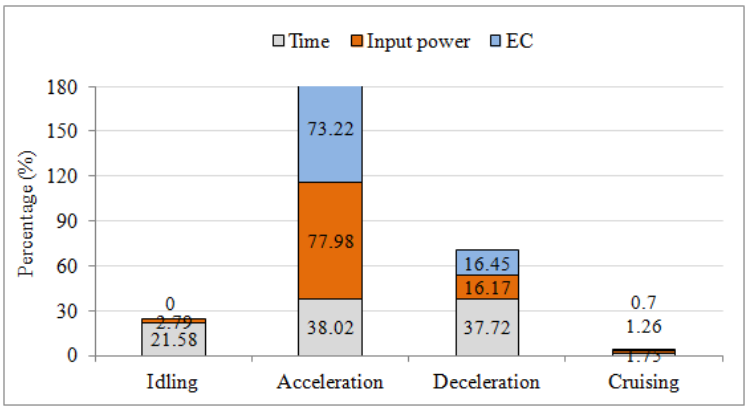

Figure 5.27. Percentage distribution of time spent, electrical input power, and EC w.r.t the drive modes of the WLTC-low.

However, Figure 5.28 shows the drive-modes distribution of the test parameters for the laboratory test conducted using the full MIDC. It illustrates the percentage distribution of time spent, EC_{ind}, PoC, and load current on each drive-modes to the total trip value of the parameters (time, EC_{ind}, PoC, load current).

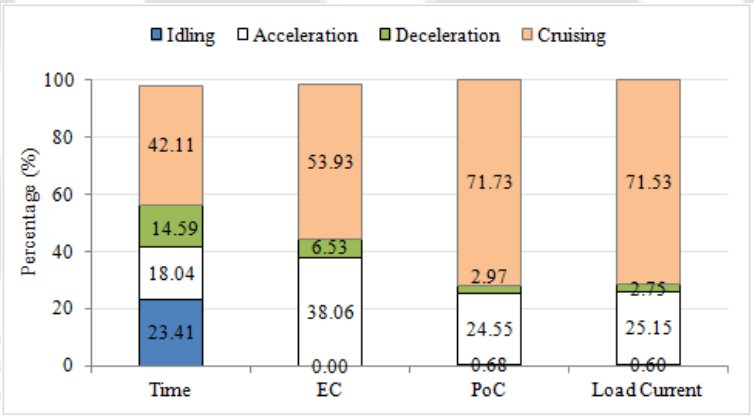

Figure 5.28. Percentage distribution of time spent, EC_{ind}, PoC, and Load current w.r.t the drive-modes on the driving cycle (MIDC).

5.6.2.4 Energy and Power Consumption Analysis for the complete MIDC

The MIDC has two parts, i.e., Phase-I and Phase-II. Phase-I has a speed limit of 50 km/h, and Phase-II has a speed limit of 90 km/h. For the complete cycle, the average values of baseline EC and PoC are 88.10 Wh/km and 2.77 kW, respectively. Due to the limitation of the electric motor speed, the vehicle reaches a maximum speed limit of 64 km/h. However, the EM can track the Phase-I of the MIDC, which has a top speed limit of 50 km/h. Figure 5.29 illustrates the EM tracking of the speed limit of Phase-I of the MIDC. The AIS-039 Rev.(1) explains the

guideline for measuring electrical EC and allows the Phase-I of the MIDC for M, N category vehicles. The test vehicle belongs to the M1 category of vehicles. The said AIS is described in the Appendix.

Figures 5.29-5.31 illustrate the dynamic nature of vehicle speed, mechanical power, battery current, motor rotation (RPM), and EC_{ind} with respect to (w.r.t.) the complete MIDC. Figure 5.30 shows the variation of dynamic conditions of the actual vehicle speed and mechanical power (kW) w.r.t the driving cycle's set speed. It observes that the actual vehicle speed could not reach the maximum cycle speed of 90 km/h due to the motor speed limitation. It also shows the regenerative power (negative mechanical power) observed mostly during the deceleration mode. It is observed that the calculated on-road EC_{ind} is sensitive to the change of load current and motor speed. Figure 5.31 indicates how closely the calculated EC_{ind} follows the load current and vehicle speed (which is again dependent on the motor speed and follows the rpm path).

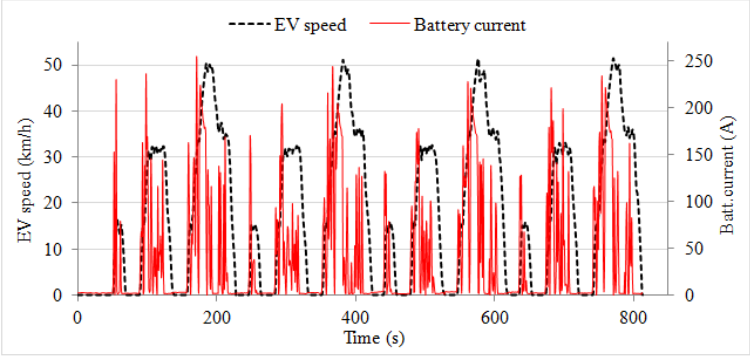

Figure 5.29. Variation of Battery current and EV speed with Phase-I of the MIDC.

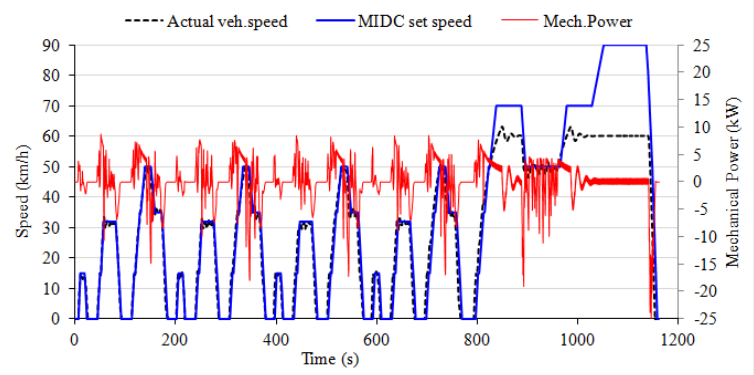

Figure 5.30. Variation of actual vehicle speed, MIDC set speed, and mechanical power.

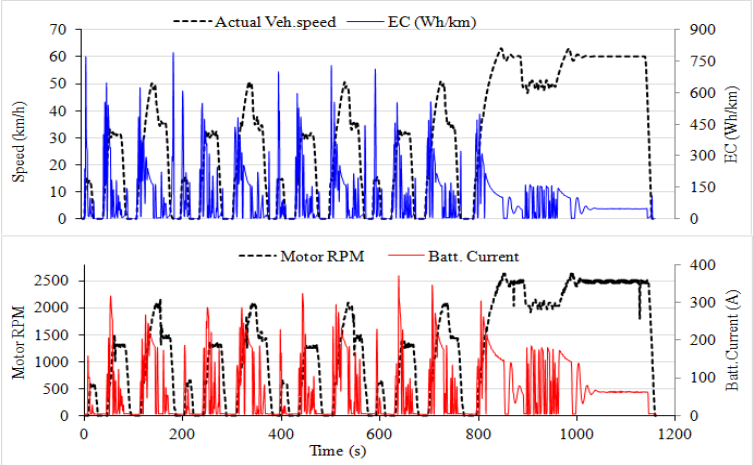

Figure 5.31. Variation of speed, motor rpm, EC_{ind}, and battery (load) current for the MIDC.

The characteristics of load current, motor speed, and mechanical power can help engineers, researchers to improve the motor and battery pack's design and performance. It is known that a higher current will lead to bigger cable-conductor size and higher I^2R losses in the motor and battery. Hence it is necessary to improve the motor design to reduce the load current to avoid the stated losses. It is also essential to know and understand the boundary operating conditions (max. & min values of current, rpm, torque, power) to avoid overloading or overloading the EM. Knowledge of electric motor rpm, maximum torque, and corresponding vehicle speed will help researchers for the right design and selection of the motor for a particular EV. The value of full load current and the average load current is also essential for designing and sizing the battery cells and battery packs. Every EV researcher and engineer desires to develop and use an energy-efficient motor for an extended electric driving range.

5.6.2.5 Comparative Analysis of Energy Consumption for Different Driving Cycles

The test results of the three laboratory tests are evaluated and compared to energy consumption. As shown in Figure 5.32, it is observed that the average electrical EC_{tot} of the test vehicle for the IDC, MIDC-I, and WLTC-low are 106.23 Wh/km, 110.91 Wh/km, and 87.35 Wh/km, respectively.

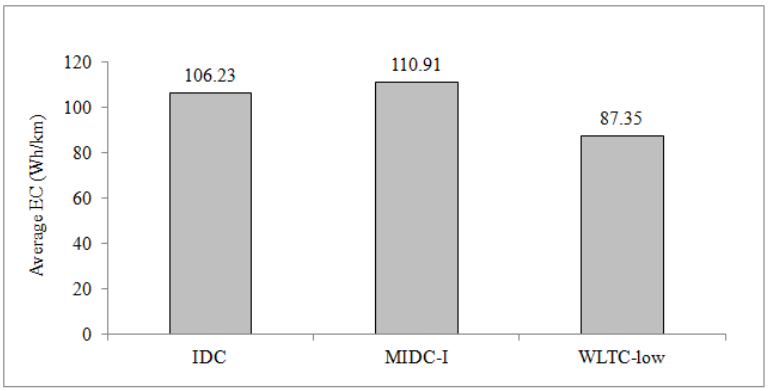

Figure 5.32. Comparison of Energy consumption w.r.t the driving cycles.

Figures 5.33-5.35 show the variation of the calculated or indirect EC w.r.t EV speed for the three cycles. The indirect EC is denoted as EC_{ind} and explained in equation (5.3). It is desired to find out the area of more EC_{ind} concentration that happened in each cycle. The figures show that the EC_{ind} value is spiked (very high) during the starting of acceleration mode in each cycle. Such a situation could be due to the higher current caused by the high torque (higher than the required) during the acceleration mode. The said figures indicate the range of EV speed and EC_{ind}, and most of the energy consumption is concentrated between 0 to 400 Wh/km; as observed, it happens mostly during the acceleration and cruising mode. The variation of power consumption (PoC) will be similar to the graphs of EC_{ind} shown in Figure 5.33-5.35, as the EC_{ind} is derived from the values of input PoC and vehicle speed.

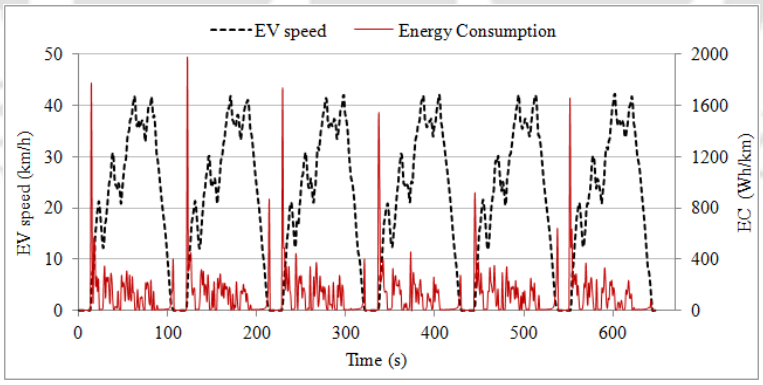

Figure 5.33. Indirect EC and EV speed for the IDC.

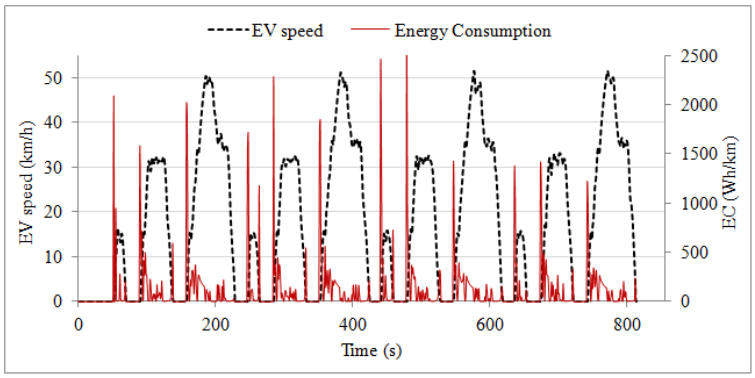

Figure 5.34. Indirect EC and EV speed for the MIDC-I.

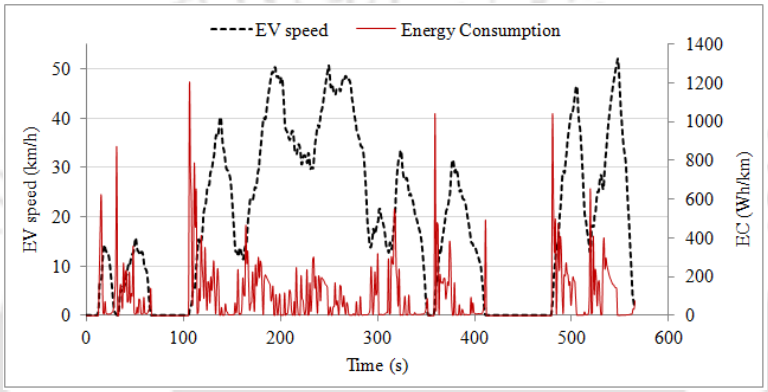

Figure 5.35. Indirect EC and EV speed for the WLTC-low.

5.7 Scope of further work and improvement

Some of the technical challenges experienced during the study in both cases are listed below. These challenges are due to the lack of proper equipment, tools, hardware, and resources. They can be improved with additional hardware and research works.

- The regenerative power that occurs during the deceleration mode is not recovered in the study due to the hardware limitations and equipment used.
- The durability of the new coupling devices is not evaluated as the total distance traveled is less than the targeted maintenance-free range of 5,000km. With the increase in battery capacity (Ah), it is expected to increase the electric range and vehicle weight. However, the literature search is done to examine the impact of vehicle weight on EC, and it has been discussed in this Chapter.

- Experiments and discussions about LiB life and stability are not done due to a lack of knowledge and experience of research and analysis on the anode, cathode materials and electrolyte used, and the BMS.
- It is planned to study and prototype a new VCU for the EV using an open ECU. The necessary algorithm development and software coding are going to be done in-house. These open ECUs are commercially available in the market. The complete EPT with the local EM, parts, and programmed VCU is planned to be sent as a kit for 'Type Approval' at an approved testing agency.

5.8 Conclusion

The laboratory study has been conducted for the two electric vehicles as per the prevailing AIS-123 (Part-3) procedure. Before and after the conversion, their performance evaluations have been done in the chassis dynamometer laboratory as per the AIS standard. The new EPT has been prototyped and implemented using the local EMs for both EVs. The methodology and test algorithm are discussed for both EVs. The EV-I has used the DC motor drive system due to high starting torque, low-cost hardware simplicity, and easy availability. The EV-II uses the local 3P-IM and standard IFOC motor controller, the local LiB pack. Prototyping for a low-cost powertrain using local IM is attempted for the EV-II during the study. The test instruments have been deployed, and performance parameters have been measured for both EVs on the dynamometer. The EV-I has been evaluated using only the IDC.

However, the IDC, MIDC-I, and WLTC-low cycles are used for the EV-II performance tests. Detailed performance evaluation and drive cycle analysis are performed. The test results have been analyzed, discussed, and presented. The uncertainty analysis has also been done for the measured parameters of the EV-II and mentioned in Appendix A.5 and described in Table A.5.2. The initial feasibility study conducted for the EV-I has given a pathway for further research and investigation for the EV-II. The study investigates EV speed variation, motor rpm, battery current, torque, EC, input, and output power during the four drive modes of each driving cycle. It attempts to determine the areas of further improvement for the motor drive system and vehicle performance. The performance evaluation and the drive cycle analysis indicate the scope of improvement in the powertrain system for better performance, I^2R losses reduction, and less EC. The study also indicates the importance of the selection of the right EM and drive system. The test results obtained from the study could be informative and useful for the local

Indian companies manufacturing EV components, traction motors, and LiBs. The data can be considered as a reference for any similar EV model having a similar EPT.

The following results are observed and experienced from the EV-I:

i. It is observed (for the test cycle) that the average vehicle speed and energy consumption of the EV are 21.84 km/hr and 94.71 Wh/km, respectively. The motor current reaches the maximum 182.90A during the acceleration-mode.
ii. The average and maximum torque are 18.01Nm and 211.21Nm, respectively.
iii. The motor current reaches 250-260A momentarily during the free-acceleration tests.
iv. The maximum power efficiency (battery to vehicle wheel) for the EV Powertrain System is 54.15%.

The following results are experienced and observed from the performance evaluation and drive cycle analysis of the EV-II:

a. During the acceleration mode, the maximum battery current observed is 260.60A for IDC, 255.01A for MIDC-I, and 200.27A for the WLTC-low cycle. The battery current is also observed, reaching 245-301A momentarily during the free acceleration tests. These results provide a useful and operating current range for the LiB. And the capacity (Ah) of the LiB needs to be double for an electric range of 50km/charge.

b. It is observed that the EC of the test vehicle is 106.23 Wh/km for the IDC, 110.91 Wh/km for the MIDC-I, and 87.35 Wh/km for the WLTC-low cycle, respectively. The EC is found higher in the acceleration mode in all the drive cycles. It shows that the vehicle needs improvement for operation in the acceleration mode. The test vehicle's top speed is 64 km/h, whereas the commercial EV has a top speed of 80 km/h and the EC of 88.00Wh/km. It indicates that the vehicle speed and EC of the test vehicle need performance improvement.

c. The average and maximum torque are 38.14Nm and 329.81Nm for the IDC, 38.10Nm, and 446.80Nm for the MIDC-I, and 35.28Nm and 334.73Nm, for the WLTC-low, respectively. The max. torque is observed higher than that of the required torque and the commercial EV. The results show the requirement for redesign and redevelop the 3P-IM to reduce the maximum torque and optimize the operating torque range.

d. The EV's maximum efficiency is observed to be in the close range of 66-67% for all three cycles, whereas the commercial EVs have 69-72% efficiency.

e. Therefore, the retrofitted EV needs improvement for the higher vehicle speed, reduced maximum battery current, better EC, and vehicle efficiency by improving the 3P-IM for higher

motor speed to meet the speed of 80km/h and right operating range of torque. Such an EV is best suited for intra-city mobility.

The experiment's results indicate the limitations of a laboratory study due to the inability to emulate actual real-world driving conditions. Many research studies reveal and conclude that laboratory tests may not give a realistic assessment of vehicle performance test data of actual on-road conditions. Thus, it has become necessary to conduct a real-world study for realistic and accurate EV data. A real-world study has been conducted for the EV-II, and the detail is described and discussed in the next Chapter 6.

Chapter 6

Real-world EV Energy Consumption and Performance Evaluation in a Tier-II Indian City

6.1 Introduction

Chapter 5 has described and discussed the laboratory study for the EVs. Several computer simulation studies and EC estimation experiments are reported in the literature review section and discussed in Chapter 2. Most of them have limitations of accurately emulating the real-world EV testing. The laboratory (dynamometer) tests are standard, accurate, repetitive, and suitable for precise comparisons between different vehicles in a controlled test condition. However, they have limitations in emulating vehicle evaluation under real-world driving conditions affected by traffic, weather conditions, and variations in road gradient and in-vehicle weights [Ray Galvin, 2017]. The laboratory testing has other limitations, such as the acceleration, deceleration, and average speed of the laboratory driving cycles are quite different from real-world tests. Another limitation of a laboratory test is that the vehicle wheels' resistance forces are derived from the car coast-down test. The coast-down test is conducted under different testing conditions, which may not precisely reflect the real-world road's resistances.

In India, the chassis dynamometer testing with MIDC does not truly represent the actual on-road (real-world) driving conditions, and the detail is discussed in the literature review section. Indian researchers need to conduct real-world studies for EV performance, total EC, and PoC for EVs in the Tier-II Indian cities for a realistic approach and real-world test data. The analysis of real-world EC characteristics is an essential foundation to study the EC factor for EVs. The EC factor is a correlation factor (value) to estimate and relate real-world EC to various EV models' laboratory EC data. The real-world EV studies are little reported in the literature from the Indian perspective.

In this chapter, the real-world study of the EV-II is described and discussed. A similar real-world study has been conducted and reported in the paper [Lairenlakpam, R., 2018]. It reports the analysis of the effect of real-world driving on vehicle parameters of an ICE vehicle. Some

of the above-stated limitations of laboratory tests are addressed in this chapter. The present study investigates the effect of real-world driving and drive-modes on the crucial EV parameters (such as total EC, battery current, input power) and vehicle performance. It also reports the real-world driving analysis to identify and understand the on-road performance and energy-efficient routes to achieve a better driving range. The knowledge of energy-efficient routes may help forecast the driving range on the traffic routes. It can also reduce the risk of running out of electricity before reaching the charging station or destination. GPS mapping for the real-world EC along the vehicle GPS path is discussed in this chapter; such a GPS mapping is seldom reported in the literature from the Indian scenario standpoint. However, the EV-I is not evaluated for real-world operation as it has a speed limit of 39 km/h and unbalanced vehicle-weight distribution (as described in Chapter 4).

Researchers may find useful information and data from such a study to establish the energy-use strategy and EC factor for the metropolitan and Tier-II cities. It may also help the researchers to figure out new methods and means to minimize the driving range anxiety among EV users and drivers. Test data from such a study may also help researchers working on a virtual test driving for powertrain applications like real-world driving simulation environment (e.g., CarMaker simulation software from IPG Germany [CarMaker IPG, 2020]. Such a solution can take the real-world test driving to the test bench, emphasizing reproducibility and flexibility. The real-world driving simulation may become a faster and economical testing solution in the future.

The present chapter is organized and discussed in six sections; namely, i) Real-world Test Description, ii) Route Selection, iii) Real-world EV Performance Tests, iv) Experimental Results and Discussion, v) Sensitivity Analysis, and vi) the chapter concludes with the real-world testing perspective and potential benefits.

6.2 Real-world Test Description

The section describes the real-world testing and evaluation for the test vehicle (EV-II) only on the selected three traffic routes (representing congested, medium, and low traffic routes) of a Tier-II Indian city (Dehradun). As discussed in Chapter 3, the two measurement methods (direct and indirect) are employed to generate the test parameters. The primary motor parameters, such as voltage, current, and motor rotation, are measured using the direct method. The indirect method offers the power-speed-based indirect EC (EC_{ind}) data, the battery's input

power (PoC), and their characteristics observed during real-world vehicle operation. An old in-use gasoline car of the same vehicle model is used as a chased car and baseline real-world vehicle emissions. The in-use gasoline car belongs to the same vehicle category and segment as the test vehicle. An onboard Portable Emissions Measurement System (PEMS) is used to measure the real-world vehicle emissions and fuel consumption for the chased in-use car for reference. The chased car is assumed to represent the test vehicle before the electric conversion. As part of this thesis's research work, the real-world vehicle emissions and FC data are measured for the chased in-use car as reference data. The said vehicle emissions and FC data are mentioned in Table A.4.1 in the Appendix. The car-chasing technique is followed for real-world EV testing [Ahmad et al., 2005]. The technique is described in Chapter 3. Figure 6.1 illustrates the car-chasing technique.

Figure 6.1. Car chasing technique for the real-world tests

All the real-world tests for both the chased in-use car and test vehicle were conducted in December'19 and February'20. Dehradun's average ambient temperature during December and February is usually 22-26°C [MCDDN, 2020]. The real-world test is done during these months to have a testing condition similar to the laboratory's temperature 20-30°C [TAP-115/116, Issue No. 4]. Thus, the vehicle's Mobile Air Conditioning (MAC) system is deactivated for real-world tests. MAC is also not utilized due to i) the smaller battery pack used for the study. ii) battery is mainly used to provide energy for traction. Apart from these reasons, some studies from the literature indicate that MAC (i.e., cooling and heating) causes about a 33% average decrease in the driving range. Heating load leads to three times more reduction of driving range than cooling load [Jong et al., 2013; Brahim et al., 2013]. The air-conditioner

consumes approximately 25% to 50% of the total power consumption on a hot summer day [Seishiro et al., 2015].

On the other hand, it is reported that the energy consumption of morning peak hours is the highest during a day with an increase of 6.57% than that in off-peak hours. The average speed is the lowest in morning peak hours, followed by evening peak hours. The average EC of peak hours is 4.59% higher than that of off-peak hours on weekdays and 5.04% on weekends and holidays [Jin et al., 2020]. Some researchers have also reported that the EC during peak hours is 8.2% higher than the off-peak hours [Ruoyun et al., 2019]. Likewise, several other literature studies have reported that more energy is consumed during peak-hour vehicle operation than the off-peak hour operation. Therefore, all the on-road tests for the test vehicle are conducted during off-peak hour traffic conditions. During peak hours, vehicle testing can increase idling mode share compared with off-peak hours and have lower average vehicle speed, as traffic congestion is more severe during peak hours. Vehicle operation during peak hours can also experience frequent stop-go operations.

The on-road test is repeated during morning peak hours only on the part of the highway due to the pandemic lockdown restrictions on non-essential vehicles' movement on all the routes except for the highway. For the test repeated on the highway, the off-peak test and peak test have an average vehicle speed of 30.68 km/h and 32.9 km/h, respectively, which are higher than that of the MIDC. The peak-hour test EC_{tot} is 2.1% higher than the off-peak test's EC_{tot} test for the highway portion. Such a marginal difference can be due to the lockdown restrictions leading to probably a new low traffic condition all the time (a new normal) as all the educational institutes are closed. Offices are working with reduced staff capacity. There is not much difference observed between the peak-hour and off-peak hour traffic on the routes.

Moreover, in Dehradun, the morning peak hour happens between 7-10 am (IST) due to the school and office goers and commuters. Evening peak hour happens between 5-7 pm. All the on-road tests have been conducted with extra care to ensure uniform test conditions, such as testing timing (for traffic conditions), battery SoCs, and tire pressure. However, this study does not consider the losses unrelated to the driving cycle and real-world driving. It also doesn't include the thermal aspect of the motor, battery, and vehicle. Future regulatory test cycles may consider peak-hour studies and driving speeds of Indian cities, especially for the megacities like New Delhi, Mumbai, Chennai, Kolkata, etc.

6.3 Route Selection and Real Driving Cycles (RDC)

The traffic route selection for the study has been described in Chapter 3. Based on the traffic route selection, the real-driving cycles (RDC) have been described in Chapter 3. The identified RDCs are the low, medium, and congested traffic routes. These routes include different traffic roads (i.e., city driving, suburban, and highway driving) for various vehicle speeds and road gradients that can be experienced in a real driving situation.

6.4 Real-world EV Performance Tests

The same test drivers have operated the EV-II and the in-use ICE car on the selected routes. The data-logger records the voltage, load current supplied by the battery to the motor controller-inverter. The laboratory test shows the electric driving range limitation of 25 km per full charge. Therefore, due to the range limitation, the test vehicle is tested for a distance of 24 km per trip. The vehicle evaluation has been conducted for three days to cover the three traffic routes and maintain uniform test timing. The test vehicle is operated and evaluated for a total distance of 31.3 km. Out of the total distance, the distance covered on the congested traffic route is 11.3 km, the medium traffic route is 12.5 km, and the low traffic route is 7.5 km, respectively.

6.5 Experimental Results and Discussion

In this section, real-world EV energy consumption and performance data are discussed and analyzed in detail. The laboratory test of the EV-II provides the baseline test parameters for the complete MIDC cycle. The laboratory cycle duration is 1160 seconds, and the distance is 10.60 km. As stated earlier, the EV test parameters are obtained using indirect and direct measurement methods. The test parameters such as battery voltage, load current, mechanical power, and vehicle speed are directly acquired using the data logger and dynamometer. The indirect method (calculation based) gives the indirect EC_{ind} and PoC and their characteristics observed during vehicle operation. The onboard instruments (power meter, data-logger) have measured and provided the test data of the EV on the three traffic routes. The PEMS has provided the baseline vehicle emissions data of the chased in-use car. The in-use car's test data is included in Table A.4.1 in the Appendix of this thesis. The vehicle emissions data provides a fair idea about the test vehicle's condition (before the electrification). The chased in-use car belongs to the same vehicle model and represents the test vehicle before conversion.

Validated methods or data are not available in the literature to quantify some non-measurable uncertainties such as driving habits, pedestrian activities, and road conditions experienced during the real-world testing in Dehradun. The real-world tests are not repeated and cannot be replicated precisely in the same driving manner and test conditions due to the above-stated uncertainties and limited resources.

6.5.1 Variation of Real-world Power and Energy Consumption

The traffic conditions in Dehradun are unpredictable, with pedestrian activities and narrow roads. Figures 6.2-6.4 show the dynamic nature of the battery current, vehicle speed and calculated electrical power, and EC obtained from the on-road testing. The description and formulas for EC_{ind} and PoC have been discussed in Chapter 3. The results show that the indirect values of EC and PoC closely relate to vehicle speed, acceleration, and frequent stop-go vehicle operations.

There is no vehicle stoppage (idling) observed on the low traffic route, leading to the highest average $EC_{ind.}$ Such a situation is shown in Figure 6.2 by the speed's dotted line, where the speed line is not reaching zero speed. However, Figure 6.3 shows several vehicle stoppages and frequent acceleration-deceleration on the medium route, causing more average EC_{ind} and more energy consumption than the congested traffic route. Figure 6.2 through 6.4 also indicates the possible range of vehicle speed, battery current, and power that can be experienced in a similar city.

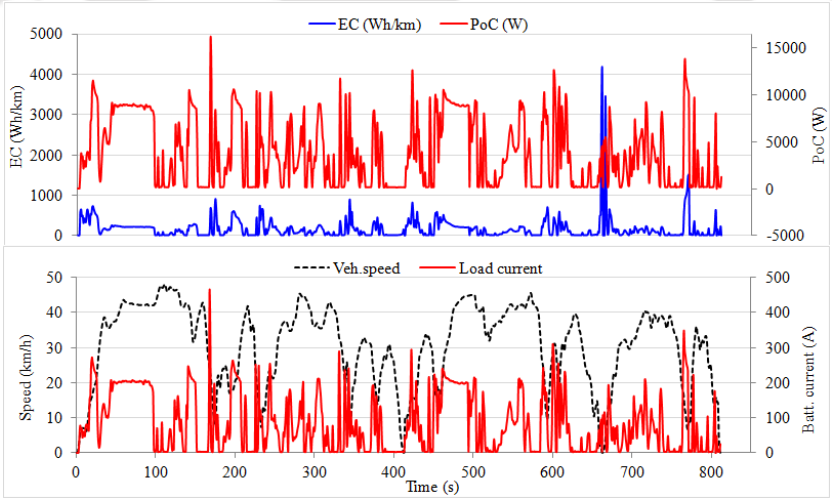

Figure 6.2. Variation of load current, vehicle speed, EC_{ind}, and PoC on the time scale for the low traffic route.

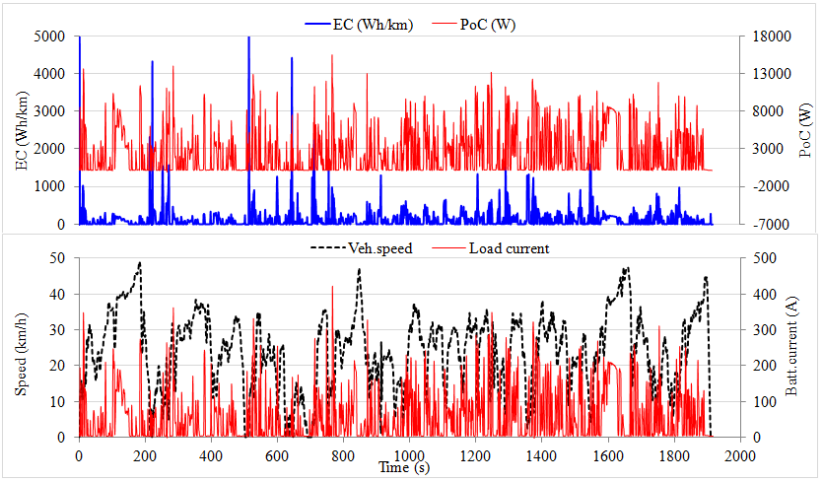

Figure 6.3. Variation of real-world EC_{ind}, PoC, load current, and vehicle speed on the time scale for the medium traffic route.

Figure 6.4 shows more vehicle stoppage with longer idle time on the congested route. It is illustrated by the dotted speed line, indicating lower average speed and less energy consumption on the road contributing to the lowest average EC_{ind}. More vehicle stops can be due to the vehicle passing through the railway station road, one of Dehradun's most congested traffic routes.

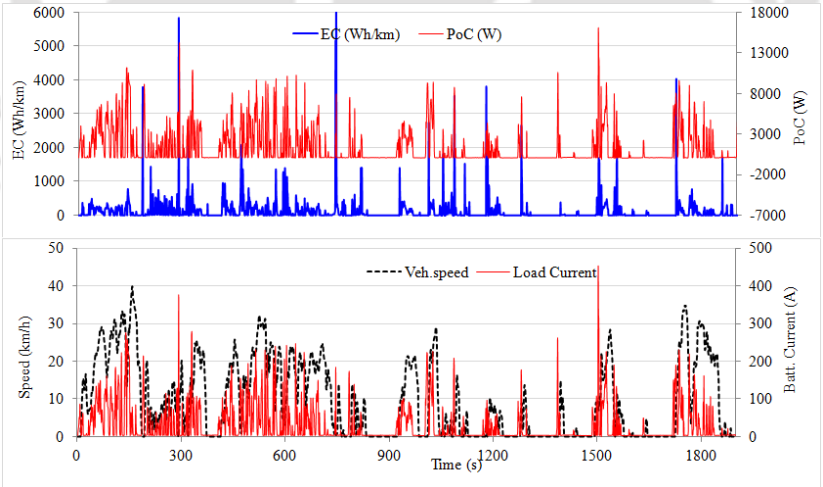

Figure 6.4. Variation of real-world EC_{ind}, PoC, load current, and vehicle speed on the time scale for the congested traffic route.

Figure 6.5 shows the change of current, voltage, and input power when the vehicle starts moving from a standstill condition (traffic stop). In Figure 6.5, markers named 1,2,3,4, and 5 illustrate the rapid increase in speed, current, and power, indicating the vehicle's movement

from the standstill condition. The battery voltage varies between 40-50 V. Such a range of test parameters can be useful for improving the motor and battery pack's design. When the battery voltage is low, then the battery current is high and vice versa to meet the 'go' operations' torque requirement.

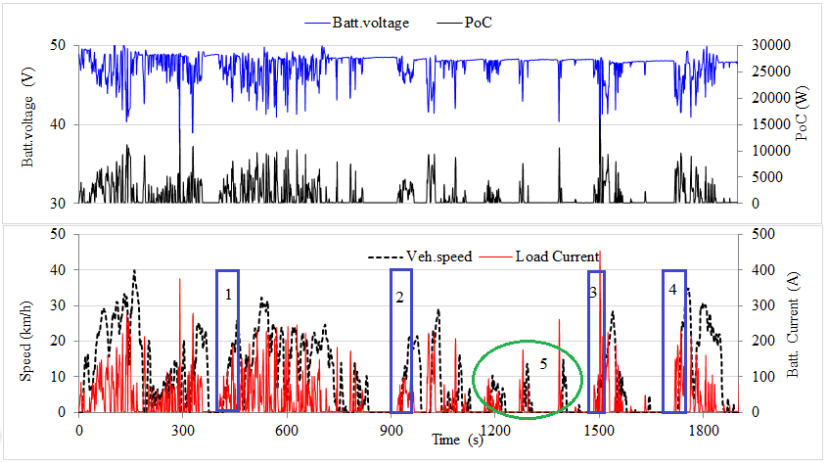

Figure 6.5. Change of load current, voltage, and PoC while moving from standstill condition on the congested traffic route.

It is reported in the literature that changes in vehicle mass does not appear to have an enormous impact on energy consumption in highway driving. Some studies in the literature show that a decrease in mass of 250 lb (~113.4 kg) results in an improvement in FE of 0.53 to 1.6 miles per gallon (mpg) for ICE technology. It is equivalent to a ratio of 0.37 to 1.2% energy consumption for percent mass change [Carlson et al., 2013]. These results do not dictate other makes and models of ICE vehicles, HEVs, and BEVs. The Nissan Leaf varies by 0.03 on the highway, 0.34 on Aggressive, and 0.42 on the city-road (% EC divided by % Mass change ratio) [Carlson et al., 2013]. The test results of similar studies on EVs are seldom reported in the literature.

6.5.2 Share of the Real-driving Drive Modes

The drive-modes of a standard test cycle are idling, acceleration, deceleration, and cruising. Likewise, real-driving consists of the same drive-modes. Figure 6.6 presents the shares of four drive-modes for all the routes. The acceleration range shares are from 12.34% to 17.11% among the three traffic conditions, and the deceleration range is 12.19% to 19.35%. The acceleration share is slightly lower for the medium and low traffic than deceleration, indicating that vehicle speeding down is usually more rapid than speeding up. From the low traffic to medium, to congested traffic route, the share of idling increases from 0% to 2.09%, and

34.31%, while cruising decreases from 67.69% to 61.87%, 38.74%, respectively. Such a case can be due to the road characteristics (variation in the speed limit and traffic crossings) of the three routes, as drivers are more likely to stop frequently in congested driving or at traffic crossings on the medium and congested roads.

The percentage contribution of acceleration and cruising during highway driving is higher than city driving, indicating more highway driving energy consumption. There is no idling-mode observed on the low traffic route, meaning more EC requirement. The analysis indicates that EV driving is more energy efficient in congested traffic, which is one of the main reasons for operating HEVs in electric mode while driving on city roads where EV mode is more efficient, whereas ICE mode is more efficient on highways. It is also observed that no electrical energy is consumed during the deceleration mode for the EV. Instead, regenerative power is generated during deceleration. However, a detailed analysis of the regenerative power is not discussed and covered in this thesis. Vehicle testing may increase idling and acceleration share during peak hours compared with off-peak hours due to more traffic congestion during peak hours. The share of acceleration and deceleration mode may also get changed depending on the moderate or aggressive driving. However, the percentage share of all drive-modes is likely to remain the same if the vehicle is re-tested on the same routes at the same day-timing until road infrastructure and traffic management get changed.

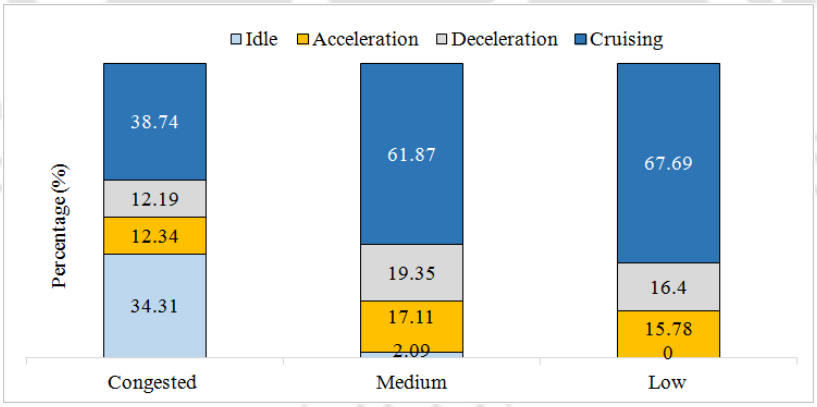

Figure 6.6. The share of driving modes for the different traffic routes.

6.5.3 Analysis of Real-Driving Cycle's Drive-modes for EV parameters

As stated, the four drive-modes are idling, acceleration, deceleration, and cruising. The load current, EC, and PoC data are divided into these four modal categories for the road data. It is a standard practice to define and follow the limits for acceleration and deceleration as per the document of 'Type Approval Procedure' (TAP) [TAP-115/116, Issue No. 4]. The percentage

of time spent in the different drive modes is based on the procedure's limits. The drive-mode definitions and limitations are recalled as follows.

- Idle - speed equals zero km/h.
- Acceleration - Speed greater than 0.139 m/s^2
- Deceleration - Same as acceleration except that acceleration should be negative.
- Cruising - Speed greater than 5km/h and acceleration greater than 0.139 m/s^2.

However, for real-world driving, there is a fifth drive-mode called 'Creeping' having to speed less than 5 km/h, acceleration, and deceleration less than 0.1 m/s^2 [Nesamani et al., 2011]. The creeping mode is commonly used for real-world studies, especially for on-road testing on heavy traffic routes where vehicle speed less than 5 km/h can happen due to traffic congestion.

The Microsoft-Excel software enables us to i) save all the test data as macro-enabled and ii) use the computer program in the Excel software that segregates the drive-modes along with the corresponding test data. The computer program is the same one used for the laboratory study except for the row and column positions. The program calculates the percentage (%) distribution of time spent, load current, EC_{ind}, and PoC for each traffic route drive mode. The program is described in the Appendix.

Figures 6.7-6.10 illustrate the percentage distribution of time spent, EC_{ind}, PoC, and load current on each of the four drive-modes to the total trip value for the parameters (time, EC_{ind}, PoC, load current). Figure 6.7 shows the drive-modes distribution with test parameters for the laboratory test. MIDC has Phase-I of 780 seconds and 4.03 km (out of the total cycle of 1160 seconds and distance of 10.60 km). MIDC has Phase-II of higher-speed operation, long-distance, and significant contribution by cruising mode, as described and discussed in the previous section. Therefore, as shown in Figure 6.7, the cruising mode has the highest duration of steady-speed vehicle operation and, subsequently, the highest contribution to PoC for the cycle. The second highest contribution is made by acceleration mode for the cycle.

Figures 6.8-6.10 show the drive-modes distribution for real-world tests. It can be observed from the figures that the vehicle idling is more on the congested route having an idle-percentage of 34.31% of the total trip duration. In contrast, the other two routes have a lesser idle-percentage (time). Such a situation indicates that EC is less on the congested route as the motor

drive system does not consume any energy for traction during idling mode (zero speed). The laboratory's (MIDC) idling percentage is 23.41%, as shown in Figure 6.7.

It is also observed from the test results, especially from Figures 6.8 and 6.9, that the acceleration and cruising mode are the most critical contributors to the total power and energy consumption on the low and medium traffic routes. For illustration, cruising and acceleration mode's cumulative power consumption is 83.60% on the low traffic, 79.32% on medium traffic, and 71.30% on congested traffic routes, respectively. Hence the cumulative EC of cruising and acceleration mode is highest on the low traffic, high on the medium than the congested route.

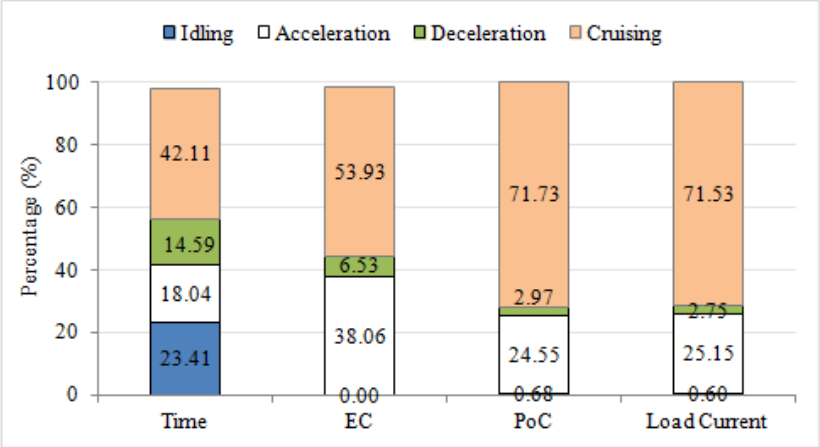

Figure 6.7. Percentage distribution of time spent, EC_{ind}, PoC, and Load current w.r.t the drive-modes on the driving cycle (MIDC).

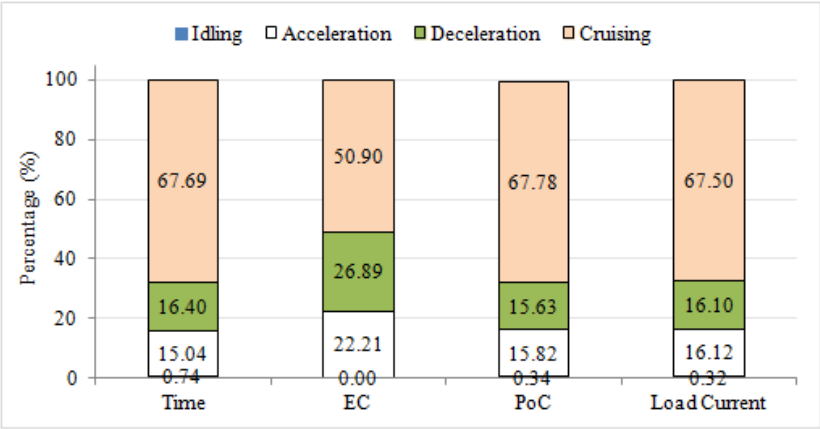

Figure 6.8. Percentage distribution of time spent, EC, PoC, and Load current w.r.t the drive-modes on the low traffic route.

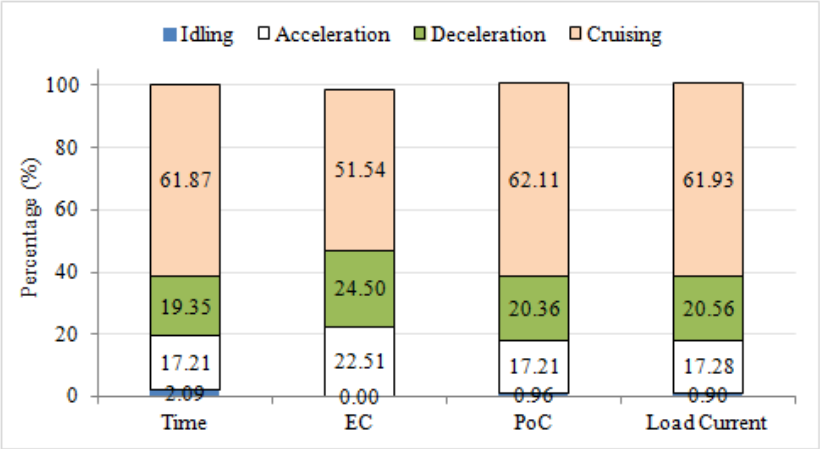

Figure 6.9. Percentage distribution of time spent, EC_{ind}, PoC, and load current w.r.t the drive-modes on the medium traffic route.

The creeping mode is observed on the congested route and has a vehicle speed of less than 2 km/h. Figure 6.10 shows that the creeping-mode spending 3.5% of the total trip time on the congested route, contributing 15.90% to the total trip energy consumption. However, the drive-modes' percentage contribution may vary depending on the traffic conditions on the same road.

A study reports that the difference between driving moderately and more aggressively can make approximately 30% difference in EV energy consumption, amounting to 30 g/km of CO_2 (equivalent) over the driving cycle used [Bingham et al., 2012]. Therefore, there is a scope for EC improvement during the acceleration mode with proper driver-training to avoid hard and repeated accelerations.

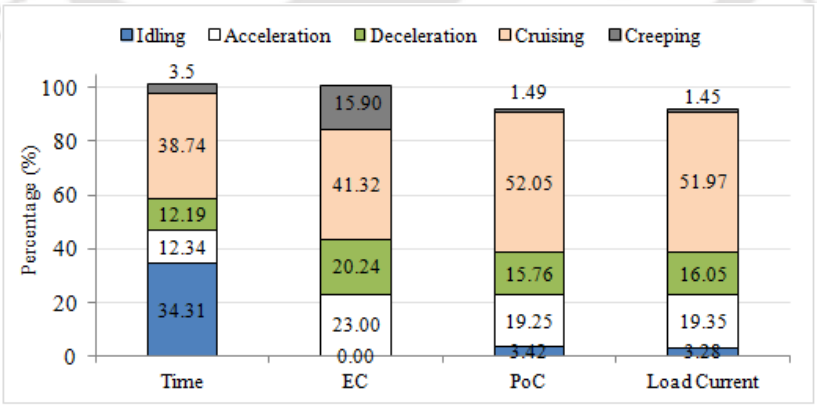

Figure 6.10. Percentage distribution of time spent, EC_{ind}, PoC, and Load current w.r.t the drive-modes on the congested traffic route.

Vehicle speed is an essential indicator of driving patterns and traffic flow that can impact vehicle energy consumption and traffic efficiency in a city. Table 6.1 presents the speed cluster

(range) distribution for the three routes. Over 77% of city driving (congested traffic) is in the cluster with an average speed of less than 20 km/h, indicating less EC. In contrast, over 78% of the highway driving lies in the cluster with an average speed of more than 20 km/h but less than 60 km/h, indicating higher EC. The above-stated observations also suggest that the EV operation is more energy-efficient in congested traffic conditions. Researchers can conduct more of such study and analysis to establish a robust scientific database and help the stack holders develop suitable charging infrastructure and routing strategies in urban areas.

Table 6.1 Vehicle speed cluster distribution

Speed range	Percentage (%)		
(km/h)	Congested	Medium	Low
0-20	77.73	33.7	21.08
20-60	22.6	65.88	78.92

6.5.4 GPS Mapping of Measured Data for Real-World Test

PEMS's software is used to analyze the EC_{ind} data and mapped along the vehicle GPS path. The software generates Figures 6.11-6.13. The software has a unique feature called 'Map Data Analysis.' The feature is applied to create GPS mapping with the location coordinates and corresponding on-road test data. Figures 6.11-6.13 show the EC_{ind} data along the GPS vehicle path for the low traffic, medium traffic, and congested traffic routes. The data represented by each dot is the EC_{ind} sampled for every 15 seconds to look them decongested for the mapping. The low traffic route is the portion of the National Highway (NH-72). The analysis observes more cruising mode with higher load current, causing higher EC_{ind} on the low traffic route. Figure 6.11 shows the EC_{ind} data mapped along the GPS path, and bigger red dots represent the higher EC_{ind} on the low traffic route. The higher load current and EC_{ind} on the low traffic route is probably due to the NH route characteristic. The vehicle spends more time on a steady-speed operation that causes more EC_{ind} and higher average speed but spends no time on idle mode. There are negligible decelerations observed during such a steady-speed operation on the highway, causing no regenerative power generation. The situation stated above is also one reason for higher energy consumption on the low traffic route. Similarly, the variation of other

test parameters like load current, PoC can be mapped and analyzed along the GPS path for all the routes.

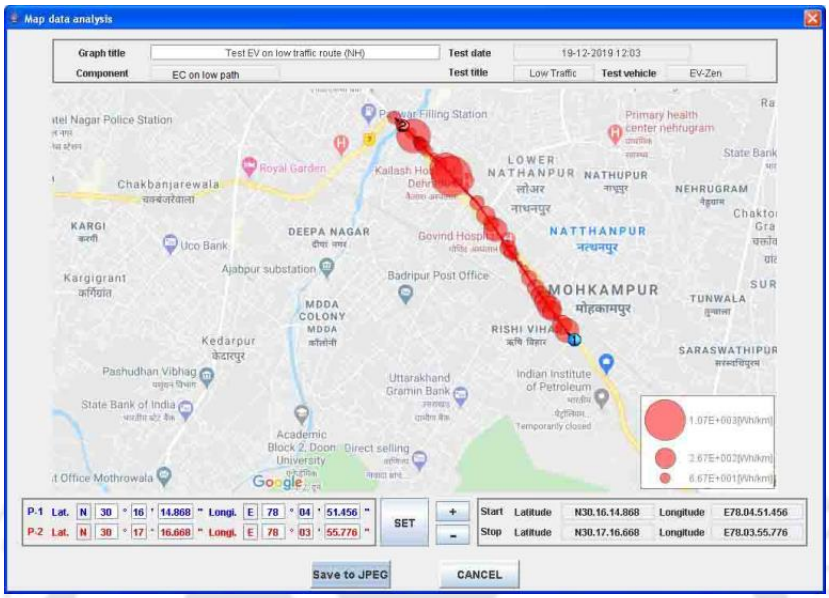

Figure 6.11. EC_{ind} data along the GPS path on the low traffic route.

Similarly, Figures 6.12-6.13 show the EC_{ind} data mapped along the GPS path of the medium and congested traffic routes. Figure 6.4 has also illustrated the highest number of vehicle stoppage (idling mode) observed on the congested road. Figures 6.4 and 6.13 are complementary to each other.

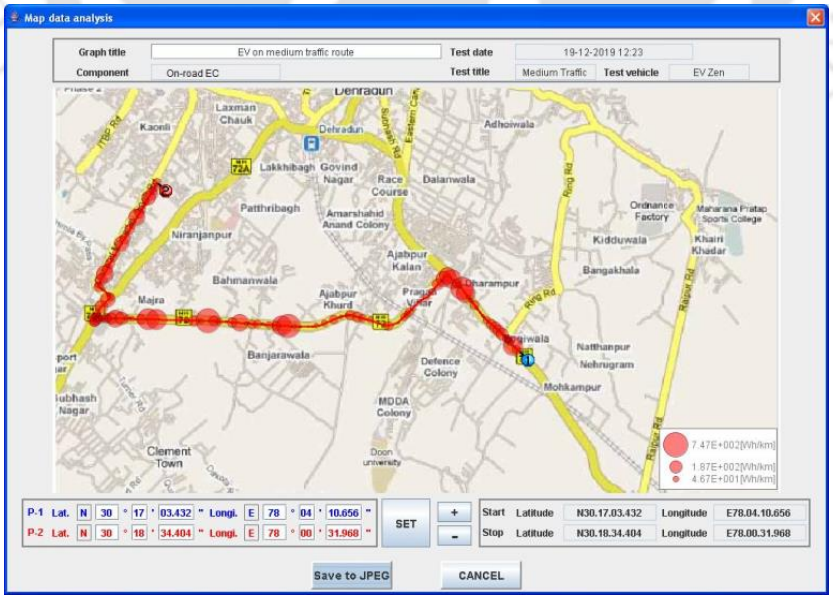

Figure 6.12. EC_{ind} data along the GPS path on the medium traffic route.

The results from such analysis highlight the possibility of energy savings strategy, energy-efficient routing, energy-efficient EV operation that can be accrued by appropriate traffic management, driver training, and long-term road infrastructure development (like over-bridge construction at major traffic crossings). The drivers can get the proper training to minimize aggressive driving and periods of repeated acceleration/deceleration on the congested and medium traffic. The training can also train drivers to allow more prolonged periods of steady-speed vehicle movement and information on corresponding energy saving. They can also be trained and informed about the energy benefits obtained by minimizing hard accelerations during avoidable overtaking.

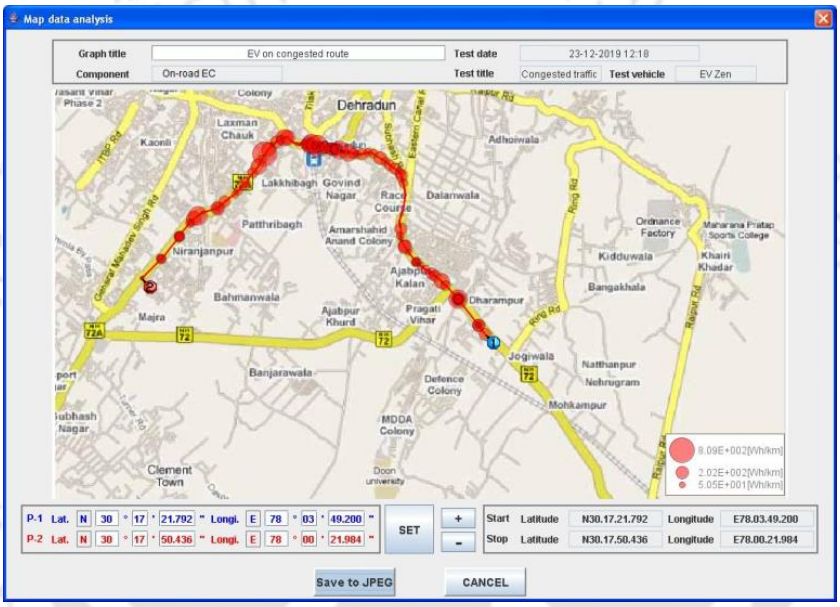

Figure 6.13. EC_{ind} data along the GPS path on the congested traffic route.

6.5.5 Comparative Analysis for the Real-world and Laboratory Data

The section emphasizes the difference between the real-world test data and the laboratory data. It has been reported and discussed the significant difference between the laboratory (certification) cycle and the real-world driving cycle in terms of crucial driving and test parameters. Laboratory cycles demonstrate a large variation from real-world cycles, especially in acceleration and average speed, pointing to a gap between real-world testing and laboratory testing.

The simple equation (6.1) provides the percentage difference between the real-world and laboratory test data. The percentage of the real-world data is calculated w.r.t the laboratory data. The statistical analysis estimates the average EC_{ind} (Wh/km) of each route.

Percentage (%) of the difference of 'x' parameter is given by

$$x\,(\%) = \frac{(\text{real.world value} - \text{laboratory value})}{\text{laboratory value}} * 100 \qquad -- \qquad (6.1)$$

Table 6.2 shows the route-wise distribution of the statistical values of the real-world PoC (kW), load current (A), and vehicle speed (km/h) on the three traffic routes and their difference with the laboratory data. The average speed (of all the three routes) and average total EC_{tot} of the real-world driving tests are 21.37 km/h and 145.83 Wh/km, respectively. The congested route has the lowest average speed than the other routes and laboratory tests, indicating slower traffic and less EC. The average speed is highest on the low traffic route, leading to more EC. The table also shows the range of maximum battery current, 365-445A, which can happen on the city's roads. The range can be useful for the battery companies, other stakeholders, and researchers associated with the charging infrastructure. The total electrical EC_{tot} for the laboratory and real-world tests are given in Table 6.2. The statistical analysis of the laboratory and real-world test data may help to establish the EC correlation factor for the EV in the future.

Table 6.2. Distribution of average vehicle speed, Battery current, and EC of the EV-II

Traffic routes in Dehradun		**Congested**	**Medium**	**Low (highway driving)**	**Lab. (MIDC)**
Distance traveled (km)		11.30	12.50	7.50	10.60
Speed (km/h)	Max.	39.50	48.80	48.00	63.14
	Avg.	9.56	23.88	30.68	29.30
Battery current (A)	Max	444.88	416.21	459.96	365.92
	Avg.	29.51	56.38	85.68	61.00
PoC (kW)	Max	15.72	15.27	16.20	14.48
	Avg.	2.32	2.50	3.84	2.17
Total EC_{tot}	--	125.08	145.72	166.85	88.10

Table 6.3 indicates the maximum and average values of acceleration and deceleration for each test. The maximum acceleration of each real-world test is much higher than the acceleration limit of 1.04 m/s^2 for phase-I and 0.833 m/s^2 for phase-II of MIDC, defined in the TAP

document [TAP-115/116, Issue No. 4, Part XIV, Chapter-3]. However, the laboratory test's maximum acceleration is 1.62 m/s^{2,} which is closer to the acceleration defined in the TAP. The frequency of acceleration is known for the laboratory cycle; however, it is difficult to predict the real-driving tests. The higher acceleration in real-world tests is one of the reasons for higher EC than the laboratory test. The table also indicates the boundary condition of real-driving acceleration and deceleration during the operation of the EV in Dehradun. The boundary condition can be used as an indicator or limit for driver's training. It is reported that aggressive driving behavior involves a decrease in the battery range, which the driver must consider [Roberto et al., 2015]. Such on-road test data indicates a need to equip the vehicle with a system that interacts with drivers to provide information about their behavior at the wheel.

Table 6.3. Route-wise acceleration and deceleration.

Traffic Routes in Dehradun		**Congested**	**Medium**	**Low**	**Lab.**
Acceleration (m/s^2)	Max.	3.86	5.03	2.67	1.62
	Avg.	0.63	0.67	0.62	0.13
Deceleration (m/s^2)	Max.	-3.19	-4.47	-2.64	-1.71
	Avg.	-0.64	-0.67	-0.66	-0.13

It is observed that the average real-world PoC is highest on the low traffic, followed by the medium and congested route, respectively. The analysis has revealed that vehicle operation experiences relatively steady-speed with a higher average speed on the highways, causing continuous power consumption from the primary energy source. Least deceleration and braking are observed on the highways, due to which negligible regenerative power is detected. Similarly, real-world EC_{ind} is higher than the laboratory result by 41.97% on the congested, 65.40% on the medium, and 89.39% on the low traffic routes. It is observed that the average indirect EC gets increased as the traffic conditions become lower or lesser. Similar trends of higher real-world EC are observed in other studies reported in the literature [Paffumi et al., 2015; Chiara et al., 2019]. Highway driving presents the highest energy consumption during driving speed of 50-70 km/h [Paffumi et al., 2015]. The relationship between traffic congestion and energy consumption underlying EVs can change with higher energy consumption connected to an increased average traffic speed [Chiara et al., 2019].

Figures 6.14-6.17 show the difference between the total EC_{tot}, maximum, and average values of load current, vehicle speed, and PoC measured in the real world and the laboratory. It is

observed that the EC_{tot} is higher than the laboratory test data by 1.42 times on the congested traffic, 1.65 times on the medium traffic, and 1.89 times on low traffic routes, respectively. Figure 6.14 shows that all the real-world EC_{tot} are higher than the laboratory data. Similar trends of higher real-world test results than the laboratory result are also observed and reported in the paper [Kezhen et al., 2017; Jan Dornoff et al., 2020].

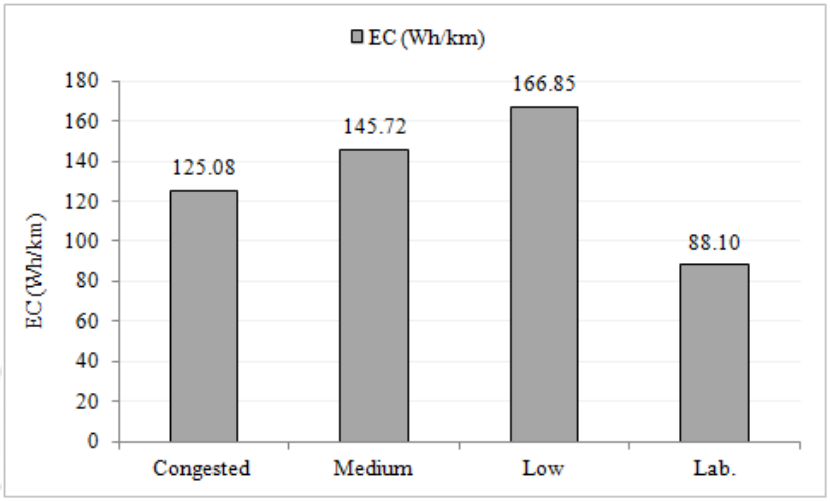

Figure 6.14. Comparison of total electrical EC_{tot}

Figures 6.15-6.16 indicate the range of maximum and average load currents and PoCs for the EV. The graphs show the operating boundary conditions of the load current and PoC (input power) that can happen while operating the test vehicle in the real-world. A maximum current of 460 A can occur on the low traffic route. Such data-range and current data can be beneficial and informative to the battery researchers, manufacturers, and relevant auto industry stack holders. Figure 6.17 shows the range of maximum and average vehicle speed that the EV or a similar EV can achieve and experience while operating in Dehradun.

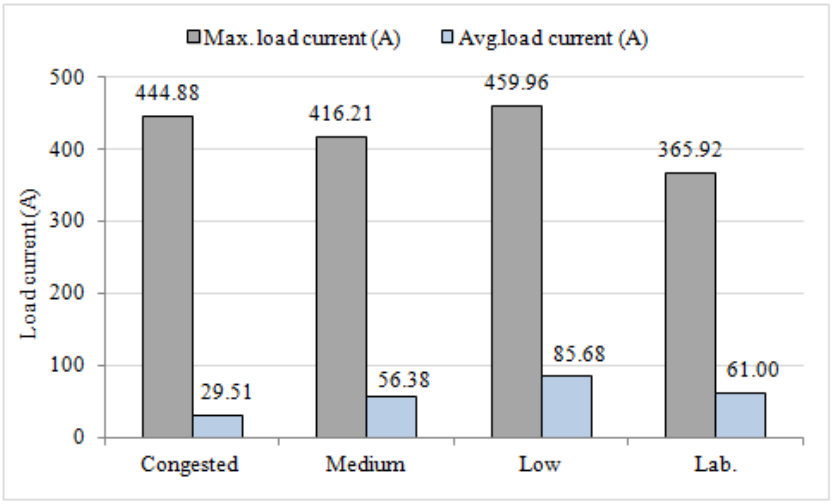

Figure 6.15. Difference between maximum and average load currents.

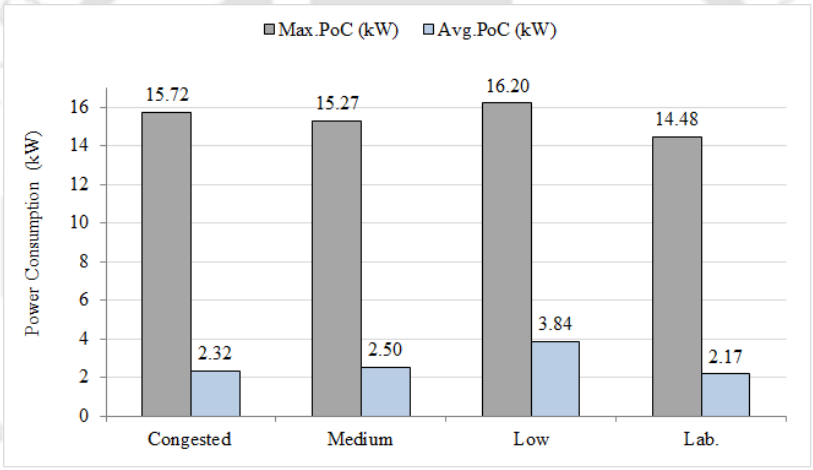

Figure 6.16. Difference between maximum and average power consumption.

The average speed is the key information for the average EC of an EV in real-world operation as higher average speed leads to higher EC_{ind} and EC_{tot}. As shown and discussed, the average vehicle speed is lowest on the congested route and highest on the low traffic route. The maximum speed of 63.14 km/h is achieved in the laboratory, and speed hardly reaches 49 km/h in real-world driving, owing to different traffic congestion on the routes. Research works in EV are in the initial stage in India. Such vehicle performance data from real-world tests can be useful for EV companies and EV motor manufacturers. Therefore, engineers and researchers need to conduct more experiments and investigate energy-efficient algorithms, controllers, devices, routes, and methods to achieve more electric driving range and better EV performance.

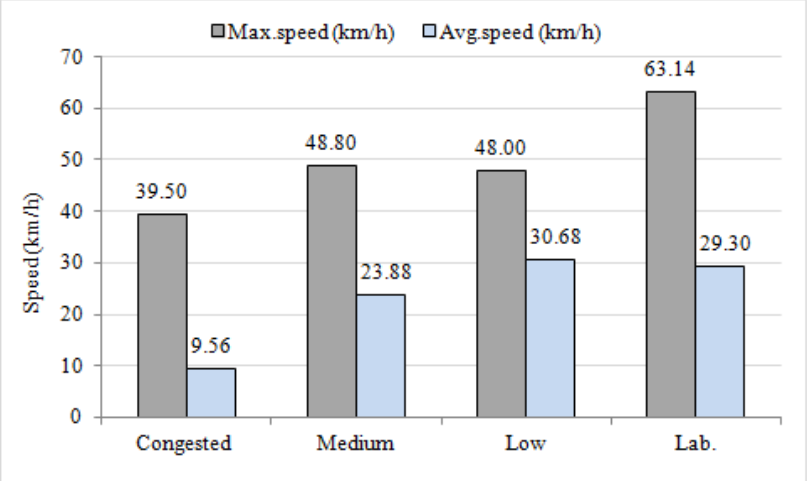

Figure 6.17. Difference between maximum and average vehicle speeds.

6.5.6 Sensitivity Analysis for EC and Driving range

The sub-section presents the sensitivity analysis (single variable method) of the variables that influence the energy consumption and driving range. The variables are kerb weight and battery capacity (Ah). Sensitivity analysis is a method that determines how the target variables are affected by changes in input variables. It is done by changing one parameter (single-variable) while keeping the other parameters at the reference value. It is performed to predict the outcome of a specific range of input variables. The 'What-if analysis' of Microsoft-Excel software is used for the analysis. The sensitivity analysis is done for the study, considering the average values (of all the three traffic routes) given in Table 6.2 and vehicle kerb weight given in Table A.1.1 and A.1.2 in Appendix.

The vehicle parameters (range and battery current) are varied for a range of (0 to 140) with an incremental factor of -20 to +20 from the reference case. The kerb weight is varied for a range of -20% to +20% from the reference case. The vehicle's mass is varied from 564 kg to 846 kg keeping 705 kg as the reference case. Figures 6.18 and 6.19 show the results of the analysis. Figure 6.18 shows the change in battery capacity (kWh) with the change in range, indicating a higher battery capacity (kWh) requirement for a higher range. Figure 6.19 shows the impact of kerb weight on the range, predicting the reduction of range with increased kerb weight.

Vehicle weight is one of the parameters of EVs that affects their dynamic and range characteristics. Some of the research studies report that the driving range of an EV is directly affected by battery capacity, which affects the battery's weight, which means more the battery

capacity more the battery weight. If one uses a 1.1 kWh lithium battery weighing 10 kg, a medium-class EV can travel a distance of 8 ± 1 km [Berjoza and Jurgena, 2017].

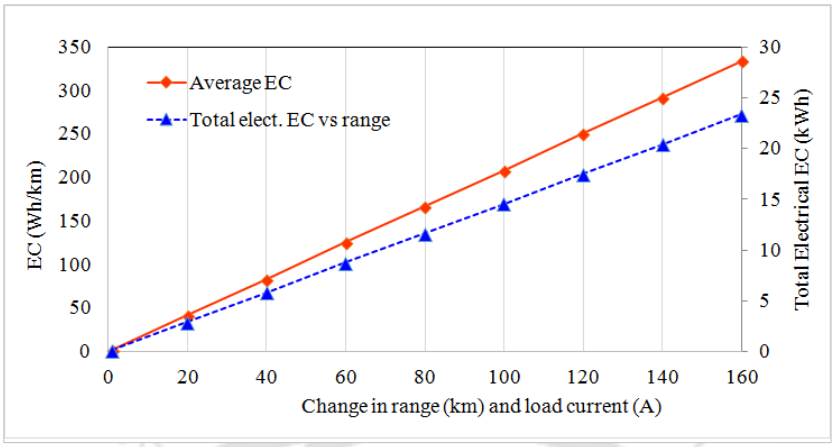

Figure 6.18. Prediction of range with total electrical energy consumption

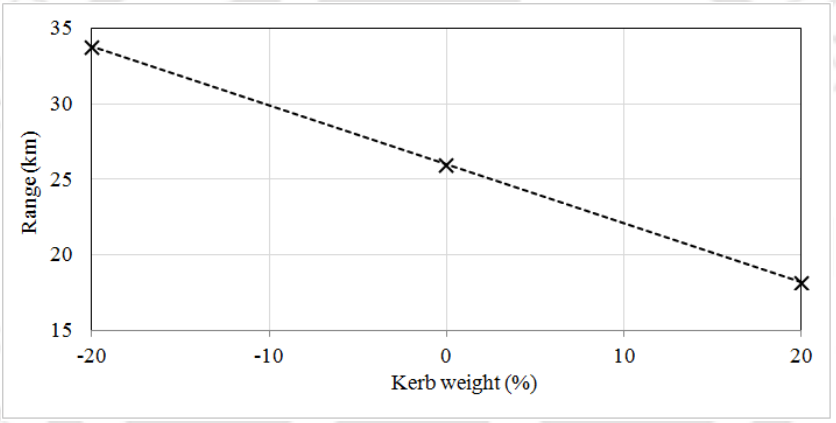

Figure 6.19. Variation of range with Kerb weight

Under normal circumstances, vehicle weight gets increased directly with the battery capacity, and the simplest way to increase EV range is the use of batteries with higher capacity (kWh) [Berjoza and Jurgena, 2017]. The electric driving range is an essential indicator that directly affects the exploitation cost of an EV. This indicator for EVs with high capacity and weight batteries (Kia Soul EV, Tesla) is 80–95% higher than for the EVs with a low gross weight [Berjoza and Jurgena, 2017; Martin Mruzek et al., 2016]. The higher the km indicator, the higher the weight batteries are used in the EV, and the more it is loaded. The above-stated sensitivity analysis is carried out with reference to the methods used in the literature [Berjoza and Jurgena, 2017; Martin Mruzek et al., 2016; Jithin et al., 2018].

It is essential and of great interest to design a mathematical model to perform an in-depth investigation of the effects of the kerb weight, the weight of batteries, various resistance forces on the performance parameters such as energy consumption, range per battery charge, acceleration intensity, maximum acceleration, etc. Such a simulation model can provide interrelationships among the parameters and compare the calculated data with experimental road data in future research.

6.6 Conclusion

The chapter has described and discussed the real-world vehicle data and the performance of the EV-II. It examines the effect of real-world driving and four drive-modes on the EC, PoC, and vehicle performance for the EV in the Tier-II Indian city. It is among the first attempts to investigate the real-world performance of an EV in the Indian context. The analysis used in this research study is based on the standard driving and real-driving cycle analysis. The analysis gives the percentage distribution of drive-modes to the load current, EC_{ind}, PoC, load current of the test vehicle. The study uses the locally developed prototype EV powertrain having the local 3-ph induction motor. It identifies the congested route as the most energy-efficient route for the EV in the Tier-II city. The low traffic condition test shows that most of the driving points are within a specific torque vs. speed range. Therefore, it is vital to improving the motor design with the operating points within the high-efficiency region for operation in low traffic conditions. The comparative analysis of test results reveals the gap between the real-world and laboratory data. The sensitivity analysis has been carried out for the variables that influence the EC and driving range. Generating and making available such data may help the researchers conduct more studies on the possible methods and means to reduce the battery current range and address the drivers' range anxiety. Based on the analysis, the following observations have arrived from the test results:

- The laboratory estimation of the total electrical EC and PoC (using MIDC) does not provide real-world data for Dehradun.
- The study indicates that the dynamometer cycle (MIDC) needs review as the laboratory test does not closely represent the real-world tests.
- It observes that the EV operation is more energy-efficient on the congested traffic route because of more traffic stops (idling mode), lower average speed, and less cruising on the route that results in less energy consumption.

- The low traffic route has no traffic stops (idling-mode) and the highest average vehicle speed, indicating more EC.
- The acceleration and cruising mode combined accounts for 64-75% of the total EC_{ind} on all the traffic routes. The acceleration and cruising modes are the main contributors to the total EC_{ind} and PoC for all the traffic routes.
- The average real-world EC of all the routes is 145.83Wh/km, and the average laboratory EC is 88.10 Wh/km.
- The total electrical EC_{tot} is 125.08Wh/km for the congested, 145.72Wh/km for the medium, and 166.85Wh/km for the low traffic routes.
- The study indicates that the average real-world EC_{ind} is higher than the laboratory test results by 41.97%, 65.40%, and 89.39% in congested, medium, and low traffic routes.
- The study results, especially the load current characteristics, can be a guideline and useful information for improving the motor and battery pack design. Higher current will lead to having bigger cable-conductor size and higher I^2R losses in the motor and battery.
- The study offers a further scope of vehicle performance improvement in terms of higher speed, reduced load current, and improvement in regeneration capability for extended range.

Chapter 7

Conclusions and Future Work

In this thesis, the electric conversion of the two gasoline cars into the experimental EVs has been carried out and presented. The EV conversion process has been described and demonstrated. The electric powertrain has been prototyped and implemented using the local EMs for both EVs. In the first case, the first car (Maruti-800) is converted into the EV-I that has used the DC motor drive system. Due to the EV-I limitations, the second car (Maruti-Zen) is converted into the EV-II in the second case. The EV-II has used the local-make 3P-IM, LiB pack, and a standard IFOC motor controller. Performance evaluations and drive cycle analysis for both EVs have been conducted in the chassis dynamometer laboratory as per the AIS standard. The EV-I has been evaluated using only the IDC. However, the IDC, MIDC-I, and WLTC-low cycles are used for the EV-II performance tests. The performance evaluation and the drive cycle analysis indicate the areas of improvement in the powertrain system for better performance. The analysis indicates the scope of improvement for I^2R losses reduction and less EC. Due to the limitations and inability of the laboratory study to represent the actual real-world driving conditions, the real-world study has been conducted.

The second part of the research work has described the real-world study that emphasizes real-world EC_{ind} and EV-II performance. The field study investigates the effect of real-world driving and drive-modes on the battery current, EC_{ind}, PoC, and vehicle performance for the EV-II in the Tier-II Indian city. It is among the first attempts to systematically compare real-world test data with an EV's laboratory data in the Indian context. The principal analysis done in this study is based on the driving cycle and real-driving cycle analysis. The statistical, comparative, uncertainty, and sensitivity analysis are performed for the EV-II for its laboratory data and real-world test data. The test results reveal the gap between real-world data and laboratory data. Providing such information may help the researchers conduct more studies on the possible methods and means to address drivers' range anxiety.

The following conclusions are drawn from the study:

- The system integration and weight distribution analysis of the EV subsystems has been performed and discussed.
- The study has attempted to investigate a supercapacitor's effect on the electric range using the SC bank of 48 V, 189 F.
- It has been observed that a fully charged SC-bank can power the EV-II for a short distance of around 200 meters (m) before the controller cuts the power off to the 3P-IM. Therefore, it is concluded that the SC bank alone cannot be used to power the EV. However, the SC bank can work in conjunction with the battery so that the SC can absorb the regenerative power and reduce the average energy consumption of the primary energy source (battery).

Laboratory observations for the EV-I:

- It is observed (for the test cycle) that the average vehicle speed and energy consumption of the EV are 21.84 km/hr and 94.71 Wh/km, respectively. The motor current reaches the maximum 182.90A during the acceleration-mode.
- The average and maximum torque are 18.01Nm and 211.21Nm, respectively.
- The motor current reaches 250-260A momentarily during the free-acceleration tests.

Laboratory observations for the EV-II:

- During the acceleration mode, the maximum battery current observed is 260.60A for IDC, 255.01A for MIDC-I, and 200.27A for the WLTC-low cycle. The battery current is also observed, reaching 245-301A momentarily during the free acceleration tests. These results provide a useful and operating current range for the LiB, and the capacity (Ah) of the LiB needs to be double for an electric range of 50km/charge.
- The EC is observed higher in the acceleration mode in all three driving cycles. It shows that the vehicle needs improvement for operation in the acceleration mode. The test vehicle’s top speed is 64 km/h, whereas the commercial EV has a top speed of 80 km/h and the EC of 88.00Wh/km.
- The average and maximum torque are 38.14Nm and 329.81Nm for the IDC, 38.10Nm, and 446.80Nm for the MIDC-I, and 35.28Nm and 334.73Nm, for the WLTC-low, respectively. The results show the requirement for redesign and redevelopment of the 3P-IM to reduce the maximum torque and optimize the operating torque range.
- The EV’s maximum efficiency is observed to be in the close range of 66-67% for all three cycles.

- Therefore, the converted EV-II needs improvement for the higher vehicle speed, reduced maximum battery current, better EC, and vehicle efficiency by improving the 3P-IM for higher motor speed to meet 80km/h and the proper operating range torque. Such an EV is best suited for intra-city mobility.

The laboratory test results indicate the limitations of a laboratory study due to the inability to emulate actual real-world driving conditions. Many research studies reveal and conclude that laboratory tests may not give a realistic assessment of vehicle performance test data of actual on-road conditions. Thus, it has become necessary to conduct a real-world study for realistic and accurate EV data.

The following observations are reached based on the real-world study for the EV-II:

- The laboratory estimation of the EC and PoC (using MIDC) does not provide realistic real-world data for the city.
- It observes that the EV operation is more energy-efficient on the congested traffic route because of more traffic stops (idling mode), lower average speed, and less cruising on the route that results in less energy consumption.
- The acceleration and cruising mode combined accounts for 65-75% of the total EC on all the traffic routes. The acceleration and cruising modes are the main contributors to the total EC and PoC for all the traffic routes.
- The average real-world EC of all the routes is 145.83 Wh/km, and the average laboratory EC is 88.10 Wh/km.
- The average real-world EC is 125.08 Wh/km for congested, 145.72 Wh/km for medium and 166.85 Wh/km for low traffic routes, respectively.
- The study indicates the average real-world EC is higher than the laboratory test results by 41.97%, 65.40%, and 89.39% in congested, medium, and low traffic routes, respectively.
- The research study's results, especially the load current characteristics, can be a guideline and useful information for improving the motor and battery pack design. Higher current will lead to having bigger cable-conductor size and higher I^2R losses in the motor and battery.
- It is of great interest to conduct similar real-world studies for EVs in other Tier-II Indian cities that could have different traffic and road conditions.
- Based on the study, the following research areas are identified for further future study:
  - Study and implementation of a dual gear system
  - Utilization of a higher voltage, higher rpm IM for better EV performance

- Investigation of a supercapacitor's use to reduce average EC from the battery
- Gradeability tests at different gradients for the EVs
- Attempt to use a vehicle control unit (VCU) for energy management and regenerative features.

The study has demonstrated that the electric conversion of ICE vehicles into EVs could be a solution for faster vehicle electrification and mass adoption of EVs. It is also an attempt for Research, Development, and Deployment (RD&D). It has highlighted the importance of addressing the laboratory study's limitations. The study's results have verified the usability of the new prototype EPT having the local subsystems, the system integration approach, and its practical implementation. The study has also indicated considering the real-driving features while reviewing and improving the dynamometer cycles.

Further, it strives to determine a few new research areas and improvements for better performance and mileage for the EPT system. Such a thesis study may provide useful parameters range and boundary conditions for the motor, battery developers, and researchers. It might help local researchers for more research works for the localization of EV subsystems in India. The study is on the right path for the localization of EV subsystems and mass adoption of EVs, aligning with the FAME scheme's objectives and the country's EV policies for fuel savings, vehicle pollution reduction, and intra-city mobility.

List of Publications

Journal Publications:

1. **Lairenlakpam, R.,** Kumar, P., and Thakre, G., "Experimental Investigation of Electric Vehicle Performance and Energy Consumption on Chassis Dynamometer Using Drive Cycle Analysis," SAE International Journal of Sustainable Transportation, Energy, Environment, & Policy 1(1):23–38, 2020, doi:10.4271/13-01-01-0002.
2. **Lairenlakpam, R.,** Kumar, P., and Thakre, G., "Effect of Real-World Driving and Drive Modes on Electric Vehicle Energy Consumption and Performance in a Tier-II Indian City," SAE Int. J. Sust. Trans., Energy, Env., & Policy 1(2):2020, doi:10.4271/13-01-02-0008.

Conference Publications:

1. **Robindro Lairenlakpam,** Praveen Kumar, GD Thakre, "Electric conversion of a gasoline vehicle in an electric vehicle and its performance and drive cycle analysis," IEEE Power Electronics, Drives and Energy Systems Conference (PEDES)-2018, IIT Madras, paper id: 63, 19, Dec. 2018.
2. **Robindro Lairenlakpam,** Praveen Kumar, GD Thakre, Poonam Gupta, Yograj Singh, "Effect of Different Drive Modes on Energy Consumption of an Electric Auto Rickshaw," IEEE International Transportation Electrification Conference (ITEC)-2017, Pune, paper id: S5-73, 13, December 2017.

Appendix - A

Appendix

This section describes the specifications of test vehicles, subsystems, and test equipment. Further, it describes the common analysis methods, preliminary test results, and prevailing automotive standards.

A.1 Test Vehicles Specifications

Table A.1.1: Basic specification of the test vehicle (EV-I) of the Case study-I

Vehicle Model		Maruti-800
Fuel Type		Gasoline
Engine		796 cc, 3-cylinders, four-stroke, water-cooled
Max.Torque		58.80 Nm at 3000 rpm
Max. Power		39.5 HP at 5500 rpm 29.45 kW at 5500 rpm
Kerb weight		620 kg
Transmission Gear-Ratio	1st	3.585
	2nd	2.166
	3rd	1.333
	Top	0.900
	Reverse	3.363

Table A.1.2: Basic specification of the test vehicle (EV-II) of the Case study-II

Vehicle Model	Maruti-Zen
Fuel Type	Gasoline
Engine	993 cc, 4-cylinders, four-stroke cycle with manual transmission
Max. Torque	78 Nm at 4500 rpm
Max. Power	44 kW at 6000 rpm
Kerb weight	755 kg for Manual Transmission (MT) 765 kg for Automatic Transmission

Table A.1.3: Basic specification of the reference EV model

Vehicle Model	Mahindra E_2O-Plus
Motor type	3-phase induction motor
Motor power	19 kW @ 3500 rpm
Motor torque	70 Nm @ 1000 rpm
Controller	600 A
Gear ratio	10.83:1 and direct drive transmission
Battery	Li-ion 48V, 210Ah, 84 kg
Standard electric mileage	110 km
Standard EC	88 Wh/km
Top speed	80 km/h
Kerb weight	940 kg

A.2 EV Subsystem Specifications

Table A.2.1: Specification of the EPT of the EV-I

Powertrain of EV-I	Specifications
Motor Type and weight	A DC series motor, 4.5 kW, 1800 rpm; 50 kg
Motor controller and weight	Curtis controller (1204M); 2 kg
Main Contactor	48 V, 150 A rated
A foot pedal	5 kΩ
Gearbox and transmission	Gear ratio: 0.9:1, differential to wheels
Coupling plate, parts, mounting parts	8 kg, newly developed.
Battery type Battery weight	48 V, 80 Ah Li-polymer battery; 26 kg.

Table A.2.2: Specification of the EPT of the EV-II

Powertrain of EV-II	**Specifications**
Motor type, rpm and weight	The local 3-phase induction motor of 8.0 kW, rated 2920 rpm; 48 kg
Motor Torque	78 Nm @ 1112
Motor controller-inverter and weight	The vehicle control unit (VCU), IFOC (500A) with electronic foot pedal (potentiometer) as the accelerator
Gearbox and transmission	Gear ratio: 1.28:1, direct-drive and differential to wheels
Supporting & mounting plate, mechanical parts, and axle connectors and joints.	8 kg (newly developed).
Battery type (small swappable LiB pack) Battery weight, Battery cycles at 1C/1C (75A) to 80% of capacity	48 V (nominal), 75 Ah per battery unit; Peak current 200 A 26 kg Cell volt. 3.3-4.1 V up to 3000 cycles
Battery Charger	Input voltage: 210-230 Vac, 50Hz Output current / voltage : 40 A,58.8 Vdc
Charging time (approx.)	2 hrs 40min; SoC from 41 V to 51.5 V

Table A.2.3: Specification of the 3P-IM, IFOC controller, and LiB pack of the EV-II

Powertrain Sub-systems	**Specifications**
Motor type, Power Motor Torque Motor Voltage Battery Voltage Speed Frequency	3-phase Induction 8.0 kW 78 Nm 32 V 48 V 2920 rpm 100 Hz
Motor controller-inverter Nominal Voltage 2 Min RMS Current rating (A) 60 Min RMS Current rating (A)	Curtis 1238-6501 (IFOC + Power Inverter); 48-80 V 550 A
Battery type (small swappable LiB pack) Battery weight, Battery cycles at 1C/1C (75A) to 80% of capacity	48 V (nominal), 75 Ah per battery unit; Peak current 200 A 26 kg Cell volt. 3.3-4.1 V up to 3000 cycles

Table A.2.4: Test Report for the 8 kW AC induction motor

Motor Voltage (V)	Motor Current (A)	Speed (RPM)	Torque (Nm)	Frequency (Hz)	Input Power (kW)
No Load Test					
31.52	27.79	2976	0	99.30	0.274
Blocked Rotor Test					
3.66	145.48	0	0	24.80	0.44
8.89	145.10	0	0	99.32	1.09
Characteristic Load Test					
31.32	145.10	2866	21.19	99.32	6.97
31.41	186.43	2834	25.89	99.32	8.94
30.90	201.82	2510	31.39	89.30	9.80
31.42	152.82	2562	25.89	89.30	7.61
31.20	182.53	2260	32.96	79.40	8.95
31.36	248.15	2186	40.41	79.40	12.17
29.26	238.15	1926	43.16	69.46	11.02
30.76	290.20	1848	52.97	69.46	14.14
30.84	345.23	1688	71.41	59.59	16.70
29.97	270.73	1650	58.86	59.59	12.79
30.73	408.16	1288	102.02	49.66	19.75
31.05	232.73	1112	78.48	39.72	10.94
30.19	342.54	825	125.56	30.02	14.80
28.59	332.52	809	125.56	30.02	14.47

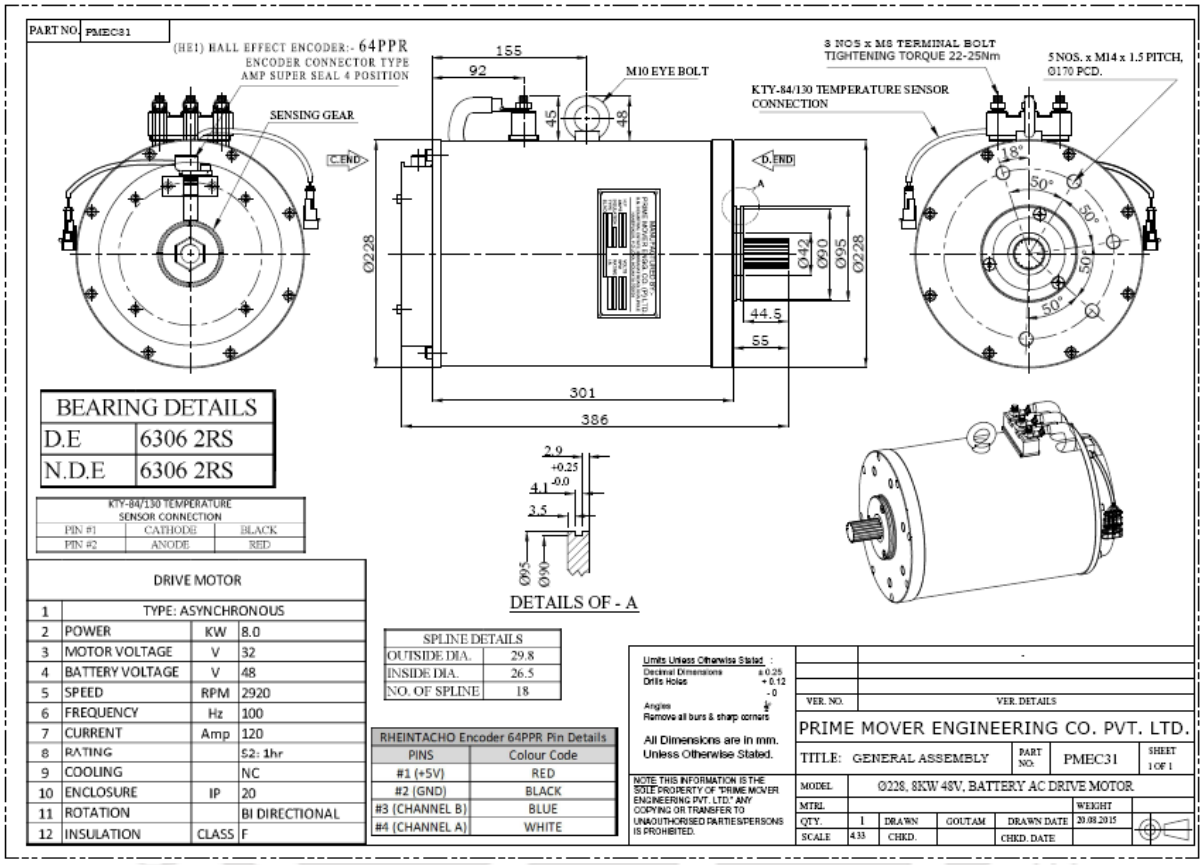

Figure A.2.1 Design specification of the 3P-Induction Motor

Table A.2.5: Energy Source Specifications

Energy Sources	**Specifications**
Battery type (small swappable LiB pack) Battery weight, Battery cycles at 1C/1C (75A) to 80% of capacity	48V (nominal), 75Ah per battery unit; Peak current 200A 26 kg Cell volt. 3.3-4.1V up to 3000 cycles
Single Supercapacitor	
Rated Capacitance Maximum Capacitance Maximum ESRDC Test Current for Capacitance Rated Voltage Absolute Maximum Voltage Absolute Maximum Current Typical Usable Specific Power, Pd Minimum Stored Energy, E_{stored}: Typical Stored Energy, Estored**Safety** Short Circuit Current, typical (Current possible with short circuit from rated voltage)	3,400.00 Farad (F) 3,740.00 F 0.28 mΩ 100.00 A 2.85 V 3.00 V 2,500.00 A 8.50 kW/kg 3.84 Wh; 4.00 Wh 10,000.00 A
Supercapacitor Bank	
Number of single SC	18
Bank voltage	51.3V
Bank Capacitance	189 F

Table A.2.6: Specifications for the Battery Management System (BMS) for LiBs

Parameter Description		Criterion
Voltage	Charging voltage	DC:58.8V, CC/CV
	Balance voltage for single cell	4.20±0.025V
Current	Balance current for single cell	126±10mA
	Current consumption	≤20μA
	Max. continuous charging current	80A
	Max. continuous discharging current	120A
Over Charge Protection	Over charge detection voltage	4.25±0.025V
	Over charge detection delay time	0.5-2 s
	Overcharge release voltage	4.05±0.05V
Over-Discharge Protection	Over discharge detection voltage	3.0±0.062V
	Over discharge detection delay time	10ms-300ms
	Over discharge release voltage	2.0±0.062V
Overcurrent Protection	Over current detection voltage	0.62V
	Over-current detection current	400±50A
	Detection delay time	5ms-15ms
	Release condition	Cut load
Short Circuit Protection	Detection condition	
	Detection Delay time	200-500μs
	Release condition	Cut load
Resistance	Protection Circuitry (MOSFET)	≤20mΩ
Temperature	Operating Temperature Range	-40 - +85°C
	Storage Temperature Range	-40 - +125°C

Table A.2.7: Specifications of the Li-Battery Charger

Parameter	**Specification**
Battery Charger	Input voltage: 210-230 Vac, 50 Hz Output current: 40 A Output voltage: 58.8 Vdc
Charging time (approx.)	2 hrs 40min SoC from 41V to 51V

Table A.2.8: Specification of the battery charger used for the SC bank charging

Parameter	**Specification**
Battery Charger	Model:GF-TBPU-M8P500U059 Input voltage: 180-305 Vac, 50/60Hz Input current: 5.0A Output current: 12A Output voltage: 59V
Total electrical EC for charging the battery	4.9 kW; state-of-charge (SoC) of the battery from 10% to 100%.
Charging time (approx.)	Ten hr. for SoC from 10% to 100% Eight hr. 10 min., SoC from 30% to 100%

A.3 Measuring Equipment Specifications

Table A.3.1 Basic description of the test equipment.

Equipment	Specification
DataTaker DT-80 (from Thermofisher Scientific)	Dual Ch. isolation technology, Capable of inputs Temperature, Strain, Current and Voltage data, FTP for automatic data transfer, 40Hz max. sample speed Up to 15Analog (± 50V) sensor inputs with accuracy 0.1% and 12 Digital inputs, Modbus for SCADA connection, SDI-12 (multiple networks), 1GB USB memory.
Garmin GPS 18x series sensor (WAAS DGPS)	Update rate 5Hz Position: < 3 meters, 95% typical Velocity: 0.05 m/s steady state (0.1 knot RMS steady state).
Yokogawa Power Meter (CW240)	Voltage (0-1000V), current (0-500A), Electric power (active, reactive, apparent) Power factor, the phase angle of each phase Average, minimum, maximum values of each measurement element. Data Collection Time(s): 1/2/5/10/15/30 seconds; 1/2/5/10/15/30/60 minutes 128MB memory card
Phases / Systems that can be measured (CW-240)	Single-phase 2-wire, single-phase 3-wire, single-phase 3-wire 3-current (current in neutral line), three-phase 3-wire 2-current (2-power meter method), Three-phase 3-wire 3-current (3-power meter method), three-phase 4-wire, three-phase 4-wire 4-current (current in neutral line), Scott connection (three-phase 3-wire + single-phase 3-wire)

CW Viewer AP240E is data analyzing software for the CW240 Clamp-on Power meter.

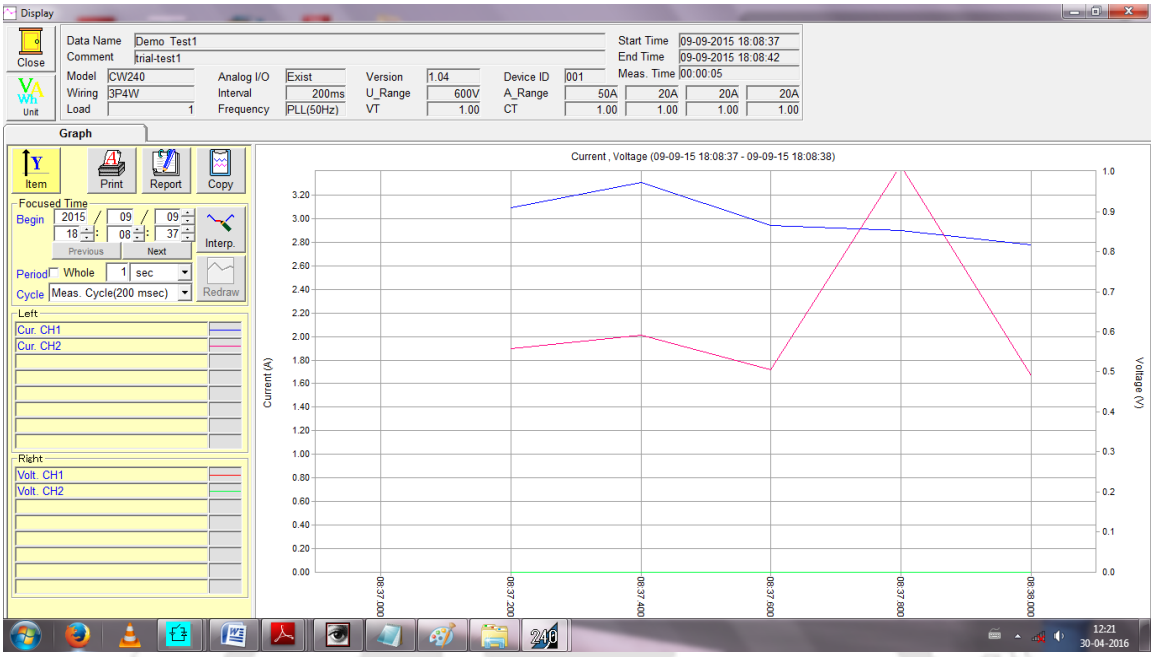

Figure A.3.1: Overview of CW240's software for data analysis

Table A.3.2. Basic specification of the PEMS.

PEMS Model	OBS-2200 from Horiba, Japan
Measuring Principle	NDIR for CO, CO_2; FID for THC; CLD for NO, NOx
Measuring Range	CO: 0-0.5 to 0-10 vol% CO_2: 0-5 to 0-20 vol% THC: 0-100 to 0-10,000ppm NO,NOx: 0-100 to 0-3000ppm
Accuracy	within ± 2.5% of full scale (FS)
Repeatability	Zero gas: within ± 1% of FS Span gas: within ± 1% of readings
Exhaust flow rate	Pitot flow meter;
	Accuracy: ±1.5% of full scale

Table A.3.3: Specification of the Digital Vehicle Weighment System

Parameter Description	**Specification**
Make:	HKM Messtechnik GmbH, Germany.
Model:	RW 2.0
Type: Total Capacity Nominal Load: Sensitivity: Accuracy: Dimension: *Hand terminal for wheel load scales* Type: HT 3.4 Display: Power supply:	Portable wheel load scale 2000 kg 500 kg / wheel 0.2 kg ± 0.4 kg 430 x 420 x 30 mm LCD, 2−line wheel and axle loads total load 10−15 V

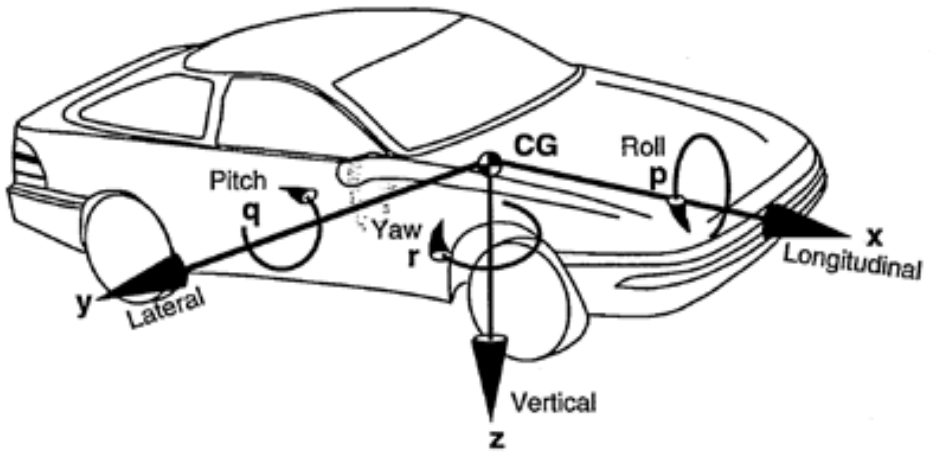

Figure A.3.2: The fundamentals of vehicle dynamics

[SAE Vehicle dynamics, 2020]

A.4 Real-Driving Emissions (RDE) data of the in-use ICE Car

Table A.4.1 indicates the real-world vehicle emissions and fuel consumption of the representative (in-use) vehicle. The results show a realistic scenario where a similar ICE car model can cause how much vehicle pollutants in the urban areas and possible benefits in terms of vehicle emissions reduction and fuel savings by the EV conversion.

Table A.4.1: Real-world vehicle emissions and FE of the in-use gasoline Car

Traffic routes		**Congested**	**Medium**	**Low**	**Lab.**
Distance traveled (km)		11.90	12.67	7.66	10.64
Speed (km/h)	Max.	41.00	49.00	48.10	90.00
	Avg.	11.78	24.1	31.70	32.50
CO (g/km)		73.59	60.05	40.03	30.79
CO_2 (g/km)		142.92	124.41	113.10	102.82
THC (g/km)		12.79	7.67	5.55	2.56
NOx (g/km)		0.49	0.46	0.42	0.21
FE (kmpl)		10.59	11.11	11.78	13.66
Ambient Temp.(°C)		21.50	20.90	21.30	24.00
Ambient Humidity (%RH)		53.00	52.60	57.10	49.00

A.5 Uncertainty Analysis

Uncertainty analysis is the prediction of the uncertainty interval, which should be associated with an experimental result, based on observations of the scatter in the raw data used in calculating the result [Moffat, R. J., 1982]. It also refers to the process of estimating how great an effect the uncertainties in the individual measurements have on the calculated result. The root-sum-square (RSS) combination is used to estimate the uncertainties for the measured parameters [Moffat, R. J., 1982; Moffat, R. J., 1988; Sahoo, B., 2011]. The relative errors of independent variables used for the uncertainty analysis are given in Table A.5.1 The calculated uncertainties (zeroth order) for the different measured parameters are given in Table A.5.2.

An example of estimating the uncertainty:

The independent variables accompanying input power measurement are voltage (V) and current (I).

Input power drawn from the battery is given by Power (P) =VI (W)

Therefore, the uncertainty in the measurement of input power,

$\Delta P = (0.0015^2 + 0.0010^2)^{1/2} = 0.0018 = 0.18\%$

Table A.5.1: Relative errors of independent variables

Independent Variables	**Relative Error (%)**
DC battery current (A)	0.10
DC battery voltage (V)	0.15
Dyno.Tractive Force (N)	0.11
Speed (dynamometer)	0.05
Roller radius (m)	0.50
Wheel radius (m)	0.50
Time (s)	0.05

Table A.5.2: Uncertainties of measured parameters

Parameter	**Uncertainty (%)**
Torque (Nm)	0.51
Input power (kW)	0.18
Speed (km/h)	0.50
Power (mech.) (kW)	0.51
Energy Consumption	0.19

A.6 Microsoft-Excel Computer Program for Data Segregation

The program is used to check the acceleration trend by checking the positive change in vehicle speed and acceleration in the adjoining cell values. First, the acceleration values are checked whether they are greater than twice the acceleration limit; if greater, it is declared acceleration. Next, from the current cell position, the acceleration values in 2 cells up and 2 cells down are checked and assigned to a random variable y1. If the y1 value is greater than the acceleration

limit, then it is declared acceleration; if not, then no-acceleration. The program flowchart is shown in Figure A.6.1. The definition and limits of drive-modes are described in Chapter 3. The values of acceleration are calculated with a simple equation as given below:

Acceleration value, $x = \frac{(A11*1000-A10*1000)}{(60*60)}$ (m/s^2) ---- Eq. A.6.1

Where A10 and A11 are the arbitrary cell numbers in the speed-data column. A11 is the higher cell number of vehicle speed, and A10 is the preceding cell number of the speed. The unit of speed in kilometers per hour (km/h).

A quick recall for the drive-mode definitions and limitations are as follows.

- Idle - speed equals zero km/h.
- Acceleration - Speed greater than acceleration limit of TAP document
- Deceleration - Same as acceleration except that acceleration should be negative.
- Cruising is also considered during constant speed operation as acceleration is zero, i.e. $(\frac{dv}{dt}) = 0$, during constant speed operation. where, v = velocity (speed) in m/s.

Flowchart for segregation of Acceleration

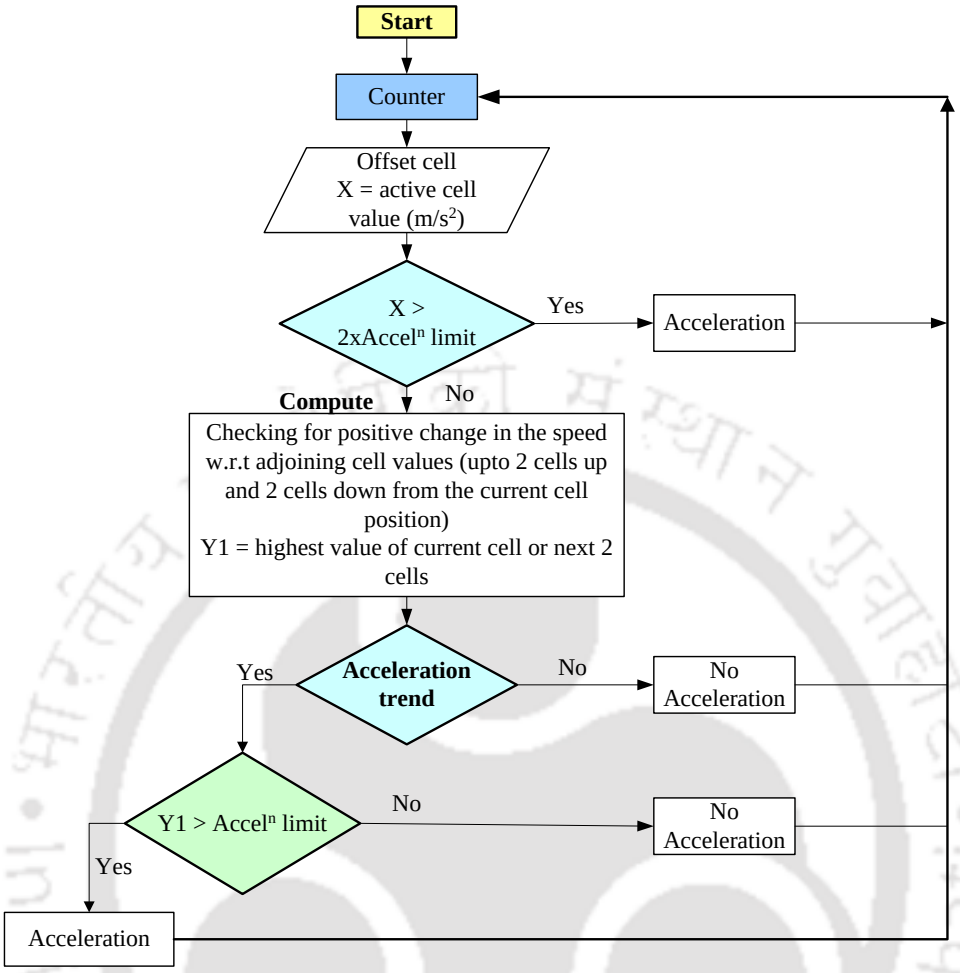

Figure A.6.1: Flowchart for data segregation for acceleration mode

A.7 Relevant IS documents and AIS standards for Electric Vehicle powertrain

A.7.1: AIS-039 (Rev.1) - Measurement of Electrical Energy Consumption for EVs

AIS-039 (Rev.1) specifies the method for measurement of electrical EC expressed in Wh/km for L, M & N categories of Electric Powertrain Vehicles as defined in Rule 2 (u) of Central Motor Vehicle Rules (CMVR). It specifies the detailed procedure for vehicle preparation, charging, discharging of the rechargeable energy storage systems, end of charge criteria, etc. Vehicle preparation includes checking the condition of the test vehicle like tyre pressure, battery condition, etc. It also defines the test condition specifying that all the tests are conducted at a temperature of between 20 °C and 30 °C. More detail on AIS-039 (Rev.1) is given in the Appendix.

The standard also specifies the test procedure, test sequence, power setting of the chassis dynamometer, Parameters, Units and Accuracy of Measurements, Application of the Cycle, and Measurement of the Distance.

It specifies the use of Part 1 of MIDC for M1, M2 (with GVW up to 3500 kg), and N category of vehicles. However, 25 Cycles of Delhi Driving Cycle is recommended for M2 (with GVW above 3500 kg) and M3 category of vehicles. Electric EC Calculation is specified as follows:

$$C = \frac{E}{D} \text{ (Wh/km)} \qquad \text{---} \qquad (1)$$

Where C is the total electrical energy consumption per kilometer (EC_{tot}) expressed in Wh/km; E is the total electrical input energy in Watt-hour (Wh) reading of the power meter, and D is the distance covered (range) in kilometer (km).

A.7.2: AIS-123 (Part 3) - CMVR Type Approval of Electric Propulsion Kit Intended for Conversion of Vehicles for Pure Electric Operation.

A.7.3: AIS-138 (Part-1), 2017 - Electric Vehicle Conductive AC Charging System.

A.7.4 G.S.R-167 (E), March 2019 - Govt. gazetted notification on the electric conversion of existing / old ICE vehicles into pure battery-powered EVs.

A.7.5: Indian Standard (IS) 14785: 2000 (R2016)

Automotive Vehicles – Determination of Road-Load Constants by Coast Down Test Method.

This standard specifies the procedure for determining the equation of road-load resistance for a vehicle, including aerodynamic and rolling resistance by coast down technique. The data is primarily intended for the road-load simulation on variable load curve chassis dynamometer, expressed as:

$F = a + bv^2$, where factors ‘a’ and ‘b’ are the constants.

This standard also defines the vehicle preparation, laden, unladen vehicle, instrumentation used, test requirements, and least square curve fitting.

References

Aayog, N., and R. M. I. (RMI), “India’s Electric Mobility Transformation: Progress to date and future opportunities,” **NITI Aayog** INDIA and RMI, Tech. Rep., April 2019.

Abousleiman, R., Rawashdeh, O., and Boimer, R., "Electric Vehicles Energy Efficient Routing Using Ant Colony Optimization," SAE Int. J. Alt. Power. 6(1): 2017.

Abhinav Soman, Karthik Ganesan, and Harsimran Kaur, “India’s Electric Vehicle Transition - Impact on Auto Industry and Building the EV Ecosystem,” October 2019, https://www.ceew.in/sites/default/files/CEEW-IndiaElectricVehicleTransitionReportPDF26Nov19.pdf, Accessed on 23rd November 2020.

Ahmad Raqib, Wan Hashim Wan Ibrahim and Ahmad Farhan, Mohd Sadullah, “Estimating Travel Time of Arterial Road using Car Chasing Method and Moving Observer Method,” Journal of Transportation Science Society of Malaysia 1, 77-87, 2005.

Ahssan, M., Ektesabi, M., and Gorji, S., “Electric Vehicle with Multi-Speed Transmission: A Review on Performances and Complexities,” SAE Int. J. Alt.Power. 7(2):169–181, 2018, doi:10.4271/08-07-02-0011.

AIS-039: Automotive Industry Standard (AIS)-039 (Rev.1) for Electric Vehicles, https://hmr.araiindia.com/Control/AIS/12222017102528AMAIS-039(Rev.1)_with_Corrigendum_1.pdf, Accessed on 10th October 2020.

AIS-123 (Part-3): CMVR Type Approval of Electric Propulsion Kit Intended for Conversion of vehicles for Pure Electric Operation. Accessed on 10th Oct.2020. https://hmr.araiindia.com/Control/AIS/110201995755AM6_AIS_123_Part3_with_Amd_1and2_F.pdf, Accessed on 17th October 2020.

AIS-138 (Part-1): Indian Automotive Industry Standard (AIS)-138 (Part-1), 2017. https://hmr.araiindia.com/Control/AIS/210201752832PMAIS138_Part1.pdf, Accessed on 17th October 2020.

Amit Kumar Singh, Ankit Dalal, Praveen Kumar, “Analysis of induction motor for electric vehicle application based on drive cycle analysis,” IEEE International Conference on Power Electronics, Drives and Energy Systems (PEDES), December 2014.

Anamika Sagar, Sh. Suneel Dave, Sh. V.P. Yadav, and Ms. Anamika Sagar, CPCB Annual Report 2018-2019, Central Pollution Control Board (CPCB), Ministry of Environment, Forest & Climate Change,

https://cpcb.nic.in/openpdffile.php?id=UmVwb3J0RmlsZXMvMTExOV8xNTk3MDM3NTM0X21lZGlhcGhvdG8xOTY1Ni5wZGY= , Accessed on 19th October 2020.

André Abelardo Tavares, Claudio Ernesto Ponce Saldias, Igor Fornasa, Luis Felipe Bianchi Carbonera, Juan Carlos Cutipa-Luque, Breno Elias Bretas de Carvalho, "Power Losses Analysis and Efficiency Evaluation of an Electric Vehicle Conversion," IEEE International ESARS-ITEC Conference, November 2018, doi: 10.1109/ESARS-ITEC.2018.8607322.

Auto-Expo, 2020, Indian Expo Mart, Greater Noida, India, Feb.2020. http://www.autoexpo-themotorshow.in/about-us/, Accessed on 12th July 2020.

Bazzi, A. M., Friedl, A. P., Choi, S., Krein, P. T., "Comparison of Induction Motor Drives for Electric Vehicle Applications: Dynamic Performance and Parameter Sensitivity Analyses," IEEE International Electric Machines and Drives Conference, Accession No.: 10729108, May 2009, doi:10.1109/IEMDC.2009.5075273.

Baoqing Deng, Mengqi Deng, and Shaojia Huang, Zhuhai, "An Overview of Chassis Dynamometer in the Testing of Vehicle Emission," MATEC Web of Conferences 175, 02015 (2018), IFCAE-IOT 2018, https://doi.org/10.1051/matecconf/201817502015.

Blaschke, F. "The principle of field orientation as applied to the new transvektor closed-loop control system for rotating field machines," Siemens Review, Vol. 34, 184, 217–220, May 1972.

Berry I.M., "The Effects of Driving Style and Vehicle Performance on the Real-World Fuel Consumption of US Light-Duty Vehicles," Thesis, Massachusetts Institute of Technology (MIT), February 2010.

Berjoza, D., Jurgena, I., "Effects of change in the weight of electric vehicles on their performance characteristics," Agronomy Research, 15(S1), 952–963, 2017.

Bin Wang, Min Xu, Li Yang, "Study on the economic and environmental benefits of different EV powertrain topologies", Energy Conversion and Management, Vol.86, 916–926, 2014.

Bingham, C., Walsh, C., Carroll, S., "Impact of driving characteristics on electric vehicle energy consumption and range," IET Intelligent Transport Systems, Vol.6, Issue:1, 29-35, March 2012.

Blaž Luin, Stojan Petelin, Fouad Al-Mansour, "Microsimulation of electric vehicle energy consumption," Energy, Vol. 174, 24-32, May 2019.

Bollen, J. C., et al. Co-Benefits of Climate Policy. PBL Report no. 500116005. Netherlands Environmental Assessment Agency. February 2009. Available at

http://www.unep.org/transport/gfei/autotool/understanding_the_problem/Netherlands%20Environment%20Agency.pdf, Accessed on 10th October, 2020.

Bor Yann Liaw, Matthieu Dubarry, "From driving cycle analysis to understanding battery performance' in real-life electric hybrid vehicle operation," Science Direct, Journal of Power Sources, 174,76–88, 2007.

Boldea, I., Tutelea, L. N., Parsa, L. and Dorrell, D., "Automotive electric propulsion systems with reduced or no permanent magnets: An overview," IEEE Trans. Ind. Electron., Vol. 61, No. 10, 5696–5711, October 2014.

Bose, B. K., Modern power electronics, and AC drives. Prentice-Hall, Upper Saddle River, NJ, USA, 2002.

Bosch, 1993. "Drivetrain Automotive Handbook," (3rd ed.) p.536. ISBN 0-8376-0330-7.

Brahim Mebarki, Belkacem Draoui, Boumediène Allaou, Lakhdar Rahmani, and Elhadj Benachour, "Impact of the Air-Conditioning System on the Power Consumption of an Electric Vehicle Powered by Lithium-Ion Battery," Modelling and Simulation in Engineering, Hindawi Publishing Corporation, Vol. 2013, Article ID 935784, 2013.

Casadei, D., Serra, G., Tani, A. and Zarri, L., "Direct torque control for induction machines: A technology status review," 2013 IEEE Workshop on Electrical Machines Design, Control and Diagnosis (WEMDCD), 117–129, March 2013.

CarMaker simulation software from IPG Germany, "Virtual testing of automobiles and light-duty vehicles," https://ipg-automotive.com/products-services/simulation-software/carmaker/, accessed on 10th November 2020.

Carlson, R., Lohse-Busch, H., Diez, J. and Gibbs, J., "The Measured Impact of Vehicle Mass on Road Load Forces and Energy Consumption for a BEV, HEV, and ICE Vehicle," SAE Int. J. Alt. Power. 2(1):2013, doi:10.4271/2013-01-1457.

Chang Chih-Ming, Siao Jheng-Cin, "Performance analysis of EV powertrain system with/without transmission," World Electric Vehicle Journal, Vol. 4, 629-634. November 2010.

Chan, C.C., "The State of the Art of Electric, Hybrid, and Fuel Cell Vehicles," Proceedings of the IEEE, Vol. 95, Issue 4, April 2007.

Chen Y, Wang J., "Design and evaluation on electric differentials for over actuated electric ground vehicles with four independent in-wheel motors," IEEE Transactions on Vehicular Technology, 61(4):1534–42, 2012.

Chiara Fioria, Vincenzo Arcidiacono, Georgios Fontaras, Michail Makridis, Konstantinos Mattas, Vittorio Marzano, Christian Thiel, Biagio Ciuffo, "The effect of electrified mobility on

the relationship between traffic conditions and energy consumption," Transportation Research Part: D, 67 (2019) 275–290, 2019.

COP21 (the 2015 Paris Climate Conference) under the Sustainable Innovation Forum by Climate Action & UNEP, Paris, 2015. http://www.cop21paris.org/about/cop21/ , Accessed on 12th October 2020.

Chugh, S., Kumar, P., and Muralidharan, M., "Development of Delhi Driving Cycle: A Tool for Realistic Assessment of Exhaust Emissions from Passenger Cars in Delhi," SAE Technical Paper 2012-01-0877, 2012, doi:10.4271/2012-01-0877.

CSE, 2020, Air Quality and Public Health Report, Centre for Science and Environment (CSE), https://www.cseindia.org/page/air-quality-and-public-health, Accessed on 30th November 2020.

Delhi EV; Delhi Electric Vehicles Policy, 2020. https://transport.delhi.gov.in/sites/default/files/All-PDF/Delhi_Electric_Vehicles_Policy_2020.pdf, Accessed on 8th November 2020.

Ehsani, M., Y Gao, S. E. Gay, Ali Emadi, "Modern Electric, Hybrid Electric, and Fuel Cell Vehicles: Fundamentals, Theory, and Design" CRC press, Book, ISBN: 0-8493-3154-4.

EIA, 2013; Energy Information Administration (EIA), U.S. Department of Energy. "Analysis Brief: India." March 18, 2013. Available at http://www.eia.gov/countries/analysisbriefs/India/india.pdf, Accessed on 16th October 2020.

Efstathios E. Michaelides, "Thermodynamics and energy usage of electric vehicles," Elsevier Energy Conversion and Management, Vol. 203, Article-112246, January 2020.

FAME India Scheme, March 2019, <https://dhi.nic.in/writereaddata/UploadFile/publicationNotificationFAME%20II%208March 2019.pdf> and https://www.fame-india.gov.in/, Accessed on 17th October 2020.

Fei Lei, Yingchun Bai, Wenhao Zhu, Jinhong Liu, "A novel approach for electric powertrain optimization considering vehicle power performance, energy consumption and ride comfort," Energy, Vol. 167, 1040-1050, January 2019.

Franco, V., Kousoulidou, M. , Muntean, M., Ntziachristos, L., Hausberger, S. and Dilara, P., "Road vehicle emission factors development: A review," Atmos. Environ., Vol. 70, 84-97, 2013.

Gaurav Bansal, Anup Bandivadekar, "Overview of India's Vehicle Emissions Control Program - Past Successes and Future Prospects," The International Council on Clean Transportation (ICCT), Washington DC 20005, 2013.

G.S.R 167 (E), March 1, 2019, Indian Federal Legislation for EV Conversion, https://morth.nic.in/sites/default/files/notifications_document/Notification_no__G_S_R_167%28E%29_dated_01_03_2019.pdf, Accessed on 17th October 2020.

Guttikunda, S. K., Goel, R., Pant, P., "Nature of air pollution, emission sources, and management in the Indian cities," Atmospheric Environment, Vol. 95, 501 – 510, 2014.

Hewu Wang, Xiaobin Zhang, Minggao Ouyang, "Energy consumption of electric vehicles based on real-world driving patterns: A case study of Beijing," Applied Energy, Vol. 157, 710-719, November 2015.

IEA (International Energy Agency), "Global EV Outlook 2019 - Scaling-up the transition to electric mobility," May 2019.

IEA (International Energy Agency), "**Global EV** Outlook 2017 – Two million and counting," 2017.

Idris, N. R. N., and Yatim, A. H. M., "Direct torque control of induction machines with constant switching frequency and reduced torque ripple," IEEE Trans. Ind. Electron., Vol. 51, No. 4, 758–767,Aug 2004.

IHME, 2013, The Global Burden of Disease 2010: Generating Evidence and Guiding Policy. Institute for Health Metrics and Evaluation (IHME), Seattle, USA.

Insaf Sagaama, Amine Kchiche,Wassim Trojet, Farouk Kamoun, "Evaluation of the Energy Consumption Model Performance for Electric Vehicles in SUMO," 2019 IEEE/ACM 23rd International Symposium on Distributed Simulation and Real Time Applications (DS-RT), doi: 10.1109/DS-RT47707.2019.8958704, October 2019.

IS 14785: 2000, Bureau of Indian Standard (BIS) for Automotive Vehicles -Determination of road-load constants by coast down test method, IS 14785: 2000.

Islam, **S. M.** and Somuah, C. B., "An efficient high-performance voltage decoupled induction motor drive with excitation control," IEEE Transactions on Energy Conversion, Vol. 4, no. 1, 109–117, 1989.

Islam, S. M., C. B. Somuah, M. S. Ahmed, and Y. L. Abdel-Magid, "Improved speed regulation of an excitation controlled induction motor," IEEE Transactions on Industry Applications, Vol. 28, no. 3, 694–702, 1992.

Jacobina, C. B., J. Bione Fo, F. Salvadori, A. M. N. Lima, and L. A. S. Ribeiro, "A simple indirect field oriented control of induction machines without speed measurement," in Conf. Record of the 2000 IEEE Ind. Appl. of Electrical Energy, Vol. 3, 1809–1813, October 2000.

Jahns, T.M., V. Blasko, 'Recent advances in power electronics technology for industrial and traction machine drives,' Proceedings of the IEEE, vol 89, Issue 6, June 2001, doi: 10.1109/5.931496,

Jaideep Singh, K.V.V Rao Srinivasa, and Jagmindar Singh, "Selection of Gear Ratio for Smooth Gear Shifting," SAE International, 2012-01-2005, 2012, doi:10.4271/2012-01-2005.

Jain, A., Robindro, L., Pathak, S., Singh, Y. et al., "Impact of Road Quality, Traffic Management and Driver Training on Vehicular Emissions and Fuel Economy-an Experimental Study on Indian Roads," SAE Technical Paper 2011-26-0040, 2011, doi:10.4271/2011-26-0040.

Jan Dornoff, Uwe Tietge, Peter Mock, "On the way to 'Real-World' CO_2 values: The European passenger car market in its first year after introducing the WLTP," Retrieved from, White Paper, The International Council on Clean Transportation (ICCT), May 2020.

Jianyong Su, RuiGao, and Iqbal Husain, "Model Predictive Control Based Field-Weakening Strategy for Traction EV Used Induction Motor," IEEE Transactions on Industry Applications, Vol. 54, No. 3, June 2018.

Jin Zhang, Zhenpo Wang, Peng Liu, Zhaosheng Zhang, "Energy consumption analysis and prediction of electric vehicles based on real-world driving data," Elsevier Applied Energy, 275 (2020) 115408, 2020.

Jinrui N, Zhifu W, Qinglian R, "Simulation and Analysis of Performance of a Pure Electric Vehicle with a Supercapacitor," IEEE Vehicle Power and Propulsion Conference, ISSN:1938-8756, 1-6,6-8 September 2006.

Jithin T J, Prasanth P, Vikas Gautam, Meheranusha V, Kumaravel S, S. Ashok, "A Sensitivity Analysis on Performance of a Typical Single Axle Battery Electric Vehicle," IEEE International Conference on Power, Energy, Control and Transmission Systems (ICPECTS), DOI: 10.1109/ICPECTS.2018.8521616, February 2018.

Jorge O. Estima, Antonio J. Marques Cardoso, 'Efficiency Analysis of Drive Train Topologies Applied to Electric/Hybrid Vehicles,' IEEE Transactions on Vehicular Technology, Vol. 61, No. 3, March 2012.

Jong Tae Lee, Seokjoo Kwon,Yunsung Lim, Mun Soo Chon, Daesik Kim, 'Effect of Air-Conditioning on Driving Range of Electric Vehicle for Various Driving Modes,' SAE International, 2013-01-0040, TSAE-13AP-0040, March 2013.

Jorge Alonso del Valle, Juan Carlos Vieraa, David Anseána, Christian Brañasb, Pablo Luquec, Daniel Álvarez Mántarasc, Yoana Fernández Pulidoa, "Design and Validation of a Tool for

Prognosis of the Energy Consumption and Performance in Electric Vehicles," Transportation Research Procedia, Vol. 33, 35-42, 2018.

Jordi-Roger Riba, CarlosLópez-Torres, LuísRomeral, Antoni Garcia, "Rare-earth-free propulsion motors for electric vehicles: A technology review," Renewable and Sustainable Energy Reviews, Vol. 57, 367–379, 2016.

Jun Bi, Yongxing Wang, Qiuyue Sai, Cong Ding, "Estimating remaining driving range of battery electric vehicles based on real-world data: A case study of Beijing, China," Elsevier Energy, 169 (2019) 833-843, 2019.

Juyal, S. S. S., Singh, M., "India leaps ahead: transformative mobility solutions for all," Tech. Rep., NITI Aayog India, and RMI, New Delhi, 2017.

Karen L. Butler, Mehrdad Ehsani, Preyas Kamath, "A Matlab-based modeling and simulation package for electric and hybrid electric vehicle design," IEEE Transactions on Vehicular Technology, Vol. 48, No. 6, November 1999.

Kazmierkowski, M. P., and A. B. Kasprowicz, "Improved direct torque and flux vector control of PWM inverter-fed induction motor drives," IEEE Trans. Ind. Electron., Vol. 42, No. 4, 344–350, August 1995.

Kerkman, R. J., Rowan, T. M. and Leggate, D., "Indirect field-oriented control of an induction motor in the field-weakening region, IEEE Transactions on Industry Applications, Vol. 28, Issue 4, 850-857, 1992. doi: 10.1109/28.148451.

Kezhen Hu, Jianping Wu, and Tim Schwanen, "Differences in Energy Consumption in Electric Vehicles: An Exploratory Real-World Study in Beijing," Journal of Advanced Transportation, https://doi.org/10.1155/2017/4695975, 2017.

Kistler vehicle dynamics, 2020
https://www.yumpu.com/en/document/read/35915021/vehicle-dynamics-corrsys-datron, Accessed on 21st November 2020.

Kumar, R., Das, S., Syam, P., and Chattopadhyay, A. K., "Review on model reference adaptive system for sensorless vector control of induction motor drives," IET Electr. Power Appl., Vol. 9, No. 7, 496–511, 2015.

Kumar, R. H., Iqbal, A., and Lenin, "R N. C., Review of recent advancements of direct torque control in induction motor drives a decade of progress," IET Power Electron., Vol. 11, No. 1, 1–15, 2018.

Lairenlakpam, R., Jain, A.K., Gupta, P., Kamei, W. et al., "Effect of Real World Driving and Different Drive Modes on Vehicle Emissions and Fuel Consumption," SAE Technical Paper 2018-01-5017, 2018, doi:10.4271/2018-01-5017.

Li, Z., Khajepour, A., and Song, J., "A Comprehensive Review of the Key Technologies for Pure Electric Vehicles," Energy 182:824-839, 2019.

Liang, Q., Tang, N., Gao, B., and Chen, H., "The Seamless Gear Shifting Control for Pure Electric Vehicle with 2-Speed Inverse-AMT," IFAC Proceedings 46(21):507-511, 2013, doi:10.3182/20130904-4-JP-2042.00023.

Lee, B., Oh, H., Han, S., Woo, S. et al., "Development of High-Efficiency Gasoline Engine with Thermal Efficiency over 42%," SAE Technical Paper 2017-01-2229, 2017, doi:10.4271/2017-01-2229.

Lukic, S.M. and Emado, A., "Modeling of Electric Machines for Automotive Applications Using Efficiency Maps," Proceedings of the Electrical Insulation Conference and Electrical Manufacturing & Coil Winding Technology Conference of IEEE, 2003, 543-550, doi:10.1109/EICEMC.2003.1247945.

Lum K.M., Fan H. S.L., Lam S.H. & Olszewski P. "Speed-flow modeling of arterial roads in Singapore," Journal of Transportation Engineering 124(3): 213-222. 1998.

Martin Mruzek, Igor Gajdáč, Ľuboš Kučera, Dalibor Barta, "Analysis of Parameters Influencing Electric Vehicle Range," 9th International Scientific Conference Transbaltica 2015, Procedia Engineering 134 (2016) 165 – 174, 2016.

Maya, B.D., "Zero-emission vehicle credits: China program design inputs brief," Tech. Rep., innovation Center for Energy and Transportation, Beijing, China, 2015.

Moffat, R. J., Department of Mechanical Engineering, Stanford University, "Contributions to the Theory of Single-Sample Uncertainty Analysis," Transactions of the ASME, 250/Vol. 104, June 1982.

Moffat, R. J., Department of Mechanical Engineering, Stanford University, "Describing the Uncertainties in Experimental Results," Experimental Thermal and Fluid Science, 1:3-17, 1988.

Monica Tutuianu, Pierre Bonnel, Biagio Ciuffo, Takahiro Haniu, Noriyuki Ichikawa, Alessandro Marotta, Jelica Pavlovic, Heinz Steven, "Development of the Worldwide harmonized Light-duty Test Cycle (WLTC) and a possible pathway for its introduction in the European legislation," Transportation Research Part:D, 40 (2015) 61–75, 2015.

Multi-gear, 2020; https://energyeducation.ca/encyclopedia/Transmission_(vehicle), Accessed on 22nd October 2020.

Mustafa Aktasa, et al., "Direct torque control versus indirect field-oriented control of induction motors for electric vehicle applications," Engineering Science and Technology, an International Journal 23 (2020), 1134-1143, 2020.

MCDDN; Meteorological Centre Dehradun, Indian Meteorological Department, Ministry of Earth Science, Govt. of India. http://rmcnewdelhi.imd.gov.in/MET_CENTRES/MCDDN/ and https://mausam.imd.gov.in/imd_latest/contents/departmentalweb.php, accessed on 7th August 2020.

Nemet, G. F., T. Holloway, and P. Meier. "Implications of Incorporating Air-Quality Co-Benefits into Climate Change Policymaking," Environmental Research Letters 5, No. 1, 4007, 2010.

NEMMP, 2012, The National Electric Mobility Mission Plan 2020, DHI, Ministry of Heavy Industries and Public Enterprises, Government of India, 2012.

Nesamani, K.S., Subramanian, K.P., Development of a driving cycle for intra-city buses in Chennai, India", Elsevier Atmospheric Environment, 45 (2011), 5469-5476, 2011.

Nesamani, K.S., Subramanian, K.P., "Impact of real-world driving characteristics on vehicular emissions," Chennai, India, UCI-ITS-WP- 05-5, December 2005.

NITI Aayog, Zero-Emission Vehicles (ZEVs), 2018: Towards A Policy Framework, http://niti.gov.in/writereaddata/files/document_publication/EV_report.pdf, Accessed on 24th November 2020.

Norbert E. Ligterink Pim, Mensch Rob F.A. Cuelenaere Stefan Hausberger David Leitner Gérard Silberholz, "Correction algorithms for WLTP chassis dynamometer and coast-down testing," European Commission, DG Clima, Framework Contract ENTR/F1/2009/030 – Lot 42016-TL-RAP-0100293115, TNO 2015 R10955, July 2015.

Omar Ellabban, Joeri Van Mierlo, Philippe Lataire, "A comparative study of different control techniques for an induction motor fed by a Z-source inverter for electric vehicles," IEEE International Conference on Power Engineering, Energy and Electrical Drives, Accession No.: 12304681, 2011, doi:10.1109/PowerEng.2011.6036554.

Paffumi, E., De Gennaro, M., Martini, G., Manfredi, U. et al., "Experimental Test Campaign on a Battery Electric Vehicle: On-Road Test Results (Part 2)," SAE Int. J. Alt. Power. 4(2):277-292, 2015.

Praveen Kumar, Prof. S. Majhi, "Introduction to Hybrid and Electric Vehicles," of NPTEL, MoHRD, 2009-2012, https://nptel.ac.in/courses/108/103/108103009/, Accessed on 18th October 2020.

Prasun Mishra, Suman Saha, Ikkurti, H.P., "Selection of propulsion motor and suitable gear ratio for driving an electric vehicle on Indian city roads," IEEE International Conference on Energy-Efficient Technologies for Sustainability, 692 – 698, April 2013.

Prabhakar, K.K., Chinthakunta, U.R., Singh, A.K., and Kumar, P., "Efficiency and performance analysis of DTC-based IM drivetrain using variable dc-link voltage for electric vehicle applications," IET Electrical Systems in Transportation, Vol.8, No.3, 205-214, 2018.

Polychronis Spanoudakis, et al., "Efficient Gear Ratio Selection of a Single-Speed Drivetrain for Improved Electric Vehicle Energy Consumption," Sustainability 2020, 12, 9254, 2020, doi:10.3390/su12219254.

Quiroga, C.A. & Bullock, D. "Travel time studies with global positioning and geographic information systems: an integrated methodology," Transportation Research C, 6: 101-127. 1998.

Rafael Basso, Balázs Kulcsár, Bo Egardt, Peter Lindroth, Ivan Sanchez-Diaz, "Energy consumption estimation integrated into the Electric Vehicle Routing Problem," Transportation Research Part D: Transport and Environment, Vol.69, 141-167, April 2019.

Ray Galvin, "Energy consumption effects of speed and acceleration in electric vehicles: Laboratory case studies and implications for drivers and policymakers," Transportation Research: Part D, 53 (2017), 234–248, 2017.

Rajashekara, K., "Present status and future trends in electric vehicle propulsion technologies," IEEE J. of Emerging and Sel. Topics in Power Electron., Vol. 1, No. 1, 3–10, March 2013.

Rahman, Z., Ehsani, M., and Butler, K., "An Investigation of Electric Motor Drive Characteristics for EV and HEV Propulsion Systems," SAE Technical Paper, 2000-01-3062, 2000, doi:10.4271/2000-01-3062.

Ren, Q., Crolla, D.A., Morris, A., "Effect of Transmission Design on Electric Vehicle (EV) Performance," 2009 IEEE Vehicle Power and Propulsion Conference, Dearborn, MI, USA, September 2009, doi: 10.1109/VPPC.2009.5289707.

Robertson, H.D., Hummer, J.E., & Nelson, D.C., 'Manual of transportation engineering studies. New Jersey: Prentice-Hall,1994.

Roberto Alvarez, Alberto Lo'pez, and Nieves De la Torre, "Evaluating the effect of a driver's behavior on the range of a battery-electric vehicle," Proc IMechE Part D: Journal Automobile Engineering, Vol. 229 (10), 1379–1391, 2015.

Ruoyun Ma, Xiaoyi He, Yali Zheng, Boya Zhou, Sheng Lu, Ye Wu, "Real-world driving cycles and energy consumption informed by large-sized vehicle trajectory data," Journal of Cleaner Production, Vol. 223, 564-574, June 2019.

Rui Zhang, Enjian Yao, "Electric vehicles' energy consumption estimation with real driving condition data," Transportation Research: Part D, 41 (2015), 177–187, 2015.

Sahoo, B., Sahoo, N., and Saha, U., "Dual Fuel Performance Studies of a Small Diesel Engine Using Green Fuels," Applied Mechanics and Materials 668(110-116):2101-2108, 2011.

Sanghpriya H. Kamble, Tom V. Mathew, G.K. Sharma, "Development of real-world driving cycle: Case study of Pune, India," Transportation Research Part:D, 14 (2009) 132–140, 2009.

SAE Vehicle dynamics, https://www.sae.org/images/books/toc_pdfs/R114.pdf, Accessed on 24th November 2020.

Seishiro Shibata, Tsuguhiko Nakagawa, "Mathematical Model of Electric Vehicle Power Consumption for Traveling and Air-Conditioning," Journal of Energy and Power Engineering 9 (2015) 269-275 doi: 10.17265/1934-8975/2015.03.006, 2015.

Shindell, D., et al. "Climate, Health, Agricultural and Economic Impacts of Tighter Vehicle-Emission Standards." Nature Climate Change 1, No. 1, 59–66, April 2011.

Shiqi Ou, et .al, 'Light-duty plug-in electric vehicles in China: An overview on the market and its comparisons to the United States," Renewable and Sustainable Energy Reviews, Vol. 112, 747-761, September 2019.

Shrikant Misal and Bangalore Divakar, "Performance Evaluation of Ultra-Capacitor in Hybrid Energy Storage System for Electric Vehicles," 7th Asia Modelling Symposium, 2013.

SIAM Annual Reports 2018-19, Society of Indian Automobile Manufacturers (SIAM), http://www.siamindia.com/scripts/industrystatistics.aspxl, data retrieved and accessed on 11th November 2020.

SIAM 2020, Industry Composition, https://www.siam.in/statistics.aspx?mpgid=8&pgidtrail=12, Accessed on 26th November 2020

Shi, T., Zhao, F., Hao, H., and Liu, Z.and "Costs, Benefits and Range: Application of Lightweight Technology in Electric Vehicles," SAE Technical Paper 2019-01-0724, 2019, doi:10.4271/2019-01-0724.

Sudhir Gupte, "Experimental analysis and feasibility study of 1400cc diesel engine car retrofitted into a hybrid electric vehicle using BLDC hub motors," Science Direct, Energy Procedia, 54, 177 – 184, 2014.

Sumit Sharma, Anju Goel, R Suresh, C Sita Lakshami, Richa Mhatta, S Sundar, "Assessment of emission test driving cycles in India: A case for improving compliance," The Energy and Resources Institute (TERI), doi: 10.13140/RG.2.1.1589.4163. Reviewed by International Council for Clean Transportation (ICCT), Gaurav Bansal, John German, Francisco Posada, Vicente Franco.

S.O.1522 (E), 6th April 2018, for Vehicle speed limit notification https://morth.nic.in/sites/default/files/notifications_document/Draft_Notification_no_S_O_1522E_dated_6_4_018_regarding_Revised_Speed_Limits_0.pdf, Accessed, 17th October 2020.

Sorniotti, A., Boscolo, M., Turner, A., and Cavallino, C., "Optimization of a Multi-Speed Electric Axle as a Function of the Electric Motor Properties," Vehicle Power and Propulsion Conference (VPPC), 2010 IEEE, 1-6, 2010, doi:10.1109/VPPC.2010.5729120.

TAP-115/116, Issue No.4, 2012, Document on Test Methods, Testing Equipment, and Related Procedures for Testing Type Approval and Conformity of Production (COP) of Vehicles for Emission as per CMV Rules 115,116 and 126, MoRTH/CMVR/TAP-115/116, Amendment No. 1, Issue No.4, Dec. 2012, https://www.araiindia.com/CMVR_TAP_Documents/Amendment%201%20to%20Tap%20Issue%204_1.pdf, Accessed on 15th October 2020.

TAP-115/116, IDC: Testing Type Approval and Conformity of Production (CoP) of Vehicles for Emission as per Central Motor Vehicle Rules 115, 116 and 126," Ministry of Road Transport and Highways, Government of India, MoRTH/CMVR-115/116 (Issue 4), Phase-III, Chapter-3, 59-64, https://araiindia.com/CMVR_TAP_Documents/Phase-03/Phase-03_Chapter03.pdf, Accessed on 15th October 2020.

TAP-115/116, MIDC: Testing Type Approval and Conformity of Production (CoP) of Vehicles for Emission as per Central Motor Vehicle Rules 115, 116 and 126," Ministry of Road Transport and Highways, Government of India, MoRTH/CMVR/TAP-115/116 (Issue-4), Phase-14, Chapter-3, 912-915, https://www.araiindia.com/CMVR_TAP_Documents/Phase-14/Phase-14_Chapter03.pdf.

https://www.araiindia.com/CMVR_TAP_Documents/Amendment%201%20to%20Tap%20Issue%204_1.pdf, Accessed on 15th October 2020.

TAP-115/116, Issue No. 4, Part-XIV, Chapter-3, Details of Standards for Tailpipe Emissions from Petrol, CNG, LPG, and Diesel Engined Vehicles and Test Procedures Effective for Mass Emission Standards (Bharat Stage IV) For M and N Category Vehicles not exceeding 3.5 Tons GVW, Document no. MoRTH/CMVR/ TAP-115/116, Issue No. 4, PART XIV, Chapter-3, https://www.araiindia.com/CMVR_TAP_Documents/Part-14/Part-14_Chapter03.pdf, Accessed on 15th October 2020.

UK Auto, 2020, https://www.thehindu.com/news/international/uk-to-ban-sale-of-new-petrol-and-diesel-cars-from-2030-reports/article33100396.ece, accessed on 16th November 2020.

Van Mierlo, J. , Maggetto, G., Van de Burgwal, E. and Gense, R., "Driving style and traffic measures-influence on vehicle emissions and fuel consumption," Proc. Inst. Mech. Eng. Pt. D: J. Automobile Eng., Vol. 218, 43-50, 2004.

Vasudevan, M., Arumugam, R., "High Performance Sensorless Direct Flux and Torque Control Scheme for Induction Motor Drives," National Power System Conference, IIT Madras, December, 2004.

Wang, J., Li, W., Zhang, X., Yi, P. et al., "Road Dynamic Simulation for Vehicle Driveline Experiments," SAE Technical Paper 2018-01-5016, 2018, doi:10.4271/2018-01-5016.

Walker, P.D., Abdul Rahman, S., Zhang, N., Zhan, W., Lin, Y., Zhu, B., "Modelling and simulation of a two-speed electric vehicle," Springer, Sustainable Automotive Technologies, 193-198, 2012.

Walker, P.D., Rahman, S.A., Zhu, B., and Zhang, N., "Modelling, Simulations, and Optimisation of Electric Vehicles for Analysis of Transmission Ratio Selection," Advances in Mechanical Engineering, 5, 2013, doi:10.1155/2013/340435.

Walker, P.D., Roser, H., Zhang, N., and Fang, Y., "Comparison of Powertrain System Configurations for Electric Passenger Vehicles," SAE Technical Paper 2015-01-0052, 2015, doi:10.4271/2015-01-0052.

Wang, H., Song, X., Saltsman, B., and Hu, H., "Comparative Studies of Drivetrain Systems for Electric Vehicles," SAE Technical Paper 2013-01-2467, 2013, doi:10.4271/2013-01-2467.

West, J. G. W., "DC, induction, reluctance and PM motors for electric vehicles," Power Engineering Journal, Vol. 8, No. 2, 77–88, April 1994.

Wu, G., Zhang, X., and Dong, Z., "Powertrain Architectures of Electrified Vehicles: Review, Classification and Comparison," Journal of the Franklin Institute, 352(2):425-448, 2014, doi:10.1016/j.jfranklin.2014.04.018.

Williamson, S.S., Lukic, S.M., and Emadi, A., "Comprehensive Drive Train Efficiency Analysis of Hybrid Electric and Fuel Cell Vehicles Based on Motor-Controller Efficiency Modeling," IEEE Transactions on Power Electronics 21(3):730-740, 2006, doi:10.1109/tpel.2006.872388.

World Economic Forum (WEF), 2019, https://www.weforum.org/agenda/2019/02/china-is-winning-the-electric-vehicle-race/, Accessed on 30th November 2020.

Xinkai Wu, David Freese, Alfredo Cabrera, William A. Kitch, " Electric vehicles energy consumption measurement and estimation," Transportation Research Part: D, 34 (2015) 52–67, 2015.

Xinmei Yuan, Chuanpu Zhang, Guokai Hong, Xueqi Huang, Lili Li, "Method for evaluating the real-world driving energy consumptions of electric vehicles," Energy, 141,1955-1968, 2017.

Xue, X. D., Cheng, K. W. E., and Cheung, N. C., "Selection of electric motor drives for electric vehicles," in Power Engineering Conference, 2008. AUPEC '08, Australasian Universities, 1–6, 2008.

Xuewei Qi, Guoyuan Wu, Kanok Boriboonsomsin, Matthew J. Barth, 'Data-driven decomposition analysis and estimation of link-level electric vehicle energy consumption under real-world traffic conditions,' Transportation Research Part D: Transport and Environment, Vol. 64, 36-52, October 2018.

Yang Y, Liu J, Hu T. An energy management system for a directly-driven electric scooter. Energy Convers Manage, 52:621–9, 2011.

Yin, Q., Wu, Z., and Rui, X., "Parameter Design and Optimization of Electric Vehicle," Transportation Electrification Asia-Pacific (ITEC Asia-Pacific), 2014 IEEE Conference and Expo, 1-7, 2014, doi:10.1109/ITECAP.2014.6940949.

ZEV, 2016 "Governor's interagency working group on zero-emission vehicles: ZEV zero-emission vehicles on California roadways by 2025," Tech. Rep., 2016.

Zeraoulia, M. , Benbouzid, M. E. H. and Diallo, D., "Electric motor drive selection issues for hev propulsion systems: A comparative study," IEEE Trans. Vech. Tech., Vol. 55, No. 6, 1756–1764, November 2006.

Zhang Qi, JieYang, RuoJia,FanWang, "Investigating Real-World Energy Consumption of Electric Vehicles: A Case Study of Shanghai," Science Direct, Procedia Computer Science, 131, 367–376, 2018.

Zhenhe Li, Amir Khajepour, Jinchun Song, "A comprehensive review of the key technologies for pure electric vehicles," Energy, Vol. 182, 824-839, September 2019.

Zhi Yang, Fei Shang,Ian P.Brown,and Mahesh Krishnamurthy,' Comparative Study of Interior Permanent Magnet, Induction, and Switched Reluctance Motor Drives for EV and HEV Applications,' IEEE Transactions on Transportation Electrification, Vol. 1, No. 3, October 2015.

Zhuo Yang, Baoqing Deng, Mengqi Deng and Shaojia Huang, Zhuhai, "An Overview of Chassis Dynamometer in the Testing of Vehicle Emission," MATEC Web of Conferences 175, 02015 (2018), IFCAE-IOT, 2018, https://doi.org/10.1051/matecconf/201817502015.